DEUTSCHES ELEKTRONEN-SYNCHROTRON

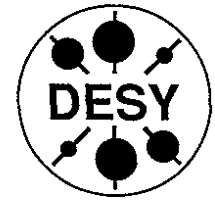

DESY 94-242
December 1994

Rigorous Bounds on Survival Times in Circular Accelerators and Efficient Computation of Fringe-Field Transfer Maps

G. H. Hoffstätter

Department of Physics and Astronomy,
Michigan State University, East Lansing, USA

ISSN 0418-9833

NOTKESTRASSE 85 - 22603 HAMBURG

To be sure that your preprints are promptly included in the
HIGH ENERGY PHYSICS INDEX,
send them to (if possible by air mail):

DESY
Bibliothek
Notkestraße 85
22603 Hamburg
Germany

DESY-IfH
Bibliothek
Platanenallee 6
15738 Zeuthen
Germany

DESY 94-242
December 1994

ISSN 0418-9833

RIGOROUS BOUNDS ON SURVIVAL TIMES IN CIRCULAR ACCELERATORS AND EFFICIENT COMPUTATION OF FRINGE–FIELD TRANSFER MAPS

By

Georg Heinz Hoffstätter

A DISSERTATION

Submitted to
Michigan State University
in partial fulfillment of the requirements
for the degree of

DOCTOR OF PHILOSOPHY

Department of Physics and Astronomy

1994

ABSTRACT

RIGOROUS BOUNDS ON SURVIVAL TIMES IN CIRCULAR ACCELERATORS AND EFFICIENT COMPUTATION OF FRINGE-FIELD TRANSFER MAPS

By

Georg Heinz Hoffstätter

Analyzing stability of particle motion in storage rings contributes to the general field of stability analysis in weakly nonlinear motion. A method which we call pseudo invariant estimation (PIE) is used to compute lower bounds on the survival time in circular accelerators. The pseudo invariants needed for this approach are computed via nonlinear perturbative normal form theory and the required global maxima of the highly complicated multivariate functions could only be rigorously bound with an extension of interval arithmetic. The bounds on the survival times are large enough to be relevant; the same is true for the lower bounds on dynamical apertures, which can be computed. The PIE method can lead to novel design criteria with the objective of maximizing the survival time. A major effort in the direction of rigorous predictions only makes sense if accurate models of accelerators are available. Fringe fields often have a significant influence on optical properties, but the computation of fringe-field maps by DA based integration is slower by several orders of magnitude than DA evaluation of the propagator for main-field maps. A novel computation of fringe-field effects called symplectic scaling (SYSCA) is introduced. It exploits the advantages of Lie transformations, generating functions, and scaling properties and is extremely accurate. The computation of fringe-field maps is typically made nearly two orders of magnitude faster.

This thesis is dedicated
to Johann Sebastian Bach
and to his inspiring dedications.

ACKNOWLEDGEMENTS

All too often acknowledgements seem to be misused to emphasize the quality of the presented work by mentioning invitations, journeys, and support; mostly before thankfulness towards the most important supporters of private life is expressed. In order to clarify priorities and to separate my gratitude for selfless work of others from acknowledgements of professional support, which tends to shed light on my own work, I will distinguish between private and professional acknowledgements.

Private: Deep reverence goes to my wife Anke, who, with happiness, endured my education and the inconveniences it brought with it. Without doubt, the liveliness she and our three children, Samuel, Lydia, and Tabea bring to our home contribute much to my work. The time and energy spent by my parents Heinz and Elisabeth for fostering my general curiosity and my interest in history is deeply appreciated.

Although his name has the touch of professionalism, I want to express my gratitude towards Prof. Dr. Martin Berz here for being a personal friend and advisor and for shaping my scientific personality in many ways. Much of the idealistic and financial support mentioned below was initiated by him. It is due to his support that my family could settle down in Michigan quickly, and the academic group gathered around him contributed much to my stimulating experience at the National Superconducting Cyclotron.

The members of this group, Meng Zhao, Khodr Shamseddine, Weishi Wan, Dr. Ralf Degenhardt, and Kyoko Fuchi all share a part of the credit of the presented work due to their discussions and friendship. I am also deeply indebted to Prof. Dr. Harald Rose for the energy and happiness with which he introduced me to physics research and guided me towards the field of particle optics.

Professional: The financial support of The German National Scholarship Foundation (Studienstiftung des Deutschen Volkes) has made my education, starting from undergraduate times, much smoother than it would have been otherwise. And it is also from their generous support that I could visit Prof. Dr. Martin Berz's group, which finally lead to the completion of this dissertation. This support was followed up by generous funds due to a National Superconducting Cyclotron Fellowship and a Scholarship of the College of Natural Science at Michigan State University. I am also thankful for the Quadrille Ball Fellowship of the Germanistic Society of America. The financial support for participating in the conference on Numerical Analysis with Automatic Result Verification (Lafayette, LA 1993) and in the Fourth International Conference on Charged Particle Optics (Tsukuba, Japan 1994) granted by the conference committees is appreciated.

The visit to the 1992 United States Particle Accelerator Summer School at Stanford University and the received instruction and encouragement by Prof. Dr. Karl Brown and Prof. Dr. Roger Servranckx became important to my work. The real fun of a scientific career starts when others become interested in your work and I am therefore very thankful to the conference committee of the 1994 Crystal City APS meeting to invite me for a talk on the computation of fringe-field effects.

Many thanks go to Dr. Desmond Barber, who invited me to DESY to introduce him into the code COSY INFINITY and to give a talk about my work. For the same reason thanks go to Prof. Dr. Harald Rose, who invited me to a seminar talk on the fringe-field aspects of the work which will be presented. Many aspects of interval arithmetic became clear to me in discussions with Dr. Dietmar Ratz and Olaf Knüppel from Karlsruhe and Hamburg respectively, who I thank for the time they took to introduce me into the tricks of interval optimization.

Contents

LIST OF TABLES ix

LIST OF FIGURES xi

Foreword 1

1 Normal Form Theory 5

1.1 Normal Form Theory for Order n Symplectic Maps 6

1.2 First Order Transformations 11

1.3 Nonlinear Transformations 12

1.4 Invariants 25

1.5 Real Normal Forms 27

1.6 Action-Angle Variables 35

1.7 Pseudo Hamiltonians 42

1.8 Parameter Dependent Normal Forms 44

1.9 General Normal Form Theory 46

2 Long Term Estimates for Weakly Nonlinear Motion 50

2.1 Introduction to the PIE Method 51

2.1.1 History . . . 52
2.2 Pseudo Invariant Estimation (PIE) . . . 54
2.3 Normal Form Transformations and Pseudo Invariants . . . 58
2.4 Maps to Test the Method . . . 61
2.4.1 The Physical Pendulum . . . 61
2.4.2 Henon Map for One Degree of Freedom . . . 62
2.4.3 Coupled Pendulum . . . 63
2.4.4 The IUCF Ring . . . 65
2.4.5 The PSR II Ring . . . 66
2.4.6 The Demo Ring . . . 66
2.5 The Pseudo Invariant and How to Parameterize Regions . . . 67
2.6 Analysis of Pseudo Invariants . . . 73
2.7 Influence of Resonances . . . 76
2.8 Symplectic Representations . . . 87

3 Optimization by Scanning **92**

3.1 Refinements and Examples . . . 95
3.1.1 Dividing Phase Space . . . 95
3.1.2 Time Evaluation . . . 96
3.1.3 Parameter Dependence . . . 97

4 Rigorous PIE with Interval Arithmetic **101**

4.1 Interval Arithmetic . . . 102

4.2 Interval Chains and Optimization . . . 106
4.3 Parameterizing Regions for the IC-PIE Method . . . 112
4.4 Comparison Between Intervals and Interval Chains . . . 113
4.5 Refinement of the Rigorous Estimates . . . 116
4.5.1 Analysis of Multi-Turn Maps . . . 117
4.5.2 Random Parameters . . . 123
4.6 Using Taylor Maps with Remainder Bound . . . 124

5 Symplectic Scaling (SYSCA) **126**

5.1 Integration in DA . . . 129
5.2 Evaluating Propagators in DA . . . 130
5.3 Desirable Properties of an Arbitrary Order Fringe-Field Approximation 135
5.3.1 Order n Symplecticity . . . 136
5.3.2 Accuracy for a Wide Range of Apertures . . . 138
5.3.3 Usability for Arbitrary Orders . . . 139
5.4 The Principles and Usefulness of SYSCA . . . 139
5.5 Examples . . . 148
5.6 The Lie Exponent . . . 154
5.7 The Generating Function for the Linear Map . . . 156
5.8 Transformation between Cartesian and Canonical Coordinates . . . 159

LIST OF REFERENCES **162**

List of Tables

2.1 Smallest resonance denominators for the physical pendulum and the Henon map with a tune of 0.379. 74

2.2 Resonance denominators for the map of the coupled pendulum. . . . 76

2.3 Resonance denominators for the map of the IUCF ring. 77

2.4 Resonance denominators for the map of the PSR II ring. 78

2.5 Resonance denominators for the map of the Demo ring. 79

2.6 Maximum of the deviation function after symplectifying the map by adding higher orders. 89

2.7 The maximum of the deviation function as a function of the turns when the map is represented by a generating function. 90

3.1 Minimum number of turns required to move from the initial region to the forbidden region. The initial emittance was chosen to be half the acceptance. The maps were evaluated in order eight, whereas the pseudo invariants were computed to the indicated order. Scanning was performed with 20^k points for k relevant dimensions. 94

3.2 Number of map applications used for improving the estimation. . . . 97

3.3 Lower bounds on the turns of particles for initial emittance of one half the acceptance and lower bounds on the stable emittances for 10^8 turns obtained by various variations of the PIE method. 100

4.1 Predictions of the number of stable turns as a function of the order of the polynomials describing the normal form transformation for the physical pendulum with a maximum elongation of 1/10 rad. Because of energy conservation, the map is known to be permanently stable. . 114

4.2 Predictions of the number of stable turns for the Henon map at tune 0.13, strength parameter 1.1, and starting position $(x, a) = (0.01, 0)$ as a function of the order of the normal form transformation. 115

4.3 Predictions of the number of stable turns as a function of the order of the approximate invariant for the Los Alamos PSR II storage ring for the motion in a phase space of 100 mm mrad. 115

4.4 Decreasing width of the remainder interval with evaluation order. . . 121

4.5 Remainder intervals for multi-turn maps. 122

4.6 Lower bounds on the turns of particles for an initial emittance of one half the acceptance, obtained by the IC-PIE method. 123

4.7 Maximum error of the Taylor map in the phase space region of interest. 125

4.8 Results of the IC-PIE bounds on the survival time of particle motion for rigorous description of the systems by a Taylor map with remainder intervals. 125

5.1 Tilt angle and opening aberration for various fringe-field models. . . 151

List of Figures

2.1 a) The initial region $\mathcal{O}$ and the allowed region $\mathcal{A}$ of phase space $\mathcal{P}$ with $\mathcal{O} \subset \mathcal{A} \subset \mathcal{P}$. b) The gap Δf that has to be bridged. 57

2.2 Phase Diagram for 2000 turns in an accelerator for four initial conditions. The left picture shows the motion displayed in standard particle optical coordinates x and a, and the right picture shows the same motion in normal form coordinates. 60

2.3 9 particles tracked for 500 turns through the Henon map. The starting conditions were $x = 0.1 \cdot j$, $j \in \{1, \ldots, 9\}$ and the kick strength was 1.1. The tune in figure a) is 0.255 and in figure b) 0.29. 63

2.4 9 particles tracked for 500 turns through the coupled pendulum. The starting conditions were angles $x/l_0 = 0.01 \cdot j$ for $j \in \{1, \ldots, 9\}$. This corresponds to a maximum emittance of 4050mm mrad. The horizontal and vertical tunes in figure a) are 0.36 and 0.78, and in figure b) 0.37 and 0.78. 64

2.5 a) Layout of the IUCF ring, only dipoles and quadrupoles are shown. b) x–p_x phase space positions for 500 turns. The initial conditions are $(x = 5j, y = 5) \cdot 10^{-4}$ with $j \in \{1, \ldots, 10\}$. 66

2.6 a) Layout of the PSR II ring, only dipoles and quadrupoles are shown. b) x-p_x phase space positions for 500 turns. The initial conditions are $(x = 5 \cdot j, y = 5 \cdot j) \cdot 10^{-3}$ with $j \in \{1, \ldots, 8\}$. 67

2.7 a) Layout of the Demo ring, only dipoles and quadrupoles are shown. b) x-p_x phase space positions for 500 turns. The initial conditions are $(x = 5 \cdot j, y = 5 \cdot j) \cdot 10^{-3}$ with $j \in \{1, \ldots, 8\}$. 68

2.8 The motion on nonlinear invariants in the phase space section x-p_x in figure a) and y-p_y in figure b). The allowed and the forbidden region and the definition of $||\vec{z}||$ is depicted in figure c). 71

2.9 Fluctuation of the pseudo invariant on the surface of the allowed region. Elliptic beam shapes ($s = \circ$) and rectangular beam shapes ($s = \square$) were used for the left and the right picture respectively. The four cases and the emittances used are the coupled pendulum ($\epsilon_1 = 0.6\epsilon, \epsilon_2 = 0.4\epsilon$), the IUCF ring ($\epsilon_1 = 0.3\epsilon, \epsilon_2 = 0.7\epsilon$), the PSR II ($\epsilon_1 = 0.05\epsilon, \epsilon_2 = 0.95\epsilon$), and the Demo ring ($\epsilon_1 = 0.4\epsilon, \epsilon_2 = 0.6\epsilon$). 72

2.10 Invariant defect for the physical pendulum on an invariant ellipse. The coordinates are 0 to ϵ from left to right and 0 to 2π from front to back. The range of the depicted function is $[-2.36 \cdot 10^{-12}, 5.63 \cdot 10^{-12}]$. . . . 74

2.11 Invariant defect for the Henon map on an invariant ellipse. The coordinates are 0 to ϵ from left to right and 0 to 2π from front to back. The range of the depicted function is $[-5.59 \cdot 10^{-8}, 5.56 \cdot 10^{-8}]$. 75

2.12 Invariant defect for the coupled pendulum on a pseudo invariant torus. The coordinates are in $[0, 2\pi] \times [0, 2\pi]$. The range of the depicted function is $[-2.55 \cdot 10^{-13}, 7.36 \cdot 10^{-13}]$. 77

2.13 Invariant defect for the map of the IUCF ring on a pseudo invariant torus. The coordinates are in $[0, 2\pi] \times [0, 2\pi]$. The range of the depicted function is $[-6.84 \cdot 10^{-9}, 6.00 \cdot 10^{-9}]$. 78

2.14 Invariant defect for the map of the PSR II ring on a pseudo invariant torus. The coordinates are in $[0, 2\pi] \times [0, 2\pi]$. The range of the depicted function is $[-1.76 \cdot 10^{-9}, 1.65 \cdot 10^{-9}]$. 79

2.15 Invariant defect for the map of the Demo ring on a pseudo invariant torus. The coordinates are in $[0, 2\pi] \times [0, 2\pi]$. The range of the depicted function is $[-7.22 \cdot 10^{-9}, 6.95 \cdot 10^{-9}]$. 80

2.16 Regions of resonances for two degrees of freedom up to order a) 6, b) 12. 82

2.17 Variation of the maximum δ of the deviation function d_f with tune for the Henon map of a) order 8, b) order 4. The scale is logarithmic and inverted. Staying out of resonance holes yields long survival time predictions with the PIE. 84

2.18 Variation of the maximum δ of the deviation function d_f with tune for the 8^{th} order map of the physical pendulum. The scale is logarithmic and inverted. Due to the existence of an invariant, resonance denominators do not cause a problem during normal form computation. 85

2.19 Variation of the maximum δ of the deviation function d_f with tune for the 8^{th} order map of the PSR II. The scale is logarithmic and inverted. The whole horizontal and vertical tune space is covered: $\nu_x \times \nu_y \in [0, 1] \times [0, 1]$. The range of d_f is from $2.2 \cdot 10^{-10}$ to $1.9 \cdot 10^{-7}$. 86

2.20 Variation of the maximum δ of the deviation function d_f with tune for the 8^{th} order map of the Demo ring. The scale is logarithmic and inverted. The range of d_f is from $1.3 \cdot 10^{-9}$ to $1.9 \cdot 10^{-4}$. 88

2.21 Quality of normal form invariants when the map is represented by a generating function for the four examples with two degrees of freedom: a) the coupled pendulum, the range of the displayed function is $[-2.15, 9.45] \cdot 10^{-13}$, b) IUCF: $[-1.16, 1.11] \cdot 10^{-8}$, c) PSR II: $[-2.63, 2.63] \cdot 10^{-9}$, d) Demo: $[-6.36, 8.49] \cdot 10^{-9}$. For the order 8 symplectic Taylor maps, the corresponding figures were displayed previously. 91

3.1 Figure a) depicts $F(x)$ and figure b) $D(x)$ in the allowed region. The variation of the pseudo invariant relative to $||\vec{z}||$ is shown in figure c). 93

3.2 Dividing phase space approximates the area under the displayed curve by several rectangles to obtain the bound on the survival time. Without this improvement, the PIE method would only give the area of the drawn rectangle. 96

3.3 a) slow increase of the pseudo invariant over many turns, b) periodic change of the pseudo invariant after relatively few turns. 97

3.4 The figures display the variation of the deviation function in the allowed region for the six examples. From top left to bottom right these are a) Pendulum, b) Henon map, c) Coupled pendulum, d) IUCF, e) PSR II, f) Demo. 98

4.1 Top left: The function of which an upper bound should be found. Others: Covering the region of interest with smaller intervals reduces the overestimation of the maximum. 107

5.1 Definition of fringe-field and main-field maps. 127

5.2 Time consumption of integration in DA relative to main-field map computation with the propagator for different expansion orders. From top left to bottom right: dipole, quadrupole, hexapole, octupole. . . . 132

5.3 Accuracy of SCOFF for different orders, a random choice of Taylor coefficients would be close to one. From top left to bottom right: dipole, quadrupole, hexapole, octupole. 134

5.4 Tracking through a 15° dipole, displayed in conventional coordinates on the left and in normal form coordinates on the right. The figures on the top display accurate tracking data, those in the middle were created by the 5^{th} order Taylor map, and the bottom pictures were produced by 5^{th} order symplectic generating function tracking. 137

5.5 The coordinates of the particle trajectories in two elements scale with the factor α if the elements scale with the factor α and the fields scale with the factor $1/\alpha$. 142

5.6 Schematic outline of the procedures leading to the reference representation and from the reference representation to the general transfer map. 147

5.7 left: $(x|xxa)$ for a quadrupole as a function of the field at the pole tip. right: Error Δ of the approximation of $(x|xxa)$ with different expansion orders for the reference representation at B=2T. 148

5.8 Factor of time advantage of SYSCA to numerical integration with accuracy of 10^{n-9} as a function of the expansion order. From top left to bottom right: dipole, quadrupole, hexapole, octupole. 150

5.9 Relative deviation of predicted field settings with SCOFF and SYSCA from the correct settings for five quadrupoles. The standard fringe-field approximation of TRANSPORT is given as a reference; the deviation is mainly due to the neglect of quadrupole fringe fields. 151

5.10 Beam spots with SYSCA (left) and SCOFF (right) approximation. The plot produced with the exact fringe fields can not be distinguished from the plot produced with SYSCA. Note the difference in scale. . . 152

5.11 500 turn tracking without (left) and with (right) fringe fields trough an 1Gev proton storage ring. 152

5.12 5000 turn tracking with fringe fields obtained by numerical integration (left), SYSCA (middle), and a non-symplectic fringe-field approximation (right). The initial position of the particle is $(x, y) = (3\text{cm}, 3\text{cm})$ with no initial inclinations x' and y'. 153

Foreword

Predictions of accelerator performance require an accurate model of particle optical devices and accurate computation schemes to evaluate the motion of particles in each element of the accelerator. Usually it is considered an accurate description of an accelerator when the motion of a single particle can be computed with a small error. However, having such an accurate model available only allows one to evaluate the accelerator's influence on a limited number of particles. Thus, any approach computing single particle motion can only evaluate the action of the accelerator in a subset of phase space of measure zero. Completely rigorous predictions of accelerator performance can therefore only be achieved when the accelerator's action can be evaluated on the entire relevant phase space region. The presented work deals with both problems, rigorous predictions and accurate computation of charged particle motion in optical systems. The predictions concern the survival time of particles in storage rings.

This dissertation is naturally divided into three interrelated parts. These are a detailed chapter on normal form theory; the description, application, and rigorous evaluation of what we call the pseudo invariants estimation (PIE) method for survival time bounds; and finally a chapter on the DA based tool of symplectic scaling. Each of these parts has a detailed introduction including references and comments about the history and purpose of the approaches which will be developed. Please refer to the pages (5), (50), and (126) for these specific introductions.

All parts of this work use transfer maps $\vec{M}$ of dynamical systems that map initial phase space coordinates $\vec{z}_i$ into coordinates $\vec{z}_f$ which are considered final in some sense. This transfer map can also depend on n_p parameters δ_i, $i \in \{1, \ldots, n_p\}$ of the physical system involved, leaving $\vec{z}_f = \vec{M}(\vec{z}_i, \vec{\delta})$. In the applications which will be presented, the dynamical system is a particle moving in an accelerator or storage ring. Following the belief that the quality of a Ph.D. thesis increases with a decrease of the presentation of well known material, the so -called DA method of manipulating and computing all derivatives of a transfer map up to order n, will not be introduced in detail but will only be described shortly. It is based on the possibility of introducing "$=_n$" as an equivalence relation, equating functions which have the same partial derivatives at the origin up to order n. Taking derivatives at the origin is not a restriction, since the origin can be shifted to any reference point by transformation. Traditionally, equivalence in this sense is expressed by considering functions as equal up to order n, since the partial derivatives specify the Taylor expansion up to order n. The theory of constructing a differential algebra on the set of equivalence classes created by "$=_n$" is introduced with rigor in [Ber92a]. When it is relevant to the presented work, it will be used and restated that agreement up to order n can be expressed by an equivalence relation. Often we will refer to Taylor maps, which represent an equivalence class. The terminology of Taylor maps rather than equivalence classes is used, since many readers will be acquainted with manipulating Taylor maps up to order n. It should, however, be realized that no approximation is made when Taylor maps are used. To the contrary, all partial derivatives which are equated with "$=_n$" are exact. Therefore, computations within the differential algebra of derivative classes leads to all partial derivatives up to order n without any approximation.

In normal form theory, which is treated in chapter (1), a map $\vec{M}$ will be transformed by means of a nonlinear transformation $\vec{A}$ into a normal form map $\vec{N}$ $=_n$

$\vec{A} \circ \vec{M} \circ \vec{A}^{-1}$. The Taylor expansion of $\vec{N}$ has as many vanishing Taylor coefficients as possible. As usual, the symbol "$\circ$" describes the composition of maps. Although $\vec{A}$ is a Taylor map and all arguments are performed with respect to "$=_n$", strict statements about the partial derivatives, which are the Taylor coefficients, can be drawn. Normal form theory will serve to obtain functions f which are invariants of the map $\vec{M}$ up to order $n+1$ and thus $f \circ \vec{M} =_{n+1} f$. For weakly nonlinear dynamics, these functions are approximate invariants, or pseudo invariants, of the transfer map. This is, for instance, the case for particles moving close to the central periodic orbit in a storage ring, which is represented by the origin of phase space.

For the PIE method, a pseudo invariant f will be found which is suitably chosen to let $f(\vec{z})$ describe the distance between a particle with coordinates $\vec{z}$ and the central orbit. At this orbit, $f(\vec{z}) = 0$. $\mathcal{A} = \{\vec{z} | f(\vec{z}) \leq \epsilon\}$ is a volume in phase space which contains the origin. In an application of the map $\vec{M}$ on $\vec{z}$, the so described distance from the origin changes by $d_f(\vec{z}) = (f \circ \vec{M})|_{\vec{z}} - f(\vec{z})$. Where evaluating a function f at $\vec{z}$ is written as $f|_{\vec{z}}$, which is equivalent to $f(\vec{z})$. If the maximum δ of d_f on the phase space volume $\mathcal{A}$ can be found, it can rigorously be said how far a particle can move away from the closed orbit in one turn. It can also be stated rigorously that particles in the phase space volume $\mathcal{O}$ with $\mathcal{O} = \{\vec{z} | f(\vec{z}) \leq c - N\delta\}$ will not leave the volume $\mathcal{A}$ for N applications of the map. Analyzing the prospects of this approach and bounding the maximum of d_f rigorously by an extension of interval arithmetic is the main subject of the chapters (2), (3), and (4). First results of this method were reported in [BH94b].

This approach is only rigorous for single particle motion, since the one turn map is computed for a single particle. Particle loss due to residual gas scattering, beamstrahlung in the collision region, space charge effects, and other collective effects are not considered.

A substantial effort for making predictions of accelerator performance rigorous, like the introduction of interval chains in section (4.2) or the development of differential algebra with remainder intervals (RDA) in [BH94a], is only useful if the transfer maps of accelerators can be described accurately. In chapter (5) it will be shown that often the influences of fringe fields are very relevant, especially for higher order derivatives of the transfer map. The well established DA method of obtaining Taylor maps of particle optical elements by evaluating Lie derivatives can only compute transfer maps of main field regions, and numerical integration in DA is very time consuming. For the method of symplectic scaling (SYSCA), it will be analyzed how known scaling properties of maps in geometric coordinates can be used to scale symplectic representations of the transfer map of a Hamiltonian system. The representations used are various generating functions and exponential Lie operators. To apply SYSCA, a symplectic representation is computed by integration in DA as a function of the magnetic field of one specific particle optical element and a specific particle. The Taylor expansion of this function is stored to a file. Scaling this symplectic representation of the fringe-field map for a different particle or for a different size of the optical element is much faster than the conventional methods which leads to accurate fringe-field maps and it is also much more accurate than a number of conventional approximations which will be mentioned. Additionally, this method leads to maps which are symplectic up to order n. Several examples will demonstrate the usefulness of this method.

Chapter 1

Normal Form Theory

The idea of normal form transformations for simplifying differential equations is very old (according to [Nay93] it goes back to Euler's days). After Poincaré's work on maps in nonlinear dynamics [Poi99], normal form transformations were used for maps by Birkhoff [Bir27] and many others after him. Reference [Tur91] gives a detailed account of the history of normal forms. For symplectic maps, the possibility of normal form transformations was mentioned in [DF76] and computationally performed for Taylor maps in high orders in [FBI89]. In these approaches the symplecticity was guaranteed by the use of exponential Poisson-bracket operators. In [Ber93b] a method of computing the normal form of maps was demonstrated which can be applied to non-symplectic maps as well. This approach can be evaluated in a straightforward way with DA-based programs and was implemented in the code COSY INFINITY [Ber92b]. This chapter will explain this method, and it will be shown that it can be used to obtain pseudo invariants for symplectic maps.

We will use the symbol "$=_n$" to indicate that the left and right hand side of an equation have the same partial derivatives at the origin up to order n; in other words, the Taylor expansions of the left and the right hand side agree up to order n. It can be shown that "$=_n$" is an equivalence relation and therefore establishes equivalence classes. A differential algebra of these equivalence classes can be constructed [Ber92a]

which can be used to formulate relationships for the partial derivatives of functions. This theory establishes in a rigorous way that the well known method of evaluating a function of a Taylor expansion leads to the correct Taylor expansion of the resulting function and therefore to correct partial derivatives.

All arguments will be performed with Taylor maps, but it is worthwhile to keep in mind that an n^{th} order Taylor map, i.e. a map whose vector components are polynomials of order n, is one representative of an equivalence class established by "$=_n$". What is found for Taylor maps is also true for partial derivatives.

1.1 Normal Form Theory for Order n Symplectic Maps

Conventions: Some notations will be used often, therefore we want to define them now. J_{2d} is the $2d \times 2d$ matrix with

$$J_{2d,ij} = \begin{cases} 1 & \text{for } i \text{ odd and } j = i+1 \\ -1 & \text{for } i \text{ even and } i = j+1 \\ 0 & \text{else} \end{cases} . \tag{1.1}$$

The identity function will be symbolized by $\vec{z}$, i.e. $z_l(\vec{x}) = x_l$ for all $\vec{x}$. Often an incorrect notation is used by writing expressions like $(\vec{f}^T\vec{\partial})^k\vec{z}$, while $\vec{z}$ is understood to be an element of $\mathbb{R}^{2d}$ and $\vec{f}$ is a function $\mathbb{R}^{2d} \to \mathbb{R}^{2d}$. This must be wrong, since $\vec{z} \in \mathbb{R}^{2d}$ can not be differentiated. Sometimes this problem is corrected by using the identity $\vec{I}$ to write $(\vec{f}^T\vec{\partial})^k\vec{I}$. Since this notation can become very peculiar and unconventional, a slightly different but very useful notation is advocated. The clarity of the incorrect notation can be conserved by simply choosing $\vec{z}$ to be the identity map. This convention will be used consequently. Elements of $\mathbb{R}^{2d}$ will usually be denoted by $\vec{x}$.

At this point attention should also be drawn to another incorrect use of notation.

For a function $g : \mathbb{R}^{2d} \to \mathbb{R}$, $g(\vec{f})$ is incorrectly written, since g acts on elements of $\mathbb{R}^{2d}$, not on functions like $\vec{f}$. The correct notation for a concatenation of functions is $g \circ \vec{f}$. This clear notation can become important to avoid misunderstandings. An example is the ambiguity of $g(\vec{f}+\vec{z})$, which could either mean $g \circ (\vec{f}+\vec{z})$ or $g \cdot (\vec{f}+\vec{z})$. Strictly speaking it is also incorrect to write $g \circ \vec{x}$ for $\vec{x} \in \mathbb{R}^{2d}$, since "$\circ$" concatenates functions, and $\vec{x}$ is not a function. In this chapter the notation $g(\vec{x})$ is usually used; whenever this would cause confusion, $g|_{\vec{x}}$ is written for the evaluation of the function g at $\vec{x}$. Now enough about these trivialities, which are only mentioned to advocate correct use of notations.

The partial derivative of f with respect to its i^{th} variable is written as $\partial_i f$. If f only depends on one variable, ∂f will denote the derivative. Multidimensional maps will be denoted by capital vectors, e.g. $\vec{M}$, and their $2d \times 2d$ Jacobi matrix by the capital letter, e.g. M; so $M_{ij} = \partial_j M_i$. The Gauss bracket or integer part "[...]" will often be used. All the maps we will mention will be assumed to be sufficiently differentiable, such that all partial derivatives at the origin equated by "$=_n$" will be defined. All the maps we will mention will be origin preserving. Since this restriction will be implied for every map, we will not mention it further. Concatenation of functions is denoted by "$\circ$".

Before we state the theorem about normal forms, we will define some terminology and review some properties of symplectic matrices.

Definition 1.1.1 (Order n Symplecticity)

A $2d$ dimensional map $\vec{M}$, with a Jacobi matrix M that satisfies the symplectic condition up to order $n-1$,

$$M J_{2d} M^T =_{n-1} J_{2d} \ , \tag{1.2}$$

is called order n symplectic. The set of all order n symplectic maps which are $\mathbb{C}^{2d} \to$

$\mathbb{C}^{2d}$ is denoted by $\mathcal{SP}_n^{2d}(\mathbb{C})$. Correspondingly, $\mathcal{SP}_n^{2d}(\mathbb{R})$ symbolizes the set of all order n symplectic maps from $\mathbb{R}^{2d}$ into $\mathbb{R}^{2d}$.

A Jacobian satisfying $M J_{2d} M^T =_{n-1} J_{2d}$ satisfies $\det(M)^2 =_{n-1} 1$. Therefore, an inverse of the matrix $M(\vec{0})$ exists. All operations which lead to a matrix inverse via Kramer's rule can be performed with the Taylor expansions of the elements of M. Neglecting all orders higher than $n-1$ yields a matrix M_I with the property $M M_I =_{n-1} M_I M =_{n-1} Z$, which symbolizes the unit matrix. The unit matrix is denoted by Z, since it is the Jacobian of the identity map $\vec{z}$.

$$M^T J_{2d} M =_{n-1} -J_{2d} M_I (M J_{2d} M^T) J_{2d} M =_{n-1} J_{2d} \tag{1.3}$$

Therefore, just as there are two conditions for symplectic matrices, there are two equivalent conditions for order n symplectic maps,

$$\{\vec{M} | M^T J_{2d} M =_{n-1} J_{2d}, \vec{M}\} = \{\vec{M} | M J_{2d} M^T =_{n-1} J_{2d}, \vec{M}\} \ , \tag{1.4}$$

where the maps are either $\mathbb{R}^{2d} \to \mathbb{R}^{2d}$ or $\mathbb{C}^{2d} \to \mathbb{C}^{2d}$.

Theorem 1.1.2 *For $\mathbb{F}$ being either $\mathbb{R}$ or $\mathbb{C}$, the concatenation of $\vec{A} \in \mathcal{SP}_m^{2d}(\mathbb{F})$ and $\vec{B} \in \mathcal{SP}_n^{2d}(\mathbb{F})$ is order* $\min(m,n)$ *symplectic.*

Proof: Let us first establish the Jacobian C of the concatenation $\vec{C} = \vec{A} \circ \vec{B}$,

$$C_{ij} = \partial_j A_i(\vec{B}) = \sum_{l=1}^{2d} \partial_j B_l \{(\partial_l A_i) \circ \vec{B}\} \text{ or } C = A(\vec{B}) B \ . \tag{1.5}$$

Now the theorem follows immediately, because

$$C J_{2d} C^T = A(\vec{B}) B J_{2d} B^T A^T(\vec{B}) =_n (A^T J_{2d} A) \circ \vec{B} =_{\min(m,n)} J_{2d} \ . \tag{1.6}$$

Definition 1.1.3 (Non-Degenerate Maps)

The eigenvalues of the Jacobian at the origin $M(\vec{0})$ of a map $\vec{M}$ are called the linear

eigenvalues of $\vec{M}$. We call a map non-degenerate if all its linear eigenvalues have multiplicity one.

Theorem 1.1.4 *If λ is an eigenvalue of a symplectic matrix N, then also λ^{-1} is an eigenvalue of N and they both have the same multiplicity.*

Proof: The symplectic condition $NJ_{2d}N^T = J_{2d}$ yields $N^{-1} = J_{2d}N^TJ_{2d}^{-1}$, which shows that N^{-1} and N^T are similar matrices, since $J_{2d}^{-1} = -J_{2d}$. Therefore, N and N^{-1} have the same characteristic polynomial; this proves theorem (1.1.4). This also shows that non-degenerate symplectic matrices cannot have 1 as an eigenvalue. We will always arrange the eigenvalues of symplectic matrices to get $\lambda_{2i-1}\lambda_{2i} = 1$.

Definition 1.1.5 (Resonance of Order m)

The $2d$ eigenvalues λ_l of a non degenerate symplectic matrix, which are ordered to give $\lambda_{2i-1}\lambda_{2i} = 1$, are said to be in resonance of order m if there is a set of d integers k_i with $\sum_{i=1}^{d}|k_i| = m+1$ and $\prod_{i=1}^{d}\lambda_{2i}^{k_i} = 1$.

Definition 1.1.6 (Order n Inverse)

A map $\vec{A}^{-1,n}$ with $\vec{A}^{-1,n} \circ \vec{A} = \vec{A} \circ \vec{A}^{-1,n} =_n \vec{z}$ is called an order n inverse of $\vec{A}$.

Theorem 1.1.7 *Let order n symplectic map $\vec{M}$ be origin preserving, i.e. $\vec{M}(\vec{0}) = \vec{0}$. Then $\vec{M}$ has an order n symplectic order n inverse.*

Proof: First it will be established that every map with a non-singular Jacobian at the origin has an order n inverse. We use the linear map $\vec{M}_1 =_1 \vec{M}$, which has an inverse, and we write $\vec{N} = \vec{M} \circ \vec{M}_1^{-1} - \vec{z}$ which has $(\vec{\partial}N_l)|_{\vec{0}} = 0$ for all its components. Now,

$$\vec{M}^{-1,n} =_n \vec{M}_1^{-1} \circ (\vec{z} + \sum_{i=1}^{n}(-1)^i\vec{N}^i) \,, \tag{1.7}$$

where raising a map to power i means concatenating it i times with itself. Inserting shows that $\vec{M}^{-1,n}$ is indeed an order n inverse of $\vec{M}$:

$$\vec{M}^{-1,n} \circ \vec{M} \;=_n\; \vec{M}_1^{-1} \circ (\vec{z} + (-1)^n\vec{N}^{n+1})\vec{M}_1 =_n \vec{z} \tag{1.8}$$

$$\vec{M} \circ \vec{M}^{-1,n} \;=_n\; (\vec{z} + \vec{N}) \circ (\vec{z} + (-1)^n \sum_{i=1}^{n}\vec{N}^i) =_n \vec{z} \,. \tag{1.9}$$

Since the Jacobian of $\vec{M}$ at the origin is a symplectic map, its determinant is plus one [MH91], and there is an order n inverse of $\vec{M}$. Since the unit matrix Z is the Jacobian of the identity $\vec{z}$, it can be written $Z =_{n-1} (M^{-1,n} \circ \vec{M})M$ and therefore

$$\{(M^{-1,n} \circ \vec{M})MJ_{2d}M^T(M^{-1,nT} \circ \vec{M})\} \circ \vec{M}^{-1,n} =_{n-1} M^{-1,n}J_{2d}M^{-1,nT} =_{n-1} J_{2d} \,, \tag{1.10}$$

which finally proves order n symplecticity of the order n inverse.

It is worthwhile to remark that the equivalence classes of origin preserving order n symplectic maps form a group, if "$=_n$" is introduced as an equivalence relation.

With these definitions and with the aforementioned conventions, we will set out to prove the main theorem about symplectic normal forms. This theorem deals with general order n symplectic maps from $\mathbb{R}^{2n}$ into $\mathbb{R}^{2n}$ and leads to a complex normal form map; therefore it is not very intuitive. For the special case of maps $\vec{M}$ with linear eigenvalues of modulus one, theorem (1.5.4) on real normal forms will be shown later, which has a graphic interpretation. In this case the real normal form map produces rotations in d two dimensional subspaces up to order n. The amplitudes of these rotations will be seen to be invariants of $\vec{M}$ up to order $n+1$. However, such invariants can also be found for the general case. The general theorem will be formulated first and specific cases will be considered later.

Theorem 1.1.8 (Symplectic Normal Forms)

A non-degenerate map $\vec{M} \in \mathcal{SP}_n^{2d}(\mathbb{R})$ with linear eigenvalues which are not in resonance to any order $m \le n$ can be transformed by means of a map $\vec{A}$ and an order

n inverse $\vec{A}^{-1,n} \in \mathcal{SP}_n^{2d}(\mathbb{C})$ *to* $\vec{N} =_n \vec{A} \circ \vec{M} \circ \vec{A}^{-1,n} \in \mathcal{SP}_n^{2d}(\mathbb{C})$ *such that there are* $2d$ *polynomials* f_l, $l \in \{1, \ldots, 2d\}$, *of order* $[(n-1)/2]$ *which satisfy the conditions*

$$f_{2i-1} f_{2i} =_{[(n-1)/2]} 1 \quad \text{and} \quad f_{2i} \partial_i f_{2j} =_{[(n-3)/2]} f_{2j} \partial_j f_{2i} \; \forall i, j \in \{1, \ldots, d\} \tag{1.11}$$

and describe the $2d$ *components of* $\vec{N}$ *by*

$$N_l =_n z_l (f_l \circ \vec{a}) \quad \text{with} \quad a_i = z_{2i-1} z_{2i} \; \forall i \in \{1, \ldots, d\} \; . \tag{1.12}$$

Maps $\vec{N}$ and $\vec{A}$ with the given properties are called a normal form map of $\vec{M}$ and a normal form transformation for $\vec{M}$ respectively. In special cases, further restrictions are imposed on f_l, which will be the subject of another theorem. We will prove that in first order such a transformation exists and then proceed by induction to higher orders. This proof is chosen because it illustrates a method with which a normal form map and a normal form transformation can be computed.

1.2 First Order Transformations

The map $\vec{M}$, which has no constant part $\vec{M}(\vec{0})$, will now be transformed to have a diagonal linear part. Let $M(\vec{0})$ denote the Jacobi matrix at the origin. This matrix can be diagonalized, since it is non-degenerate by the assumption of the theorem. The linear transformation that diagonalizes $M(\vec{0})$ will be denoted by $\vec{A}_1$. In order to illustrate that $\vec{A}_1$ can always be chosen symplectic, we will review some properties of symplectic matrices. A discussion of such properties is, for example, given in [MH91].

Theorem 1.2.1 *The eigenvectors* $\vec{v}_l$ *and* $\vec{v}_k$ *corresponding to eigenvalues* λ_l *and* λ_k *of a symplectic matrix with* $\lambda_l \lambda_k \neq 1$ *are* J_{2d} *orthogonal, i.e.* $\vec{v}_l^T J_{2d} \vec{v}_k = 0$.

Proof:

$$(\lambda_l \lambda_k - 1) \vec{v}_l^T J_{2d} \vec{v}_k = \vec{v}_l^T (N^T J_{2d} N - J_{2d}) \vec{v}_k = 0 \tag{1.13}$$

Theorem 1.2.2 *If a non-degenerate symplectic matrix* B *has only eigenvalues of multiplicity one, then there is a symplectic transformation* C, *possibly complex, to* $\mathrm{diag}(\lambda_1, \ldots, \lambda_{2d})$ *which satisfies* $\lambda_{2i-1} \lambda_{2i} = 1$.

Proof: Since the matrix B is non-degenerate, the eigenvectors $\vec{v}_l$ are linearly independent. Because $\det(J_{2d}) \neq 0$, the vectors $J_{2d} \vec{v}_l$ are also linearly independent. Therefore, with theorem (1.2.1), $\vec{v}_l^T J_{2d} \vec{v}_k \neq 0$ when $\lambda_l \lambda_k = 1$. Let us order the eigenvalues to have $\lambda_{2i-1} \lambda_{2i} = 1$ and scale the eigenvectors to get $\vec{v}_{2i-1}^T J_{2d} \vec{v}_{2i} = 1$; then the matrix C^{-1} with column vectors $\vec{v}_l$ is symplectic. According to the proof of theorem (1.1.4) its inverse C is also symplectic. Furthermore $CBC^{-1} = \mathrm{diag}(\lambda_1, \ldots, \lambda_{2d})$ with $\lambda_{2i-1} \lambda_{2i} = 1$.

Let us choose $\vec{A}_1^{-1} = \sum_{i=1}^{2d} \vec{v}_i z_i$ with the eigenvectors $\vec{v}_l$ of $\vec{M}(\vec{0})$ according to theorem (1.2.2). After the transformation $\vec{A}_1$, the Jacobi matrix of the n^{th} order Taylor map $\vec{N}_1$ with $\vec{N}_1 =_n \vec{A}_1 \circ \vec{M} \circ \vec{A}_1^{-1}$ has the property

$$N_{1,lk}(\vec{0}) = \lambda_l \delta_{lk} \; \forall lk \in \{1, \ldots, 2d\} \quad \text{and} \quad \lambda_{2i-1} \cdot \lambda_{2i} = 1 \; . \tag{1.14}$$

With this choice, $\vec{A}_1, \vec{A}_1^{-1}, \vec{N}_1 \in \mathcal{SP}_n^{2d}(\mathbb{C})$; $\vec{N}$ has the structure of the theorem about symplectic normal forms to first order, i.e. $\vec{N}_l =_1 z_l (f_l \circ \vec{a})$ with $f_l = \lambda_l$.

1.3 Nonlinear Transformations

We will break down the rest of the proof, which addresses the nonlinear structure, in three parts.

1. Prove that there are transformations $\vec{A}$ and $\vec{A}^{-1,n}$ which transform $\vec{M}$ to normal form structure $N_l = z_l (f_l \circ \vec{a})$ for some polynomial f_l. This part was already proven in the literature [Ber93b]. For completeness and since it does not take much space, it will be proven here as well.

2. Show that requiring order n symplecticity for $\vec{N}$ is equivalent to the conditions for f_l which are imposed by the theorem on symplectic normal forms.

3. Prove that $\vec{A}$ and $\vec{A}^{-1,n}$ can be chosen order n symplectic.

After having performed the first order transformation, we proceed by applying maps $\vec{A}_2, \ldots, \vec{A}_n$ which successively transform $\vec{M}$ from second order up to order n,

$$\vec{N}_{m-1} =_n \vec{A}_{m-1} \circ \ldots \circ \vec{A}_1 \circ \vec{M} \circ \vec{A}_1^{-1} \circ \ldots \circ \vec{A}_{m-1}^{-1,n} . \tag{1.15}$$

Every map $\vec{A}_i$ is chosen so as not to have an influence on any order below i. Since we are only interested in partial derivatives up to order n, we choose all maps $\vec{N}_m$, $\vec{A}_m$, and $\vec{A}_m^{-1,n}$ to be polynomial maps of order n. We assume that the components of $\vec{N}_{m-1}$ already have the structure $N_{m-1,l} =_{m-1} z_l(f_l \circ \vec{a})$ to order $m-1$. The map $\vec{N}_{m-1}$ is then said to be in normal form up to order $m-1$. We now look for a transformation $\vec{A}_m$ which only affects the orders greater or equal to m and transforms the map into normal form to order m.

The linear part of the map $\vec{N}_1$, which also is the linear part of the maps N_i with $i \in \{1, \ldots, m-1\}$, is denoted by $\vec{L}$. According to section (1.2), the Jacobian L is a diagonal matrix.

$$\begin{aligned} \vec{N}_m &=_n \vec{A}_m \circ \vec{N}_{m-1} \circ \vec{A}_m^{-1,n} \\ &=_m (\vec{z} + \vec{T}_m) \circ \vec{N}_{m-1} \circ (\vec{z} + \vec{T}_m)^{-1,m} \\ &=_m (\vec{z} + \vec{T}_m) \circ \vec{N}_{m-1} \circ (\vec{z} - \vec{T}_m) \\ &=_m \vec{N}_{m-1} + \vec{T}_m \circ \vec{L} - \vec{L} \circ \vec{T}_m . \end{aligned} \tag{1.16}$$

$\vec{T}_m$ is a polynomial map which only has m^{th} order contributions. This map $\vec{T}_m$ has to be chosen suitably in order to eliminate as many Taylor terms of $\vec{N}_{m-1}$ as possible. To find the proper choice for $\vec{T}_m$, we write it as a Taylor expansion. For simplification

of notation, we use the norm $||\vec{k}|| = \sum_{l=1}^{2d} |k_l|$ and denote the l^{th} component of $\vec{T}_m$ by

$$T_{m,l} = \sum_{\vec{k}}^{||\vec{k}||=m} (T_{m,l}|\vec{k}) z_1^{k_1} \cdot \ldots \cdot z_{2d}^{k_{2d}} . \tag{1.17}$$

With this notation, it then follows that the l^{th} component of the commutator of $\vec{L}$ and $\vec{T}_m$ has the Taylor expansion

$$\begin{aligned} & L_l \circ \vec{T}_m - T_{m,l} \circ \vec{L} \\ = & \sum_{\vec{k}}^{||\vec{k}||=m} (T_{m,l}|\vec{k}) \{\lambda_1 z_1^{k_1} \cdot \ldots \cdot z_{2d}^{k_{2d}} - (\lambda_1 z_1)^{k_1} \cdot \ldots \cdot (\lambda_{2d} z_{2d})^{k_{2d}}\} \\ = & \sum_{\vec{k}}^{||\vec{k}||=m} (T_{m,l}|\vec{k}) (\lambda_l - \lambda_1^{k_1} \cdot \ldots \cdot \lambda_{2d}^{k_{2d}}) \cdot z_1^{k_1} \cdot \ldots \cdot z_{2d}^{k_{2d}} . \end{aligned} \tag{1.18}$$

For simplicity we will employ the notation $\vec{\lambda}^{\vec{k}} = \prod_{l=1}^{2d} \lambda_l^{k_l}$. Most Taylor coefficients in $\vec{N}_{m-1}$ are cancelled when

$$(T_{m,l}|\vec{k}) \cdot (\lambda_l - \vec{\lambda}^{\vec{k}}) = (N_{m-1,l}|\vec{k}) . \tag{1.19}$$

$D_l(\vec{k}) = (\lambda_l - \vec{\lambda}^{\vec{k}})$ is called the resonance denominator. The terms that can be eliminated and the proper choice of $\vec{T}_m$ depends on this denominator. We will show that with the choice

$$(T_{m,l}|\vec{k}) = \begin{cases} (N_{m-1,l}|\vec{k})/D_l(\vec{k}) & \text{if } D_l(\vec{k}) \neq 0 \\ 0 & \text{if } D_l(\vec{k}) = 0 \end{cases} \tag{1.20}$$

for all orders up to n, $\vec{N}$ has normal form structure. Later we will prove that this definition of $\vec{T}_m$ allows $\vec{A}_m$ and $\vec{A}_m^{-1,n}$ to be chosen $\in \mathcal{SP}_n^{2d}$. It is worthwhile to note that the choice of 0 in the case of $D_l(\vec{k}) = 0$ is arbitrary. Other choices do not influence the m^{th} order due to cancellation in the commutator. However, these terms do influence the order $m+2$ and can further be chosen to cancel higher orders of the map. Since this process, called minimal normal form [MW92, MW93], does not conserve the order n symplecticity of $\vec{A}$, it will not be analyzed here.

All terms in $\vec{N}_{m-1}$ for which the resonance denominator does not vanish can be eliminated. Two cases can be distinguished in which the denominator vanishes.

1. $D_{2i-1}(\vec{k}) = 0$ if $k_{2j-1} - k_{2j} = \delta_{ij}$ and $D_{2i}(\vec{k}) = 0$ if $k_{2j-1} - k_{2j} = -\delta_{ij}$, because $\lambda_{2i-1}\lambda_{2i} = 1$. The corresponding Taylor coefficient cannot be eliminated, except by deliberately choosing maps $\vec{M}$ with coefficients $(N_{m-1,l}|\vec{k})$ that vanish for these $\vec{k}$.

2. Even if the first case does not apply, $D_l(\vec{k})$ can vanish. For this to happen, $\prod_{i=1}^{d} \lambda_{2i-1}^{k_i}$ *must have nontrivial solutions for integers* k_i *with* $\sum_{i=1}^{d} |k_i| \leq m+1$. Such a case is called resonant and is excluded by the conditions in the symplectic normal form theorem.

All coefficients in the polynomial $N_{m-1,2i-1}$, except those with $k_{2i-1} - k_{2i} = \delta_{ij}$, will be eliminated by the transformation $\tilde{A}_m$. With an equivalent consideration for $N_{m-1,2i}$, this means

$$N_{m,2i-1} =_m \sum_{\vec{k}}^{\|k\|\leq m} (N_{m,2i-1}|\vec{k}) z_{2i-1} (z_1 z_2)^{k_1} \dots (z_{2d-1} z_{2d})^{k_{2d-1}} , \qquad (1.21)$$

$$N_{m,2i} =_m \sum_{\vec{k}}^{\|k\|\leq m} (N_{m,2i} \quad |\vec{k}) z_{2i} \quad (z_1 z_2)^{k_1} \dots (z_{2d-1} z_{2d})^{k_{2d-1}} . \qquad (1.22)$$

To order m, the map $\vec{N}_m$ has normal form structure $N_{m,l} =_m z_l (f_l \circ \vec{a})$, which is the structure we strive to obtain to order n. Performing these steps up to order n will lead to a map $\vec{N} = \vec{N}_n$ with normal form structure up to the evaluation order n.

Now we come to the second task of establishing the conditions on the functions f_l.

Theorem 1.3.1 *Let the* $2d$ *components of* $\vec{N}$ *have the form*

$$N_l =_n z_l (f_l \circ \vec{a}) \text{ with } a_i = z_{2i-1} z_{2i} \; \forall i \in \{1, \dots, d\} . \qquad (1.23)$$

Then the conditions

$$f_{2i-1} f_{2i} =_{[(n-1)/2]} 1 \text{ and } f_{2i} \partial_i f_{2j} =_{[(n-3)/2]} f_{2j} \partial_j f_{2i} \; \forall i, j \in \{1, \dots, d\} \qquad (1.24)$$

are necessary and sufficient for $\vec{N}$ *to be order* n *symplectic.*

Proof: We use the functions $g_l = f_l \circ \vec{a}$ and write the Jacobian N of $\vec{N}$ as

$$N = \begin{pmatrix} N_{11} & \dots & N_{1n} \\ \vdots & & \vdots \\ N_{n1} & \dots & N_{nn} \end{pmatrix} \qquad (1.25)$$

with the 2×2 matrices

$$N_{il} = \begin{pmatrix} \partial_{2l-1}(z_{2i-1} g_{2i-1}) & \partial_{2l}(z_{2i-1} g_{2i-1}) \\ \partial_{2l-1}(z_{2i} \quad g_{2i} \quad) & \partial_{2l}(z_{2i} \quad g_{2i} \quad) \end{pmatrix} . \qquad (1.26)$$

With this notation, we can write the symplectic condition as

$$N J_{2d} N^T =_{n-1} J_{2d} \iff \qquad (1.27)$$

$$\sum_{l=1}^{d} N_{il} J_2 N_{jl}^T =_{n-1} J_2 \delta_{ij} \; \forall i, j \in \{1, \dots, n\} . \qquad (1.28)$$

For every combination i, j, this 2×2 matrix equation yields component wise four equations. Altogether there are $4n^2$ equations. We will denote the relation in the α^{th} row and the β^{th} column by $< \alpha, \beta >$.

Case $< 1, 1 >$:

$$\begin{aligned}
& \textstyle\sum_{l=1}^{d} \quad \partial_{2l-1}(z_{2i-1} g_{2i-1}) \partial_{2l}(z_{2j-1} g_{2j-1}) \\
& - \quad \partial_{2l}(z_{2i-1} g_{2i-1}) \partial_{2l-1}(z_{2j-1} g_{2j-1}) \\
& = \textstyle\sum_{l=1}^{d} \quad z_{2i-1} z_{2j-1} (\partial_{2l-1} g_{2i-1} \partial_{2l} g_{2j-1} - \partial_{2l} g_{2i-1} \partial_{2l-1} g_{2j-1}) \\
& + \quad z_{2j-1} g_{2i-1} \partial_{2i} g_{2j-1} - z_{2i-1} g_{2j-1} \partial_{2j} g_{2i-1} \\
& = \textstyle\sum_{l=1}^{d} \quad z_{2i-1} z_{2j-1} z_{2l-1} z_{2l} \{ (\partial_l f_{2i-1} \partial_l f_{2j-1} - \partial_l f_{2i-1} \partial_l f_{2j-1}) \circ \vec{a} \} \\
& + \quad z_{2i-1} z_{2j-1} \{ (f_{2i-1} \partial_i f_{2j-1} - f_{2j-1} \partial_j f_{2i-1}) \circ \vec{a} \} =_{n-1} 0 \\
& \iff \quad f_{2i-1} \partial_i f_{2j-1} =_{[(n-3)/2]} f_{2j-1} \partial_j f_{2i-1}
\end{aligned} \qquad (1.29)$$

Case $< 1,2 >$:

$$\begin{aligned}
&\textstyle\sum_{l=1}^{d} && \partial_{2i-1}(z_{2i-1}g_{2i-1})\partial_{2l}(z_{2i}g_{2i}) \\
&- && \partial_{2l}(z_{2i-1}g_{2i-1})\partial_{2l-1}(z_{2j}g_{2j}) \\
&= \textstyle\sum_{l=1}^{d} && z_{2i-1}z_{2j}(\partial_{2l-1}g_{2i-1}\partial_{2l}g_{2j} - \partial_{2l}g_{2i-1}\partial_{2l-1}g_{2j}) \\
&+ && z_{2j}g_{2i-1}\partial_{2i}g_{2j} + z_{2i-1}g_{2j}\partial_{2j-1}g_{2i-1} + g_{2i-1}g_{2j}\delta_{ij} \\
&= \textstyle\sum_{l=1}^{d} && z_{2i-1}z_{2j}z_{2l-1}z_{2l}\{(\partial_l f_{2i-1}\partial_i f_{2j} - \partial_l f_{2i-1}\partial_l f_{2j}) \circ \vec{a}\} \\
&+ && z_{2i-1}z_{2j}\{(f_{2i-1}\partial_i f_{2j} + f_{2j}\partial_j f_{2i-1}) \circ \vec{a}\} + g_{2i-1}g_{2j}\delta_{ij} =_{n-1} \delta_{ij}
\end{aligned}$$

$$\iff \quad \partial_i(z_i f_{2i-1} f_{2i}) =_{[(n-1)/2]} 1 \text{ and} \tag{1.30}$$

$$f_{2i-1}\partial_i f_{2j} + f_{2j}\partial_j f_{2i-1} =_{[(n-3)/2]} 0 \text{ for } i \neq j \tag{1.31}$$

$$\iff \quad f_{2i-1}f_{2i} =_{[(n-1)/2]} 1\ , \quad f_{2i-1}\partial_i f_{2j} + f_{2j}\partial_j f_{2i-1} =_{[(n-3)/2]} 0 \tag{1.32}$$

Equation (1.31) can be derived from $f_{2i-1}f_{2i} =_{[(n-1)/2]} 1$ and $< 1,1 >$,

$$\begin{aligned}
f_{2i-1}\partial_i f_{2j} &=_{[(n-1)/2]} f_{2i-1}f_{2j}(f_{2j-1}\partial_i f_{2j}) \\
&=_{[(n-3)/2]} f_{2i-1}f_{2j}(-f_{2j}\partial_i f_{2j-1}) \\
&=_{[(n-3)/2]} -f_{2j}^2(f_{2i-1}\partial_i f_{2j-1}) \\
&=_{[(n-3)/2]} -f_{2j}^2(f_{2j-1}\partial_j f_{2i-1}) \\
&=_{[(n-3)/2]} -f_{2j}\partial_j f_{2i-1}\ .
\end{aligned} \tag{1.33}$$

Case $< 2,1 >$:

This equation of the 2×2 matrix can be obtained from the $< 1,2 >$ case by exchanging i and j and multiplying by -1. Since $i,j \in \{1,\ldots,n\}$ are arbitrary, this leads to conditions equivalent to equation (1.32).

Case $< 2,2 >$:

The condition of the $< 2,2 >$ position can be obtained from the case $< 1,1 >$ by exchanging $2i-1$ by $2i$ and $2j-1$ by $2j$,

$$f_{2i}\partial_i f_{2j} =_{[(n-3)/2]} f_{2j}\partial_j f_{2i}\ . \tag{1.34}$$

The condition of $< 1,1 >$ can be obtained by $f_{2i-1}f_{2i} =_{[(n-1)/2]} 1$ and this line,

$$\begin{aligned}
f_{2i-1}\partial_i f_{2j-1} &=_{[(n-1)/2]} f_{2i-1}^2 f_{2i}f_{2j-1}(f_{2j}\partial_i f_{2j-1}) \\
&=_{[(n-3)/2]} f_{2i-1}^2 f_{2i}f_{2j-1}(-f_{2j-1}\partial_i f_{2j}) \\
&=_{[(n-3)/2]} -f_{2i-1}^2 f_{2j-1}^2 f_{2i}\partial_i f_{2j} \\
&=_{[(n-3)/2]} -f_{2i-1}^2 f_{2j-1}^2 f_{2j}\partial_j f_{2i} \\
&=_{[(n-3)/2]} f_{2i-1}f_{2j-1}(-f_{2i-1}\partial_j f_{2i}) \\
&=_{[(n-3)/2]} f_{2j-1}\partial_j f_{2i-1}\ .
\end{aligned} \tag{1.35}$$

This proves that the conditions (1.34) and $f_{2i-1}f_{2i} =_{[(n-1)/2]} 1$ are necessary and sufficient for the order n symplecticity of $\vec{N}$.

Finally to the third task of establishing the order n symplecticity of the normal form transformation. To show that the map $\vec{N}$ is order n symplectic and therefore, with theorem (1.3.1), satisfies all the claims of the theorem of symplectic normal forms, we are left with showing that the transformations $\vec{A}_m$ can be chosen order n symplectic with the choice of $\vec{T}_m$ presented in equation (1.20).

Definition 1.3.2 *A map $\vec{T}$ for which the Jacobian of $J_{2d}\vec{T}$ is symmetric is called Hamiltonian. Let a map $\vec{F}$ be $\mathcal{C}^{2d} \times \mathbb{R}_0^+ \to \mathcal{C}^{2d}$ and let $\vec{F}_{t^*} : \mathcal{C}^{2d} \to \mathcal{C}^{2d}$ with $\vec{F}_{t^*}(\vec{x}) = \vec{F}(\vec{x},t^*)$ $\forall \vec{x} \in \mathcal{C}^{2d}$ be Hamiltonian for all $t^* \in \mathbb{R}_0^+$. Then a differential equation for $\vec{y} : \mathbb{R}_0^+ \to \mathcal{C}^{2d}$ of the form*

$$\partial\vec{y} = \vec{F} \circ (\vec{y},t) \tag{1.36}$$

with the identity $t : \mathbb{R}_0^+ \to \mathbb{R}_0^+$ is called Hamiltonian. If the general solution of a Hamiltonian differential equation $\vec{M} : \mathcal{C}^{2d} \times \mathbb{R}_0^+ \to \mathcal{C}^{2d}$ with $\partial_{2d+1}\vec{M} = \vec{F} \circ (\vec{M},t)$ and $\vec{M}(\vec{x},0) = \vec{x}$ $\forall \vec{x} \in \mathcal{C}^{2d}$ exists, it is called a Hamiltonian flow.

Questions of existence and uniqueness are, for instance, expressed by the theorem of Picard Lindelöf and will not be stressed here.

Theorem 1.3.3 *If $\vec{M} : \mathbb{C}^{2d} \times \mathbb{R}_0^+ \to \mathbb{C}^{2d}$ is a Hamiltonian flow, then the map $\vec{M}_{t^*} : \mathbb{C}^{2d} \to \mathbb{C}^{2d}$, which is defined by $\vec{M}_{t^*}(\vec{x}) = \vec{M}(\vec{x}, t^*)\ \forall \vec{x} \in \mathbb{C}^{2d}$, is symplectic for all $t^* \in \mathbb{R}_0^+$.*

Proof: We introduce the $2d \times 2d$ matrix $M : \mathbb{C}^{2d} \times \mathbb{R}_0^+ \to \mathbb{C}^{4d^2}$ with $M_{ij} = \partial_j M_i$. For a given $t^* \in \mathbb{R}_0^+$, $M_{t^*} : \mathbb{C}^{2d} \to \mathbb{C}^{4d^2}$ defined by $M_{t^*}(\vec{x}) = M(\vec{x}, t^*)\ \forall \vec{x} \in \mathbb{C}^{2d}$ is the Jacobian of $\vec{M}_{t^*}$. Similarly we introduce the $2d \times 2d$ matrix F with $F_{ij} = \partial_j F_i$. Then,

$$\begin{aligned} \partial_{2d+1} M_{ij} &= \partial_j \partial_{2d+1} M_i = \partial_j F_i \circ (\vec{M}, t) = \sum_{l=1}^{2d} \partial_j M_l \{(\partial_l F_i) \circ (\vec{M}, t)\} , \\ \partial_{2d+1} M &= \{F \circ (\vec{M}, t)\} M . \end{aligned} \tag{1.37}$$

We define another matrix $P = M J_{2d} M^T$; then

$$\begin{aligned} \partial_{2d+1} P &= \{F \circ (\vec{M}, t)\} M J_{2d} M^T + M J_{2d} M^T \{F^T \circ (\vec{M}, t)\} && (1.38) \\ &= GP + PG^T \text{ with } G = F \circ (\vec{M}, t) . && (1.39) \end{aligned}$$

Inserting any $\vec{x} \in \mathbb{C}^{2d}$ into the first $2d$ components yields a linear ordinary differential equation for the elements of $W : \mathbb{R}^+ \to \mathbb{C}^{4d^2}$ with $W(t^*) = P(\vec{x}, t^*)\ \forall t^* \in \mathbb{R}^+$. $W(0) = J_{2d}$, because $\vec{M}_0 = \vec{z}$. Such an ODE has an unique solution. Since $\vec{F}_{t^*}$ is Hamiltonian for all $t^* \in \mathbb{R}_0^+$, $J_{2d} G$ is symmetric and therefore all components of $GJ_{2d} + J_{2d} G^T$ vanish. This establishes that $W = J_{2d}$ is the unique solution for all $\vec{x} \in \mathbb{C}^{2d}$ and therefore $P = J_{2d}$. This finally implies the symplecticity of $\vec{M}_{t^*}$,

$$M_{t^*}^T J_{2d} M_{t^*} = J_{2d}\ \forall t^* \in \mathbb{R}_0^+ . \tag{1.40}$$

Theorem 1.3.4 *For a C^∞ function $p : \mathbb{C}^{2d} \to \mathbb{C}$ and with the Poisson-bracket operator $: p :$ acting on a differentiable function h via $: p : h = \vec{\partial}^T p J_{2d} \vec{\partial} h$, $\exp(: p :)\vec{z}$ is a symplectic map.*

Proof: If $y : \mathbb{R}_0^+ \to \mathbb{C}^{2d}$ satisfies the autonomous Hamiltonian differential equation

$$\partial \vec{y} = -(J_{2d} \vec{\partial} p) \circ \vec{y} = (: p : \vec{z}) \circ \vec{y} , \quad \vec{y}(0) = \vec{y}_0 \tag{1.41}$$

then for any differentiable function $q : \mathbb{C}^{2d} \to \mathbb{C}$, we have

$$\partial (q \circ \vec{y}) = \partial \vec{y}^T \{(\vec{\partial} q) \circ \vec{y}\} = (\vec{\partial}^T p J_{2d} \vec{\partial} q) \circ \vec{y} = (: p : q) \circ \vec{y} . \tag{1.42}$$

An example for such a function $q \circ \vec{y}$ would be the right hand side of equation (1.41). The differential equation (1.41) can be solved by power expansion with respect to $t^* \in \mathbb{R}_0^+$,

$$\begin{aligned} \vec{y}(t^*) &= \vec{y}(0) + t^* (: p : \vec{z})|_{\vec{y}_0} + \frac{t^{*2}}{2} \{: p : (: p : \vec{z})\}|_{\vec{y}_0} + \ldots && (1.43) \\ &= \{\exp(t^* : p :)\vec{z}\}|_{\vec{y}_0} , && (1.44) \end{aligned}$$

in the range of convergence of this sum. $y : \mathbb{R}^+ \to \mathbb{C}^{2d}$ defined by the sum can be inserted into the differential equation (1.42) to show that it is a solution.

This gives $\vec{y}(t^*)$ for all initial conditions $\vec{y}_0$ and for all t^*. Therefore, $\exp(t : p :)\vec{z}$ is a Hamiltonian flow and, with theorem (1.3.3), $\exp(: p :)\vec{z}$ is symplectic.

The following theorem will only be needed later, but it is suitable to prove it here, since the necessary tools have just been assembled.

Theorem 1.3.5 *Let two functions $p, g : \mathbb{C}^{2d} \to \mathbb{C}$ be such that the Hamiltonian ODE $\partial \vec{y} = (: p : \vec{z}) \circ \vec{y}$ has a solution for all starting conditions $\vec{y}(0) = \vec{y}_0$ and such that the Taylor expansion of $g \circ \vec{y} : \mathbb{R}^+ \to \mathbb{C}$ around 0 converges at 1 to $(g \circ \vec{y})|_1$. Then*

$$\exp(: p :) g = g \circ (\exp(: p :)\vec{z}) . \tag{1.45}$$

Proof: The exponential operator is defined by its power series,

$$\{\exp(t^* : p :) g\}|_{\vec{y}_0} = g(\vec{y}_0) + t^* (: p : g)|_{\vec{y}_0} + \frac{t^{*2}}{2} \{: p : (: p : g)\}|_{\vec{y}_0} + \ldots . \tag{1.46}$$

With equation (1.42), we can reformulate the right hand side to

$$g(\vec{y}_0) + t^* \{\partial(g \circ \vec{y})\}|_0 + \frac{t^{*2}}{2} \{\partial^2(g \circ \vec{y})\}|_0 + \dots \tag{1.47}$$

$$= (g \circ \vec{M})|_{(\vec{y}_0, t^*)} = g \circ \{\exp(t^* : p :)\vec{z}\}|_{\vec{y}_0} \tag{1.48}$$

for $t^* = 1$. Since this holds for all $\vec{y}_0$, it proves the theorem.

Theorem 1.3.6 *If $\vec{T}$ is a homogeneous Taylor map of order m and $\vec{z} + \vec{T}$ is order m symplectic, then there is an exponential Poisson-bracket operator with*

$$\exp(: t_m :)\vec{z} =_m \vec{z} + \vec{T} . \tag{1.49}$$

Proof: With equation (1.4), we can write the symplectic condition as

$$(Z + T)^T J_{2d}(Z + T) =_{m-1} J_{2d} \Longleftrightarrow T^T J_{2d} = -J_{2d} T \tag{1.50}$$

This is equivalent to the statement that $J_{2d}T$ is symmetric or that the Jacobian of $J_{2d}\vec{T}$ is symmetric. Therefore, the potential problem $\vec{\partial} t_m = J_{2d}\vec{T}$ has a solution t_m which is a homogeneous polynomial of order $m + 1$ and

$$\exp(: t_m :)\vec{z} =_m \vec{z} - J_{2d}\vec{\partial} t_m =_m \vec{z} + \vec{T} . \tag{1.51}$$

In order to guarantee that $\vec{A}_m$ is in $\mathcal{SP}_n^{2d}(\mathbb{C})$, we only have to show that $\vec{z} + \vec{T}_m$ is order m symplectic and choose $\vec{A}_m =_n \exp(: t_m :)\vec{z}$. $\vec{A}_m^{-1,n} =_n \exp(- : t_m :)$ will be an order n inverse of $\vec{A}_m$.

We assume that all the $\vec{A}_i, \vec{A}_i^{-1,n} \in \mathcal{SP}_n^{2d}(\mathbb{C})$ for $i \in \{1, \dots, m-1\}$ and, with theorem (1.1.2), $\vec{N}_{m-1} \in \mathcal{SP}_n^{2d}(\mathbb{C})$. Before we use the symplectic condition to check the symplecticity of $\vec{z} + \vec{T}_m$, we analyze restrictions on the m^{th} order of $\vec{N}_{m-1}$, which is closely related to $\vec{T}_m$ by the equation (1.20). We separate the map $\vec{N}_{m-1}$ into two parts. The first part $\vec{F}$ contains all contributions which already have normal form

structure; therefore, it contains all $m-1$ orders and the normal form part of order m, $F_l = z_l(f_l \circ \vec{a})$. Since it is order $m-1$ symplectic, the functions f_l satisfy the condition (1.24) according to theorem (1.3.1) for $n = m-1$. The second contribution $\vec{R}$ contains the rest of order m,

$$\vec{N}_{m-1} =_m \vec{F} + \vec{R} . \tag{1.52}$$

We write the Jacobi matrices of $\vec{F}$ and $\vec{R}$ as F and R respectively and employ the 2×2 matrices notation which was used in equation (1.27). The linear part of the map $\vec{N}_{m-1}$ has the diagonal Jacobian L with

$$L_{ij} = \delta_{ij} \begin{pmatrix} \lambda_{2i-1} & 0 \\ 0 & \lambda_{2i} \end{pmatrix} , \tag{1.53}$$

and we write

$$R_{ij} = \begin{pmatrix} \partial_{2j-1} R_{2i-1} & \partial_{2j} R_{2i-1} \\ \partial_{2j-1} R_{2i} & \partial_{2j} R_{2i} \end{pmatrix} \text{ and } F_{ij} = \begin{pmatrix} \partial_{2j-1} F_{2i-1} & \partial_{2j} F_{2i-1} \\ \partial_{2j-1} F_{2i} & \partial_{2j} F_{2i} \end{pmatrix} . \tag{1.54}$$

The symplectic condition will again be analyzed for the four equations in the 2×2 matrix separately,

$$\sum_{l=1}^{n} (F_{il} + R_{il}) J_2 (F_{jl}^T + R_{jl}^T) =_{m-1} J_2 \delta_{ij} \ \forall i, j \in \{1, \dots, n\} \tag{1.55}$$

$$\Longleftrightarrow \sum_{l=1}^{n} F_{il} J_2 F_{jl}^T + L_{ii} J_2 R_{ji}^T + R_{ij} J_2 L_{ii} =_{m-1} J_2 . \tag{1.56}$$

Parts of the required manipulations are equivalent to steps in the proof of theorem (1.3.1); we will therefore skip some lines and refer to the equations (1.29) and (1.32).

Case $< 1.1 >$:

$$z_{2i-1} z_{2j-1} \{(f_{2i-1} \partial_i f_{2j-1} - f_{2j-1} \partial_j f_{2i-1}) \circ \vec{a}\}$$

$$+ \lambda_{2i-1} \partial_{2i} R_{2j-1} - \lambda_{2j-1} \partial_{2j} R_{2i-1} =_{m-1} 0 \tag{1.57}$$

$$\Longleftrightarrow f_{2i-1} \partial_i f_{2j-1} - f_{2j-1} \partial_j f_{2i-1} =_{[(m-3)/2]} 0 \tag{1.58}$$

$$\text{and } \lambda_{2i-1} \partial_{2i} R_{2j-1} - \lambda_{2j-1} \partial_{2j} R_{2i-1} =_{m-1} 0 \tag{1.59}$$

This separation can be performed, because the polynomial on the left hand side of equation (1.59) has no terms of the structure $z_{2i-1}z_{2j-1}(h \circ \vec{a})$ for any monomial h of order $[(m-1)/2]$. Such terms cannot occur, since $\vec{R}$ does not contain terms of normal form structure. However, the rest of equation (1.57) has only terms of this structure.

Case $< 1,2 >$:

$$z_{2i-1}z_{2j}\{(f_{2i-1}\partial_i f_{2j} + f_{2j}\partial_j f_{2i-1}) \circ \vec{a}\}$$

$$+\delta_{ij}(f_{2i-1}f_{2i}) \circ \vec{a} + \lambda_{2i-1}\partial_{2i}R_{2j} + \lambda_{2j}\partial_{2j-1}R_{2i-1} \quad =_{m-1} \quad \delta_{ij} \qquad (1.60)$$

$$\iff f_{2i-1}f_{2i} =_{[(m-1)/2]} 1\ , \quad f_{2i-1}\partial_i f_{2j} + f_{2j}\partial_j f_{2i-1} \quad =_{[(m-3)/2]} \quad 0 \qquad (1.61)$$

$$\text{and } \lambda_{2i-1}\partial_{2i}R_{2j} + \lambda_{2j}\partial_{2j-1}R_{2i-1} \quad =_{m-1} \quad 0\ . \qquad (1.62)$$

This separation can be performed with reasoning corresponding to that of the $< 1,1 >$ case. The polynomial of the left hand side in equation (1.62) has no terms of the structure $z_{2i-1}z_{2j}(h \circ \vec{a})$ for any monomial h of order $[(m-1)/2]$, the rest in equation (1.60), however, only have terms of this structure.

Case $< 2,1 >$:

This equation of the 2×2 matrix can be obtained from the $< 1,2 >$ position by exchanging i by j and vice versa and multiplying by -1. Since $i,j \in \{1,\ldots,n\}$ are arbitrary, this leads to conditions identical to $< 1,2 >$.

Case $< 2,2 >$:

The condition of the $< 2,2 >$ position can be obtained from the position $< 1,1 >$ by exchanging $2i-1$ by $2i$ and $2j-1$ by $2j$ and vice versa.

The conditions (1.58) and (1.61) establish that the map $\vec{F}$, which simply consists of all terms in $\vec{N}_{m-1}$ with normal form structure, is symplectic up to order m. This is a nontrivial statement, since symplecticity of $\vec{F}$ was only assumed to order $m-1$. The equations concerning the rest of the map $\vec{R}$ are essential for establishing order m symplecticity for the map $\vec{z} + \vec{T}_m$. We use the symplectic condition, which we write

with the Jacobi matrix T of $\vec{T}_m$. T is a $2n \times 2n$ matrix and, as before, the T_{ij} are 2×2 matrices,

$$T \ = \ \begin{pmatrix} T_{11} & \ldots & T_{1n} \\ \vdots & & \vdots \\ T_{n1} & \ldots & T_{nn} \end{pmatrix} . \qquad (1.63)$$

We can write the symplectic condition as

$$TJ_{2d}T^T = J_{2d} \iff \sum_{l=1}^{n} T_{il}J_2T_{jl}^T = J_2\delta_{ij} \ \forall i,j \in \{1,\ldots,n\} . \qquad (1.64)$$

Since we just performed a similar computation for $\vec{N}_{m-1}$, we can obtain the symplectic conditions by setting $\vec{F} = \vec{z}$ and $\vec{R} = \vec{T}_m$ in the equations (1.56).

Case $< 1,1 >$: $\quad \partial_{2i} \quad T_{2j-1} - \partial_{2j} \quad T_{2i-1} =_{m-1} 0$

Case $< 1,2 >$: $\quad \partial_{2i} \quad T_{2j} \quad + \partial_{2j-1}T_{2i-1} =_{m-1} 0$

Case $< 2,1 >$: $\quad -\partial_{2i-1}T_{2j-1} - \partial_{2j} \quad T_{2i} \quad =_{m-1} 0$

Case $< 2,2 >$: $\quad \partial_{2i-1}T_{2j} \quad - \partial_{2j-1}T_{2i} \quad =_{m-1} 0$

Since the third and fourth condition follow from the first and second by changing indices as pointed out earlier, and since the same symmetries with respect to indices apply to the corresponding equations for $\vec{R}$, it is sufficient to show that the first two equations always hold by means of the above equations for $\vec{R}$. Comparing the Taylor coefficients in the equations for $\vec{T}$ yields

Case $< 1,1 >$:

$$p_l = k_l + \delta_{l,2i}\ , \quad q_l = k_l + \delta_{l,2j}\ , \qquad (1.65)$$

$$0 \ = \ (T_{2j-1}|\vec{p})p_{2i} - (T_{2i-1}|\vec{q})q_{2j} \iff \qquad (1.66)$$

$$0 \ = \ (R_{2j-1}|\vec{p})p_{2i}(\lambda_{2i-1} - \vec{\lambda}^{\vec{k}}\lambda_{2j}) - (R_{2i-1}|\vec{q})q_{2j}(\lambda_{2j-1} - \vec{\lambda}^{\vec{k}}\lambda_{2i}) \iff \qquad (1.67)$$

$$0 \ = \ (1 - \vec{\lambda}^{\vec{k}}\lambda_{2i}\lambda_{2j})\{\lambda_{2i-1}(R_{2j-1}|\vec{p})p_{2i} - \lambda_{2j-1}(R_{2i-1}|\vec{q})q_{2j}\} . \qquad (1.68)$$

The last line is guaranteed by equation (1.59).

Case $< 1,2 >$:

$$\bar{p}_l - \bar{\lambda}_l + \delta_{l,2i} \ , \quad q_l - \bar{\lambda}_l + \delta_{l,2j-1} \ , \tag{1.69}$$

$$0 = (T_{2j}|\vec{p})p_{2i} - (T_{2i-1}|\vec{q})q_{2j-1} \Longleftrightarrow \tag{1.70}$$

$$0 = (R_{2j}|\vec{p})p_{2i}(\lambda_{2i-1} - \vec{\lambda}^{\vec{k}}\lambda_{2j-1}) + (R_{2i-1}|\vec{q})q_{2j-1}(\lambda_{2j} - \vec{\lambda}^{\vec{k}}\lambda_{2i}) \Longleftrightarrow \tag{1.71}$$

$$0 = (1 - \vec{\lambda}^{\vec{k}}\lambda_{2i}\lambda_{2j-1})\{\lambda_{2i-1}(R_{2j-1}|\vec{p})p_{2i} - \lambda_{2j-1}(R_{2i-1}|\vec{q})q_{2j}\} \ . \tag{1.72}$$

The last line is guaranteed by equation (1.62).

This finally shows that $\vec{A}_m$ can be chosen order n symplectic. $\vec{A}_m$ is not unique, since one could add any polynomial of orders higher than $m+1$ to t_m; this would change the terms in $\vec{A}_m$ from order $m+1$ up to order n. This implies the possibility that $\vec{A}$ might not be unique. However, the question if there are normal form transformations other than the one which is constructed here and how these would be related to $\vec{A}$ will not be analyzed here.

Performing this procedure order by order to the truncation order n gives the normal form map $\vec{N} \in \mathcal{SP}_n^{2d}(\mathbb{C})$, the normal form transformation $\vec{A} = \vec{A}_n \circ \ldots \circ \vec{A}_1 \in \mathcal{SP}_n^{2d}(\mathbb{C})$, and its order n inverse $\vec{A}^{-1,n} \in \mathcal{SP}_n^{2d}(\mathbb{C})$ with

$$\vec{N} =_n \vec{A} \circ \vec{M} \circ \vec{A}^{-1,n} \ . \tag{1.73}$$

1.4 Invariants

Definition 1.4.1 (Order n Invariants)
A function I is called an order n invariant of a map $\vec{M}$ if $I \circ \vec{M} =_n I$.

We want to show that normal form transformations can be used to find d order $n+1$ invariants, which are not related to each other by functional dependences. To formulate this clearly, we introduce the concept of independent functions.

Definition 1.4.2 *d functions $I_j : \mathbb{C}^d \to \mathbb{C}$ are called independent if there is no function $f : \mathbb{C}^{d-1} \to \mathbb{C}$ with $I_l = f \circ (I_1, \ldots, I_{l-1}, I_{l+1}, \ldots, I_d)$ for any $l \in \{1, \ldots, d\}$.*

It can easily be observed that the d components of the identity function $\vec{z}$ are independent, since z_l can have different values for the same values of $\vec{z}_k, k \neq l$ when these functions are applied to appropriate $\vec{x} \in C^d$.

Theorem 1.4.3 *If a map $\vec{I} : \mathbb{C}^d \to \mathbb{C}^d$ is locally invertible in some volume, then the components of $\vec{I}$ are independent functions.*

Proof: Assume there is a function $f : \mathbb{C}^{d-1} \to \mathbb{C}$ which satisfies

$$I_l = f \circ (I_1, \ldots, I_{l-1}, I_{l+1}, \ldots, I_d) \ . \tag{1.74}$$

Applying the local inverse $\vec{I}^{-1}$ to the right and the left hand side yields

$$z_l = f \circ (z_1, \ldots, z_{l-1}, z_{l+1}, \ldots, z_d) \tag{1.75}$$

for the domain of the inverse, which, as just observed, cannot be true for any f.

Theorem 1.4.4 (Invariants of Order Symplectic Maps)
For a non-degenerate map $\vec{M} \in \mathcal{SP}_n^{2d}(\mathbb{R})$ with linear eigenvalues which are not in resonance to any order $m \leq n$, d independent order $n+1$ invariants of $\vec{M}$ can be found.

Proof: With theorem (1.1.8), a normal form transformation can be found to order n and the d polynomials of order $n+1$ given by $I_i =_{n+1} A_{2i-1}A_{2i}$ are order $n+1$ invariants, because

$$I_i \circ \vec{M} =_{n+1} (A_{2i-1} \circ \vec{M})(A_{2i} \circ \vec{M}) \tag{1.76}$$

$$=_{n+1} (N_{2i-1} \circ \vec{A})(N_{2i} \circ \vec{A}) \tag{1.77}$$

$$= A_{2i-1}A_{2i}(\{(f_{2i-1} \circ \vec{a})(f_{2i} \circ \vec{a})\} \circ \vec{A}) =_{n+1} I_i \ . \tag{1.78}$$

The agreement up to order $n+1$ in line (1.77) follows from the fact that $A_{2i-1} \circ \vec{M} =_n N_{2i-1} \circ \vec{A}$ and that $N_{2i} \circ \vec{A}$ has no constant part, $N_{2i} \circ \vec{A} =_0 0$. Similarly in line (1.78), $\{(f_{2i-1} \circ \vec{a})(f_{2i} \circ \vec{a})\} \circ \vec{A} =_{n-1} 1$ and $A_{2i-1}A_{2i} =_1 0$. Since the polynomials $I_i =_1 z_i$, the Jacobian of the map $\vec{I}$ at the origin has determinant one and this map is therefore invertible in a volume that contains the origin, due to the implicit function theorem. With theorem (1.4.3), one concludes the independence of the functions I_i.

1.5 Real Normal Forms

For the case that the linear eigenvalues of an order n symplectic map are either real or have modulus one, it is possible to find additional properties of the functions $\vec{A}$ and $\vec{N}$. Due to these properties, it will be possible to formulate a real normal form transformation to a real normal form map. This special case is of particular importance, since all maps with 2×2 block diagonal structure in the Jacobian at the origin fall into this category.

Conventions: We will order the linear eigenvalues to obtain $|\lambda_l| = 1$ for l in $\{1, \ldots, 2r\}$ and $\lambda_k \in \mathbb{R}$ for k in $\{2r+1, \ldots, 2d\}$. An important step towards real normal forms will be the next theorem. To express this theorem, we have to define a certain subset of $\mathbb{C}^{2d}$,

$$\mathcal{C} = \{\vec{y} | \vec{y} \in \mathbb{C}^{2d} \times \mathbb{R}^{2(d-r)},\ y_{2j-1} = i y_{2j}^* \forall j \in \{1, \ldots, 2r\}\} \ . \tag{1.79}$$

It is useful to define the set of maps which take $\mathcal{C}$ into $\mathcal{C}$,

$$\mathcal{S} = \{\vec{M} | \vec{M}(\vec{y}) \in \mathcal{C} \ \ \forall \vec{y} \in \mathcal{C}\} \ . \tag{1.80}$$

Theorem 1.5.1 *If each linear eigenvalue of $\vec{M}$ in the theorem for symplectic normal forms is either real or has unit modulus, then the normal form transformation $\vec{A}$ and*

the normal form map $\vec{N}$ have the property

$$\vec{A} : \mathbb{R}^{2d} \to \mathcal{C} \ \text{ and } \ \vec{N} \in \mathcal{S} \ . \tag{1.81}$$

Proof: The eigenvalues of modulus one satisfy $\lambda_{2j-1} = \lambda_{2j}^*$. In order to make $\vec{A}_1$ symplectic, all eigenvectors are scaled to observe $\vec{v}_{2j-1}^{\,T} J_{2d} \vec{v}_{2j} = 1$. With $M(\vec{0})\vec{v}_{2j-1}^{\,*} = \lambda_{2j}\vec{v}_{2j-1}^{\,*}$ for the first $2r$ eigenvalues, one gets $\vec{v}_{2j-1} = \alpha \vec{v}_{2j}^{\,*}$. The factor α has to be purely imaginary, since

$$\alpha^{-1} = \alpha^{-1} \vec{v}_{2j-1}^{\,T} J_{2d} \vec{v}_{2j} = \vec{v}_{2j}^{\,T*} J_{2d} \vec{v}_{2j} = -\vec{v}_{2j}^{\,T} J_{2d} \vec{v}_{2j}^{\,*} = -\alpha^{-1*} \ . \tag{1.82}$$

Scaling the vectors $\vec{v}_{2j}$ to give $\vec{v}_{2j}^{\,T*} J_{2d} \vec{v}_{2j} = i$ requires $\alpha = -i$. Since for every eigenvector with real eigenvalue its real part is also an eigenvector, the eigenvectors $\vec{v}_k$ with $k > r$ are chosen to be real. We can write $\vec{A}_1^{-1} = \sum_{l=1}^{2d} \vec{v}_l z_l$ and $\vec{A}_1^{-1} \circ \vec{A}_1 = \sum_{l=1}^{2d} \vec{v}_l A_{1,l} = \vec{z}$. Multiplying with $\vec{v}_{2j-1}^{\,T} J_{2d}$ from the left reveals

$$A_{1,2j} = \vec{v}_{2j-1}^{\,T} J_{2d} \vec{z} = -i \vec{v}_{2j}^{\,T*} J_{2d} \vec{z} = i A_{1,2j-1}^* \ \ \forall j \in \{1, \ldots, r\} \text{ and} \tag{1.83}$$

$$A_{1,2k} = \vec{v}_{2k-1}^{\,T} J_{2d} \vec{z} \in \mathbb{R} \ \ \forall k \in \{r+1, \ldots, d\} \ . \tag{1.84}$$

This is equivalent to the statement $\vec{A}_1(\vec{x}) \in \mathcal{C}$ for all real vectors $\vec{x}$. The inverse $\vec{A}_1^{-1}$ must take elements of $\mathcal{C}$ into $\mathbb{R}^{2d}$. From these properties and the fact that $\vec{M}$ takes real vectors into reals vectors, we can conclude that $\vec{N}_1 \in \mathcal{S}$.

The next step is to show that all $\vec{N}_m$, which are obtained from $\vec{N}_1$ by the steps of the normal form transformation, are in $\mathcal{S}$. Assume that $\vec{N}_{m-1}$ takes elements of $\mathcal{C}$ into elements of $\mathcal{C}$. Writing the components of $\vec{N}_{m-1}$ as polynomials, this means

$$\begin{aligned} &\textstyle\sum_{\vec{k}}^{|\vec{k}| \le n} \ (N_{m-1,2j-1}|\vec{k}) y_1^{k_1} y_2^{k_2} \ldots y_{2r-1}^{k_{2r-1}} y_{2r}^{k_{2r}} \ldots y_{2d}^{k_{2d}} \\ = i \ &\textstyle\sum_{\vec{k}}^{|\vec{k}| \le n} \ (N_{m-1,2j}|\vec{k})^* y_1^{k_2} y_2^{k_1} \ldots y_{2r-1}^{k_{2r}} y_{2r}^{k_{2r-1}} \ldots y_{2d}^{k_{2d}} \cdot (-i)^{\sum_{l=1}^{2r} k_l} \ . \end{aligned} \tag{1.85}$$

These lines entail relations for the Taylor coefficients, which can be expressed most

conveniently with the $2d \times 2d$ matrix S,

$$S_{kl} = \begin{cases} 1 & \text{if } l = k+1 \quad \text{and } k \leq 2r \text{ odd} \\ 1 & \text{if } k = l+1 \quad \text{and } k \leq 2r \text{ even} \\ 1 & \text{if } k = l \qquad \text{and } k > 2r \\ 0 & \text{else} \end{cases} \tag{1.86}$$

Equation (1.85) reveals

$$(N_{m-1,2j-1}|\vec{k}) = i(N_{m-1,2j}|S\vec{k})^* \cdot (-i)^{\sum_{i=1}^{2r} k_i} . \tag{1.87}$$

Since this condition does not relate coefficients of different orders, an n^{th} order Taylor map which is in $\mathcal{S}$ has this property for any truncation order smaller than n.

According to equation (1.20), $\vec{T}_m$ has this property also, since for the resonance denominator a similar equation holds, namely

$$D_{2i-1}(\vec{k}) \;=\; (\lambda_{2i-1} - \vec{\lambda}^{\vec{k}}) = (\lambda_{2i} - \vec{\lambda}^{S\vec{k}})^* = D_{2i}(S\vec{k})^* . \tag{1.88}$$

To finally show that $\vec{A}_m =_n \exp(:t_m:)\vec{z}$ has the same property, we prove a helpful lemma for which we need another $2d \times 2d$ matrix

$$\tilde{S}_{kl} = \begin{cases} i & \text{if } l = k+1 \quad \text{and } k \leq 2r \text{ odd} \\ i & \text{if } k = l+1 \quad \text{and } k \leq 2r \text{ even} \\ 1 & \text{if } k = l \qquad \text{and } k > 2r \\ 0 & \text{else} \end{cases} \tag{1.89}$$

and the corresponding map $\vec{s}$ with $\vec{s}(\vec{y}) = \tilde{S}\vec{y}$.

Lemma 1.5.2 *If $\vec{T} \in \mathcal{S}$ and $\vec{F} \in \mathcal{S}$, then $\vec{T}^T \vec{\partial} \vec{F} \in \mathcal{S}$.*

Proof: It will be useful to remember that, for a map $\vec{M}$ and its Jacobian M,

$$\vec{\partial}\{g \circ \vec{M}\} = M^T\{(\vec{\partial} g) \circ \vec{M}\} . \tag{1.90}$$

The function which takes all $\vec{y} \in \mathcal{C}$ into $\vec{F}(\vec{y})^*$ is denoted by $\vec{F}^*$. Due to membership in $\mathcal{S}$, $\vec{T}$ and $\vec{F}$ are functions on $\mathcal{C}$ with $\vec{T} = \tilde{S}\vec{T}^*$ and $\vec{F} = \tilde{S}\vec{F}^*$. Accordingly, $\vec{F}^* \circ \vec{s}$ takes $\vec{y}^*$ into $\vec{F}(\vec{y})^*$ for all $\vec{y} \in \mathcal{C}$. From this information, the subsequent relations follow:

$$(\vec{\partial} F)|_{\vec{y}} \;=\; (\{\vec{\partial}\vec{F}^* \circ \vec{s}\}|_{\vec{y}^*})^* = \{(\{\vec{\partial}\vec{F}^* \circ \vec{s}\} \circ \vec{s}^{-1})|_{\vec{y}}\}^* \tag{1.91}$$

$$= \; (\{\tilde{S}^T \vec{\partial} \vec{F}^*\}|_{\vec{y}})^* = (\{\tilde{S}^T \vec{\partial} \tilde{S}^{-1} \vec{F}\}|_{\vec{y}})^* . \tag{1.92}$$

Now it can be concluded that

$$\vec{T}^T(\vec{y})(\vec{\partial}\vec{F})|_{\vec{y}} \;=\; \vec{T}^{T*}(\vec{y})\tilde{S}^T\{(\tilde{S}^T \vec{\partial} \tilde{S}^{-1}\vec{F})|_{\vec{y}}\}^* \tag{1.93}$$

$$= \; \tilde{S}^{-1*}\{(\vec{T}^T \tilde{S}^{T*} \tilde{S}^T \vec{\partial}\vec{F})|_{\vec{y}}\}^* = \tilde{S}\{(\vec{T}^T \vec{\partial}\vec{F})|_{\vec{y}}\}^* , \tag{1.94}$$

which proves the lemma.

To analyze the exponential Poisson-bracket operator, we observe

$$:t_m:\vec{F} = \vec{\partial}^T t_m J_{2d} \vec{\partial}\vec{F} = \vec{T}_m^T \vec{\partial}\vec{F} . \tag{1.95}$$

All terms in the expansion of the exponential map have this structure,

$$\exp(:t_m:)\vec{z} = \vec{z} + \vec{T}_m + \frac{1}{2}\vec{T}_m^T \vec{\partial}\vec{T}_m + \frac{1}{3!}(\vec{T}_m^T\vec{\partial})^2\vec{T}_m + \frac{1}{4!}(\vec{T}_m^T\vec{\partial})^3\vec{T}_m + \ldots \tag{1.96}$$

and, due to lemma (1.5.2), with $\vec{T}_m$, also $\vec{A}_m$ is an element of $\mathcal{S}$. Also the order n inverse $\vec{A}_m^{-1,n} =_n \exp(-:t_m:)\vec{z}$ is in $\mathcal{S}$. Since the concatenation of two elements of $\mathcal{S}$ is again in $\mathcal{S}$, also $\vec{N}_m =_n \vec{A}_m \circ \vec{N}_{m-1} \circ \vec{A}_m^{-1,n}$ is in $\mathcal{S}$. In this last step it is again crucial that truncating Taylor maps preserves membership in $\mathcal{S}$. Performing the normal form transformation to the evaluation order n yields therefore $\vec{N} \in \mathcal{S}$, which proves the first part of theorem (1.5.1).

The performed transformation can be written as

$$\vec{A} =_n \vec{A}_n \circ \ldots \circ \vec{A}_2 \circ \vec{A}_1 . \tag{1.97}$$

$\vec{A}_1$ takes real vectors into $\mathcal{C}$ and the concatenation of all nonlinear maps $\vec{A}_m$ is in $\mathcal{S}$. This proves the second part of the theorem (1.5.1), namely that $\vec{A}$ takes elements of $I\!R^{2d}$ into $\mathcal{C}$.

Theorem (1.5.1) has strong implications for the functions f_l of the normal form map in theorem (1.1.8).

Theorem 1.5.3 *Let $\vec{M}$ be a map satisfying the conditions of theorem (1.1.8) on symplectic normal forms. If each of the r complex linear eigenvalue of $\vec{M}$ has unit modulus, then there are r functions $\phi_j : I\!I^r \times I\!R^{d-r} \to I\!R$ with*

$$f_{2j-1} =_{[(n-1)/2]} \exp(i\phi_j) \text{ and} \tag{1.98}$$

$$f_{2j} =_{[(n-1)/2]} \exp(-i\phi_j) \text{ for } j \in \{1,\ldots,r\} , \tag{1.99}$$

$$f_k : I\!I^r \times I\!R^{d-r} \to I\!R \text{ for } k \in \{2r+1,\ldots,2d\} . \tag{1.100}$$

The phases ϕ_j satisfy the condition $\partial_j\phi_i =_{[(n-3)/2]} \partial_i\phi_j$.

Proof: From theorem (1.5.1) and with $N_l = z_l(f_l \circ \vec{a})$ where $a_j = z_{2j-1}z_{2j}$, it follows that

$$\{z_{2j-1}(f_{2j-1} \circ \vec{a})\}|_{\vec{y}} =^{'i}(\{z_{2j}(f_{2j} \circ \vec{a})\}|_{\vec{y}})^* \quad \forall \vec{y} \in \mathcal{C} . \tag{1.101}$$

Realizing that $\vec{a}(\vec{y}) \in I\!I^r \times I\!R^{d-r}$ for $\vec{y} \in \mathcal{C}$, one concludes

$$f_{2j-1}(\vec{\xi}) = \{f_{2j}(\vec{\xi})\}^* \quad \forall \vec{\xi} \in I\!I^r \times I\!R^{d-r} . \tag{1.102}$$

In order to take advantage of the requirement $f_{2j-1}f_{2j} =_{[(n-1)/2]} 1$, we write $f_{2j-1} = \exp(i\phi_j) + P_j$ and $f_{2j} = \exp(-i\phi_j) + P_j^*$,

$$(\exp(i\phi_j) + P_j)(\exp(-i\phi_j) + P_j^*) =_{[(n-1)/2]} 1 . \tag{1.103}$$

The constant part of this equation shows that P_j has no constant part. For comparing higher orders, we write

$$P_j \exp(-i\phi_j) + P_j^* \exp(i\phi_j) + P_j^* P_j =_{[(n-1)/2]} 0 \tag{1.104}$$

and assume that P_j has no contributions up to orders $m-1$. Since the constant part of f_l equals λ_l, we get up to order m that

$$P_j\lambda_j^* + Q_j\lambda_j =_m 0 . \tag{1.105}$$

Therefore, the m^{th} order of P_j must have the structure $i\lambda_j R_{m,j}$ with $R_{m,j} : I\!I^r \times I\!R^{d-r} \to I\!R$. Writing the non-constant part of ϕ_j as $\phi_j^{(n)}$ shows that

$$f_{2j-1} =_m \lambda_j\{\exp(i\phi_j^{(n)}) + iR_{m,j}\} =_m \lambda_j \exp(i\phi_j^{(n)} + iR_{m,j}) . \tag{1.106}$$

The last equation holds, since $R_{m,j}$ has no contributions to orders lower than m and therefore $\exp(R_{m,j}) =_m 1 + R_{m,j}$. $R_{m,j}$ can be chosen to be 0 by taking its contribution into $\phi_j^{(n)}$. Performing this argument up to the evaluation order n yields that up to order n, f_{2j-1} has the structure of $\exp(i\phi_j)$ for some function $\phi_j : I\!I^r \times I\!R^{d-r} \to I\!R$.

According to the theorem on symplectic normal forms (1.1.8),

$$f_{2i}\partial_i f_{2j} =_{[(n-3)/2]} f_{2j}\partial_j f_{2i} \; \forall i,j \in \{1,\ldots,d\} . \tag{1.107}$$

Writing the f_l as given by equation (1.99) yields $\partial_i\phi_j =_{[(n-3)/2]} \partial_j\phi_i$, which proves the theorem.

This finally puts us into the position of formulating a theorem on real normal form transformations.

Theorem 1.5.4 (Real Symplectic Normal Forms)
A non-degenerate map $\vec{M} \in \mathcal{SP}_n^{2d}(I\!R)$ with linear eigenvalues which are not in resonance to any order $m \le n$ and are either real or have modulus one can be transformed by a transformation $\vec{B} \in \mathcal{SP}_n^{2d}(I\!R)$ to $\vec{R} =_n \vec{B} \circ \vec{M} \circ \vec{B}^{-1,n} \in \mathcal{SP}_n^{2d}(I\!R)$ where all these maps are $I\!R^{2d} \to I\!R^{2d}$ and

$$R_{2j-1} =_n z_{2j-1}\cos\{\psi_j \circ \vec{b}\} + z_{2j}\sin\{\psi_j \circ \vec{b}\} , \tag{1.108}$$

$$R_{2j} =_n -z_{2j-1}\sin\{\psi_j \circ \vec{b}\} + z_{2j}\cos\{\psi_j \circ \vec{b}\} , \quad (1.109)$$

$$R_{2k-1} =_n z_{2k-1} g_k \circ \vec{b} , \quad (1.110)$$

$$R_{2k} =_n z_{2k}/\ g_k \circ \vec{b} , \ |\lambda_{2k}| = 1, \ \lambda_{2k} \in I\!R . \quad (1.111)$$

The function $\vec{b}$ is given by $b_j = z_{2j-1}^2 + z_{2j}^2$ for $|\lambda_{2j}| = 1$ and $b_k = z_{2k-1}z_{2k}$ for $\lambda_{2k} \in I\!R$. The functions ψ_i and g_k are $I\!R^d \to I\!R$.

Proof: We will again choose n^{th} order polynomial maps for $\vec{R}$, $\vec{B}$, and $\vec{B}^{-1,n}$. A linear transformation $\vec{C}$ and its inverse are needed to obtain these maps from the normal form theorem (1.1.8),

$$C_{2j-1} = \frac{1}{\sqrt{2}}e^{-i\pi/2}(z_{2j-1} + z_{2j}) \quad , \quad C_{2j} = \frac{1}{\sqrt{2}}e^{i\pi/2}(-z_{2j-1} + z_{2j}) ,$$

$$C_{2j-1}^{-1} = \frac{1}{\sqrt{2}}e^{i\pi/2}(z_{2j-1} + iz_{2j}) \quad , \quad C_{2j}^{-1} = \frac{1}{\sqrt{2}}e^{i\pi/2}(z_{2j-1} - iz_{2j}) ,$$
$$C_k = z_k \text{ and } C_k^{-1} = z_k \quad \text{for} \quad j \in \{1, \ldots, r\},\ k > r . \quad (1.112)$$

The easiest way to see that $\vec{C}^{-1}$ is the inverse of $\vec{C}$ is to multiply the Jacobi matrices. Since these matrices have block diagonal structure, the result is evident. All 2×2 submatrices on the diagonal have determinant one and therefore are symplectic, which establishes the symplecticity of $\vec{C}$. Let us now prove the claim $\vec{R} = \vec{C} \circ \vec{N} \circ \vec{C}^{-1}$. First evaluate $\vec{c} = \vec{a} \circ \vec{C}^{-1}$,

$$c_j = \frac{i}{2}(z_{2j-1}^2 + z_{2j}^2) = \frac{i}{2}b_j \text{ and } c_k = z_{2k-1}z_{2k} = b_k . \quad (1.113)$$

Let us write a scaling transformation $\vec{s}$ by

$$s_j = \frac{i}{2}z_j \text{ for } j \le r \text{ and } s_k = z_k \text{ for } j > r \quad (1.114)$$

and introduce the new phases $\psi_j = \phi_k \circ \vec{s}$. The functions $b_l \circ \vec{C} \circ \vec{A}$ are order $n+1$ invariants of the map $\vec{M}$, since they are related to the $I_l = a_l \circ \vec{A}$ of theorem (1.4.4)

by $\vec{s} \circ \vec{b} = \vec{a} \circ \vec{C}^{-1}$. Performing the transformation $\vec{C}$ on $\vec{R}$ leaves

$$R_{2j-1} = C_{2j-1} \circ \vec{N} \circ \vec{C} : \quad (1.115)$$

$$= \frac{1}{\sqrt{2}}e^{-i\pi/2}\{z_{2j-1}(f_{2j-1} \circ \vec{a}) + z_{2j}(f_{2j} \circ \vec{a})\} \circ \vec{C}^{-1} \quad (1.116)$$

$$=_n \frac{1}{\sqrt{2}}e^{-i\pi/2}\{(z_{2j-1} + z_{2j})\cos(\phi_j \circ \vec{a})$$
$$+ \quad i(z_{2j-1} - z_{2j})\sin(\phi_j \circ \vec{a})\} \circ \vec{C}^{-1} \quad (1.117)$$

$$=_n z_{2j-1}\cos(\psi_j \circ \vec{b}) - z_{2j}\sin(\psi_j \circ \vec{b}) . \quad (1.118)$$

Similarly we obtain

$$R_{2j} = C_{2j} \circ \vec{N} \circ \vec{C}^{-1} \quad (1.119)$$

$$=_n \frac{1}{\sqrt{2}}e^{i\pi/2}\{(-z_{2j-1} + z_{2j})\cos(\phi_j \circ \vec{a})$$
$$- \quad i(z_{2j-1} + z_{2j})\sin(\phi_j \circ \vec{a})\} \circ \vec{C}^{-1} \quad (1.120)$$

$$=_n z_{2j-1}\sin(\psi_j \circ \vec{b}) + z_{2j}\cos(\psi_j \circ \vec{b}) . \quad (1.121)$$

For real eigenvalues λ_{2k} one gets

$$R_{2k-1} =_n z_{2k-1}(g_k \circ \vec{b}) , \quad R_{2k} =_n z_{2k}/(g_k \circ \vec{b}) \text{ with } g_k = f_{2k-1} \circ \vec{s} . \quad (1.122)$$

Finally we have to establish that $\vec{B}(\vec{x}) = (\vec{C} \circ \vec{A})|_{\vec{x}}$ is a real vector. $\vec{A}$ takes $\vec{x} \in I\!R^{2d}$ into $\mathcal{C}$ and $\vec{C}$ takes elements of $\mathcal{C}$ into $I\!R^{2d}$, which establishes that $\vec{B}$ is $I\!R^{2d} \to I\!R^{2d}$. The phases ψ_j are real, since $\vec{s}(\vec{x}) \in I\!R^r \times I\!R^{d-r}$ and is taken into $I\!R$ by ϕ_j, according to theorem (1.5.3); similarly $g_k(\vec{x}) = f_{2k-1} \circ \vec{s}(\vec{x})$ is real.

Interpretation: With the help of a $2d \times 2d$ matrix which depends only on $\vec{b}$, we can formulate the real normal form map as

$$\begin{pmatrix} R_{2j-1} \\ R_{2j} \end{pmatrix} =_n \begin{pmatrix} \cos(\psi \circ \vec{b}) & -\sin(\psi \circ \vec{b}) \\ \sin(\psi \circ \vec{b}) & \cos(\psi \circ \vec{b}) \end{pmatrix} \begin{pmatrix} z_{2j-1} \\ z_{2j} \end{pmatrix} , \quad (1.123)$$

for complex λ_{2j}. For real eigenvalues λ_{2k}, a diagonal matrix can be used,

$$\begin{pmatrix} R_{2k-1} \\ R_{2k} \end{pmatrix} =_n \begin{pmatrix} g_k \circ \vec{b} & 0 \\ 0 & 1/(g_k \circ \vec{b}) \end{pmatrix} \begin{pmatrix} z_{2k-1} \\ z_{2k} \end{pmatrix} . \tag{1.124}$$

The motion generated by $\vec{R}$ is described by rotations on a circle for every $|\lambda_j| = 1$ and by motion on a hyperbola for every $\lambda_k \in I\!R$. The speed of this motion only depends on the b_l, the order $n+1$ invariants of the map $\vec{R}$. These invariants are the square amplitudes $z_{2i-1}^2 + z_{2i}^2$ of the rotations and half the square minimum distances from the origin $z_{2k-1}z_{2k}$ of the hyperbolas.

1.6 Action–Angle Variables

Definition 1.6.1 (Order n Action–Angle Variables)

Given a Taylor map $\vec{N}$; we call maps $\vec{J}$ action variables and $\vec{\alpha}$ angle variable of $\vec{N}$ if

1. *the map $(\vec{J}, \vec{\alpha})$ is order n symplectic,*
2. *the functions J_j are order $n+1$ invariants of $\vec{N}$,*
3. *up to order $n-1$, the functions $\alpha_j \circ \vec{M} - \alpha_j$ can be expressed as functions of the $\vec{J}$ only.*

The rotations in real symplectic normal form space remind one strongly of action–angle variables for periodic motion in classical mechanics. We will prove that they are indeed order n action–angle variables.

Theorem 1.6.2 Action–angle variables of normal form maps

For a normal form map $\vec{N}$ as given in theorem (1.1.8), there are order n action–angle variables $\vec{J}$ and $\vec{\alpha}$.

Following, we introduce variables and show that they satisfy the properties of order n action–angle variables for the normal form map $\vec{N}$. Let

$$J_j = z_{2j-1}z_{2j} \ , \quad \alpha_j = \frac{1}{2}\log(z_{2j}/z_{2j-1}) \ , \tag{1.125}$$

where we restrict the domain of the action–angle variables to $\{\vec{y}|\vec{y} \in \mathcal{C}, y_l \neq 0\}$.

The Jacobian of $(\vec{J}, \vec{\alpha})$ is denoted by K and has 2×2 block diagonal form. Like before, we represent these blocks by K_{kl} with $k, l \in \{1, \ldots, d\}$, i.e.

$$K_{kl} = \begin{pmatrix} z_{2k} & z_{2k-1} \\ -\frac{1}{2z_{2k-1}} & \frac{1}{2z_{2k}} \end{pmatrix} . \tag{1.126}$$

Since the determinant of each 2×2 block is one, the matrix K is symplectic. The J_j are order $n+1$ invariants of the map $\vec{N}$. Let us analyze the change of the functions α_j under action of $\vec{N}$

$$\begin{aligned} \alpha_j \circ \vec{N} - \alpha_j &= \frac{1}{2}\{\log(N_{n,2j-1}/N_{n,2j}) - \log(z_{2j-1}/z_{2j})\} & (1.127) \\ &= \frac{1}{2}\{\log(f_{2j-1}) - \log(f_{2j})\} \circ \vec{a} =_{n-1} i\phi_j \circ \vec{J} & (1.128) \end{aligned}$$

It has to be noted that the domain of the functions $\alpha_j \circ \vec{N} - \alpha_j$ does not have to be restricted. This shows that all three conditions to call $(\vec{J}, \vec{\alpha})$ order n action–angle variables of $\vec{N}$ are satisfied.

In spite of this theorem, it becomes clear that the usual concept of action angle variables is not suited for discussions in the context of Taylor expansions. This was seen in some intermediate steps when the origin had to be excluded and rises from the fact that the polar angle cannot be defined as a differentiable function at the origin. It is therefore much more suitable to stay in the real normal form space and to consider rotations and hyperbolas as the most basic concept of motion.

Definition 1.6.3 (Normal Modes)

If a map $I\!R^{2d} \to I\!R^{2d}$ can be transformed by symplectic transformations to rotations

and hyperbolic motion in d decoupled spaces, then these decoupled motions are called the normal modes of the map. The square of the radius of rotation and half the square of the distance of the hyperbolas from the origin are called normal invariants of the map.

It is worth mentioning that every map which can be transformed to action-angle variables also has normal modes. The transformation between these two notions of elementary motion can be taken from the proof of theorem (1.6.2). By this definition, a symplectic map in its normal modes has the structure of $\vec{R}$ with

$$\begin{pmatrix} R_{2j-1} \\ R_{2j} \end{pmatrix} = \begin{pmatrix} \cos(\theta_j) & -\sin(\theta_j) \\ \sin(\theta_j) & \cos(\theta_j) \end{pmatrix} \begin{pmatrix} z_{2j-1} \\ z_{2j} \end{pmatrix} , \tag{1.129}$$

for the r rotations and with a diagonal matrix for the $d-r$ cases of motion on a hyperbola

$$\begin{pmatrix} R_{2k-1} \\ R_{2k} \end{pmatrix} = \begin{pmatrix} h_k & 0 \\ 0 & 1/h_k \end{pmatrix} \begin{pmatrix} z_{2k-1} \\ z_{2k} \end{pmatrix} . \tag{1.130}$$

The functions θ_j and h_k are $\mathbb{R}^{2d} \to \mathbb{R}$, and the d components of $\vec{b}$ with $b_j = z_{2j-1}^2 + z_{2j}$ and $b_k = z_{2k-1} z_{2k}$ are invariants of $\vec{R}$.

Given a symplectic map $\vec{M}$ that can be Taylor expanded at the origin; its Taylor map $\vec{M}_n$ up to order n is order n symplectic. Our previous discussion was based on the condition that the linear eigenvalues are not in resonance up to order n. In the case that the map $\vec{M}$ has d normal modes, it is a reasonable question to ask if the resonance condition could avoid the possibility of computing the normal form map of $\vec{M}_n$. A statement about this problem can be proved most easily with the help of the following two theorems.

Theorem 1.6.4 *Symplectic maps preserve the area in all of the d $z_{2j-1} \times z_{2j}$ subspaces.*

Proof: First we need to establish the conservation of the Poisson brackets $: f : g$ under symplectic maps. We can write the derivative with the Jacobian M as $\vec{\partial}(f \circ \vec{M}) = M^T\{(\vec{\partial} f) \circ \vec{M}\}$.

$$\begin{aligned} : f \circ \vec{M} : (g \circ \vec{M}) &= \{(\vec{\partial}^T f) \circ \vec{M}\} M J_{2d} M^T \{(\vec{\partial} g) \circ \vec{M}\} && (1.131) \\ &= (\vec{\partial}^T f J_{2d} \vec{\partial} g) \circ \vec{M} = (: f : g) \circ \vec{M} . && (1.132) \end{aligned}$$

When new coordinates are defined by the map, $\vec{Q} = \vec{M}(\vec{q})$ with $\vec{q}, \vec{Q} \in \mathbb{R}^{2d}$, then the change of an area element is given by the change of the differential 2-form

$$\begin{aligned} dQ_{2j-1} \wedge dQ_{2j} &= dq_{2j-1} \wedge dq_{2j} \left(\frac{dQ_{2j-1}}{dq_{2j-1}} \frac{dQ_{2j}}{dq_{2j}} - \frac{dQ_{2j-1}}{dq_{2j}} \frac{dQ_{2j}}{dq_{2j-1}}\right) && (1.133) \\ &= dq_{2j-1} \wedge dq_{2j} (: M_{2j-1} : M_{2j})|_{\vec{q}} && (1.134) \\ &= dq_{2j-1} \wedge dq_{2j} \{(: q_{2j-1} : q_{2j}) \circ \vec{M}\}|_{\vec{q}} && (1.135) \\ &= dq_{2j-1} \wedge dq_{2j} . && (1.136) \end{aligned}$$

This is true for every of the d subspaces and proves the theorem. This proof and also another more intuitive proof can be found in the second chapter [SSC94].

Theorem 1.6.5 *Let a symplectic map in its basic modes be written as equation (1.129) and (1.130). Then there are functions $\psi_j : \mathbb{R}^d \to \mathbb{R}$ and $g_k : \mathbb{R}^d \to \mathbb{R}$ with $\theta_j = \psi_j \circ \vec{b}$ and $h_j = g_j \circ \vec{b}$.*

Proof: First we will give a graphic proof using theorem (1.6.1), after that an alternative more formalistic proof will be given. Let us analyze what conditions the theorem about area preservation in every $z_{2j-1} \times z_{2j}$ coordinate plane imposes on normal modes. Consider first the case of rotations. An area located between two similar radii and two initial angles $\phi_{1,i}$ and $\phi_{2,i}$ is transformed into an area between the same radii and two angles $\phi_{1,f}$ and $\phi_{2,f}$ by one application of the map $\vec{M}$. If area preservation is to hold, the difference between the angles is invariant. Therefore, the

phase advance can only depend on the invariants of the map. A similar argument is possible if the motion is confined to hyperbolas. If the factors g in the 2×2 matrix describing the motion,

$$\begin{pmatrix} z_{2j-1} \\ z_{2j} \end{pmatrix}_2 = \begin{pmatrix} g & 0 \\ 0 & 1/g \end{pmatrix} \begin{pmatrix} z_{2j-1} \\ z_{2j} \end{pmatrix}_1 , \tag{1.137}$$

depend only on invariants of motion, the map is area preserving. If the factors would depend on the position on the normal invariants, this condition would be violated, since not all area elements located between two hyperbolas would be conserved under application of $\vec{M}$. As a conclusion it can be stated that the functions θ_j and h_k in equation (1.129) and (1.130) only depend on the invariants of the map, which are the components of $\vec{b}$.

For the alternative more formalistic proof, we use $\vec{C}$ and $\vec{C}^{-1}$ as defined in equation (1.112) to obtain the map $\vec{N} = \vec{C}^{-1} \circ \vec{R} \circ \vec{C}$ which is an element of $\mathcal{S}$. Elements of $\mathcal{S}$ are maps which take elements of $\mathcal{C}$ into elements of $\mathcal{C}$ as defined in equation (1.79). This means that $iN_{2j-1}(\vec{y}) = N_{2j}(\vec{y})^*$, $\forall j \in \{1, \ldots, r\}$.

With the Jacobian of $\vec{N}$ written as

$$N_{ij} = \begin{pmatrix} \partial_{2j-1} N_{2i-1} & \partial_{2l} N_{2i-1} \\ \partial_{2j-1} N_{2i} & \partial_{2l} N_{2i} \end{pmatrix} , \tag{1.138}$$

the symplectic condition will again be written in 2×2 matrix notation as

$$J_2 \delta_{ij} = (N J_{2d} N^T)_{ij} = \sum_{l=1}^{n} N_{il} J_2 N_{jl}^T = \begin{pmatrix} : N_{2i-1} : N_{2j-1} & : N_{2i-1} : N_{2j} \\ : N_{2i} : N_{2j-1} & : N_{2i} : N_{2j} \end{pmatrix} , \tag{1.139}$$

where the notation $: f : g = \vec{\partial}^T f J_{2d} \vec{\partial} g$ for the Poisson bracket between f and g was used, which was already defined in theorem (1.3.4). The conditions of the $< 1, 2 >$ position and of the $< 2, 1 >$ position lead to equivalent conditions due to antisymmetry of the Poisson bracket. We are therefore left with the conditions

$$: N_{2i-1} : N_{2j-1} = 0, \; : N_{2i} : N_{2j} = 0, \; : N_{2i-1} : N_{2j} = \delta_{ij} . \tag{1.140}$$

From this it follows that

$$\begin{aligned} (: N_{2i-1} : z_{2j-1} z_{2j}) &= (: N_{2i-1} : N_{2j-1} N_{2j}) && (1.141) \\ &= N_{2j-1}(: N_{2i-1} : N_{2j}) + (: N_{2i-1} : N_{2j-1}) N_{2j} && (1.142) \\ &= N_{2j-1} \delta_{ij} . && (1.143) \end{aligned}$$

and therefore

$$z_{2j-1} \partial_{2j-1} N_{2i-1} - z_{2j} \partial_{2j} N_{2i-1} = \delta_{ij} N_{2j-1} . \tag{1.144}$$

If we write $N_l = z_l n_l$ and insert into the second line, we get

$$z_{2j-1} \partial_{2j-1} n_{2i-1} - z_{2j} \partial_{2j} n_{2i-1} = 0 , \tag{1.145}$$

from which we conclude that there is a function $g : \mathcal{C} \to I\!R$ with $h = g \circ \vec{a}$ where $\vec{a}$ is again defined by $a_i = z_{2i-1} z_{2i}$. Similar to the evaluation in the equations (1.113) to (1.122), we conclude that $\vec{R} = \vec{C} \circ \vec{N} \vec{C}^{-1}$ has the structure

$$\begin{pmatrix} R_{2j-1} \\ R_{2j} \end{pmatrix} = \begin{pmatrix} \cos(\psi_j \circ \vec{b}) & -\sin(\psi_j \circ \vec{b}) \\ \sin(\psi_j \circ \vec{b}) & \cos(\psi_j \circ \vec{b}) \end{pmatrix} \begin{pmatrix} z_{2j-1} \\ z_{2j} \end{pmatrix} , \tag{1.146}$$

for rotations and

$$\begin{pmatrix} R_{2k-1} \\ R_{2k} \end{pmatrix} = \begin{pmatrix} g_k \circ \vec{b} & 0 \\ 0 & 1/(g_k \circ \vec{b}) \end{pmatrix} \begin{pmatrix} z_{2k-1} \\ z_{2k} \end{pmatrix} \tag{1.147}$$

for motion on hyperbolas.

Theorem 1.6.6 *If a symplectic map $\vec{M}$ can be transformed to normal modes by a symplectic transformation $\vec{B}$, and $\vec{M}$ as well as $\vec{B}$ can be Taylor expanded up to order n, then the Taylor map $\vec{M}_n$ can be transformed to normal form by means of the method presented in the proof of theorem (1.1.8).*

Proof: The map $\vec{M}$ can be written with the existing transformation $\vec{B}$ and $\vec{R}$ as

$$\vec{M} = \vec{B}^{-1} \circ \vec{R} \circ \vec{B} . \tag{1.148}$$

One can compute $\vec{A} = \vec{C}^{-1} \circ \vec{B}$ with $\vec{C}^{-1}$ from equation (1.112). Since with the given assumptions, all the involved maps have Taylor expansions to order n, this relation holds with respect to $=_m$ for all $m \in \{1, \ldots, n\}$. Therefore,

$$\vec{M} =_n \vec{A}^{-1} \circ \vec{N} \circ \vec{A} \tag{1.149}$$

where, due to theorem (1.6.5), $\vec{N}$ has the structure of a normal form map given in theorem (1.1.8). Assigning the linear transformation $\vec{A}_1 =_1 \vec{A}$ gives the linear transformation for the theorem (1.1.8) on order n symplectic normal forms. This transformation can be used to compute $\vec{N}_1 =_n \vec{A}_1 \circ \vec{M} \circ \vec{A}_1^{-1}$. The second order expansion of $\vec{A} \circ \vec{A}_1^{-1}$ yields the map $\vec{z} + \vec{T}_2$, which eliminates all second order terms of $\vec{N}_1$ which do not have normal form structure. It is order 2 symplectic and can therefore be used to compute $\vec{A}_2 = \exp(: t_2 :)\vec{z}$. Similarly all subsequent orders are treated with

$$\vec{z} + \vec{T}_m =_m \vec{A} \circ \vec{A}_1^{-1} \circ \ldots \circ \vec{A}_{m-1}^{-1,n} . \tag{1.150}$$

Continuing this strategy to order n shows that all the $\vec{T}_m$ exist and that there is no problem with vanishing $D_l(\vec{k})$, even when there are resonances of the linear eigenvalues. This shows that under the assumed conditions all the $(N_{m,l}|\vec{k})$ in equation (1.20) vanish whenever $D_l(\vec{k})$ vanishes due to resonances described in part 2 after equation (1.20).

Theorem (1.6.6) gives rise to a very useful corollary which can be used as the basis for computer proofs to establish that a system does not have d invariants of motion or to establish that a Hamiltonian system is not integrable.

Corollary 1.6.7 (Excluding Invariants) *Given a Taylor expandable symplectic map $\vec{M} : \mathbb{R}^{2d} \to \mathbb{R}^{2d}$. If at any order during the normal form transformation a division by a vanishing resonance denominator becomes necessary and the numerator at that point does not vanish, then the map $\vec{M}$ does not have d invariants of motion.*

Corollary 1.6.8 (Excluding Integrability) *If a Hamiltonian equation of motion has an unique Taylor expandable time step one map $\vec{M}$ and the normal form transformation procedure would at some order require a division of a non vanishing coefficient by a vanishing resonance denominator, then the Hamiltonian system is not integrable.*

Constructing computer proofs, of course, requires completely rigorous arithmetic. Such computations can be achieved with interval arithmetic techniques [Moo88].

1.7 Pseudo Hamiltonians

Theorem 1.7.1 *For a non-degenerate map $\vec{M} \in \mathcal{SP}_n^{2d}(\mathbb{R})$ with linear eigenvalues which are not in resonance to any order $m \leq n$ and all have modulus one, a function $H : \mathbb{R}^{2d} \to \mathbb{R}$ can be found with*

$$\vec{M} =_n \exp(: H :)\vec{z} . \tag{1.151}$$

Proof: According to theorem (1.5.3), there are d polynomials ϕ_i of order $[(n-3)/2]$ with the property that the Jacobian of $\vec{\phi}$ is symmetric. This implies that the potential problem $\vec{\partial}\Phi = \vec{\phi}$ has a solution Φ which is a polynomial of order $[(n-1)/2]$.

In order to prove $\vec{N} =_n \exp(-i : \Phi \circ \vec{a} :)\vec{z}$, the following observation will be instrumental:

$$\begin{aligned}
: \Phi \circ \vec{a} : \{z_{2j-1}(h \circ \vec{a})\} &= z_{2j-1} \sum_{k=1}^{d} \{\partial_{2k-1}(\Phi \circ \vec{a})\partial_{2k}(h \circ \vec{a}) - \partial_{2k}(\Phi \circ \vec{a})\partial_{2k-1}(h \circ \vec{a})\} \\
&- \partial_{2j}(\Phi \circ \vec{a})(h \circ \vec{a}) \qquad (1.152) \\
&= \sum_{k=1}^{d} z_{2j-1} z_{2k-1} z_{2k} \{(\partial_k \Phi \partial_k h) \circ \vec{a} - (\partial_k \Phi \partial_k h) \circ \vec{a}\} \\
&- z_{2j-1}\{(\partial_j \Phi) \circ \vec{a}\}(h \circ \vec{a}) \qquad (1.153) \\
&=_n z_{2j-1}\{(-\phi_j h) \circ \vec{a}\} . \qquad (1.154)
\end{aligned}$$

and, due to antisymmetry of the Poisson bracket,

$$: \Phi \circ \vec{a} : \{z_{2j}(h \circ \vec{a})\} = z_{2j}\{(\phi_j h) \circ \vec{a}\} \ . \tag{1.155}$$

With these formulas the evaluation of the exponential operator becomes obvious;

$$\exp\{-i : \Phi \circ \vec{a} :\} z_{2j-1} \ =_n \ \exp\{ \ i\phi \circ \vec{a}\} z_{2j-1} \ , \tag{1.156}$$

$$\exp\{-i : \Phi \circ \vec{a} :\} z_{2j} \ =_n \ \exp\{-i\phi \circ \vec{a}\} z_{2j} \ . \tag{1.157}$$

The original map $\vec{M}$ can therefore be represented by

$$\vec{A}^{-1,n} \circ (\exp\{-i : \Phi \circ \vec{a} :)\vec{z}) \circ \vec{A} =_n \vec{M} \ . \tag{1.158}$$

In the next step, the conservation of Poisson-bracket operators under order n symplectic maps is needed.

Theorem 1.7.2 *For a map $\vec{M} \in \mathcal{SP}_n^{2d}(\mathbb{F})$ and two functions $g, f \in C_{2d}^{\infty}$*

$$: f \circ \vec{M} : (g \circ \vec{M}) =_{n-1} (: f : g) \circ \vec{M} \ . \tag{1.159}$$

The field $\mathbb{F}$ is either $\mathbb{R}$ of $\mathbb{C}$ and the functions are either real or complex respectively.

Proof: A corresponding proof for symplectic maps was given in equation (1.132). Now we merely have to check what changes by considering order n symplectic maps. With the derivative of concatenated maps written with the help of the Jacobian, we prove $\vec{\partial}(f \circ \vec{M}) = M^T\{(\vec{\partial} f) \circ \vec{M}\}$.

$$: f \circ \vec{M} : (g \circ \vec{M}) \ = \ \{(\vec{\partial}^T f) \circ \vec{M}\} M J_{2d} M^T \{(\vec{\partial} g) \circ \vec{M}\} \tag{1.160}$$

$$=_{n-1} \ (\vec{\partial}^T f J_{2d} \vec{\partial} g) \circ \vec{M} =_{n-1} (: f : g) \circ \vec{M} \ . \tag{1.161}$$

With this theorem and with theorem (1.3.5), we can reformulate equation (1.158) to a single exponential Poisson-bracket operator. The notation $H = -i\Phi \circ \vec{a} \circ \vec{A}$ yields

$$\vec{M} =_n \exp(: H :)\vec{z} \ . \tag{1.162}$$

H is called the pseudo Hamiltonian of the map $\vec{M}$. It is an order $n+1$ invariant of $\vec{M}$, since it is a function of the invariants $I_i = a_i \circ \vec{A}$ from theorem (1.4.4). This fact also becomes clear by virtue of theorem (1.3.5):

$$H \circ \vec{M} =_n H \circ (\exp(: H :)\vec{z}) =_n \exp(: H :) H =_n H \ . \tag{1.163}$$

Finally we want to show that H is $\mathbb{R}^{2d} \to \mathbb{R}$. Since the functions ϕ_j are $\mathbb{F}^r \times \mathbb{R}^{d-r} \to \mathbb{R}$ and $\partial_j \Phi = \phi_j$, we get $\Phi : \mathbb{F}^r \times \mathbb{R}^{d-r} \to \mathbb{F}$. Theorem (1.5.1) specifies that $\vec{A}$ is $\mathbb{R}^{2d} \to \mathcal{C}$, $\vec{a}$ in turn takes elements of $\mathcal{C}$ into $\mathbb{F}^r \times \mathbb{R}^{d-r}$. Taking all these facts together we find that $H = -i\Phi \circ \vec{a} \circ \vec{A}$ is a real valued function of $\mathbb{R}^{2d}$.

1.8 Parameter Dependent Normal Forms

The presented theorems also apply to maps $\vec{M} : \mathbb{R}^{2d+p} \to \mathbb{R}^{2d}$ that depend on p parameters $\vec{\delta}$. For such maps, every Taylor coefficient can be viewed as a function of fixed but arbitrary parameters. All proofs are performed as before, and finally these functions of parameters in $\vec{N}$ and $\vec{A}$ are substituted by their Taylor expansions to the evaluation order to obtain the parameter dependent Taylor maps.

For computations, one starts with a Taylor map with respect to the coordinates as well as the parameters. Then one performs all computations according to the described normal form method while taking the partial derivatives with respect to the parameters into account when equating with "$=_n$". It ought to be mentioned that in a given order m there will be contributions of coordinates to lower orders $i < m$, when parameters occupy $m - i$ orders in the corresponding term of the Taylor polynomial. It can be shown by reviewing the previous sections that in all the given proofs it was never required that a given order only contains the same order in the coordinates. Due to "$=_n$", we were only concerned about the order of partial derivatives, which can be taken with respect of coordinates as well as parameters.

One exception applies. In the parameter-free case the map was assumed to be origin preserving $\vec{M}(\vec{0}) = \vec{0}$. In the parameter dependent case $\vec{M}(\vec{0},\vec{0}) = \vec{0}$ will be required. However, $\vec{C}(\vec{\delta}^*) = \vec{M}(\vec{0},\vec{\delta}^*)$ with a $\delta^* \in I\!R^p$ does not have to be $\vec{0}$; $\vec{C}$ is a parameter dependent constant part, which has to be eliminated before performing the normal form transformation. The procedure, described subsequently, can be found in [Ber93b].

This simplification is achieved by transforming the map to a parameter dependent fixed point. To do this, we have to extend the involved maps to be $I\!R^{2d+p} \rightarrow I\!R^{2d+p}$, e.g. $(\vec{M},\vec{\delta})$. Following, $(\vec{z},\vec{\delta})$ will describe the identity function. After the required transformation $\vec{A}_0$, the n^{th} order polynomial map $\vec{N}_0 =_n \vec{A}_0 \circ (\vec{M},\vec{\delta}) \circ (\vec{A}_0^{-1},\vec{\delta})$ will have the property

$$\vec{N}_0(\vec{0},\vec{\delta}^*) =_n (\vec{0},\vec{\delta}^*)\ \forall \delta^* \in I\!R^p, \tag{1.164}$$

whereas at the parameter dependent fixed point $\vec{z}_{fix} : I\!R^p \rightarrow I\!R^{2d}$ of the original map, $\vec{M}$ has the property

$$\vec{z}_{fix}(\vec{\delta}^*) =_n \vec{M}(\vec{z}_{fix}(\vec{\delta}^*),\vec{\delta}^*)\ \forall \delta^* \in I\!R^p\ . \tag{1.165}$$

The fixed point is a function of the parameters and can be expressed by the following lines,

$$(\vec{0},\vec{\delta}^*) \ =_n\ (\vec{M}-\vec{z},\vec{\delta})|_{(\vec{z}_{fix}(\vec{\delta}^*),\vec{\delta}^*)}\ , \tag{1.166}$$

$$(\vec{M}-\vec{z},\vec{\delta})^{-1,n}|_{(\vec{0},\vec{\delta}^*)} \ =_n\ (\vec{z}_{fix}(\vec{\delta}^*),\vec{\delta}^*)\ \forall \vec{\delta}^* \in I\!R^p\ . \tag{1.167}$$

The required inverse exists, since the linear part of the map $\vec{M}$ does not have 1 as an eigenvalue. To completely understand this notation, one has to keep in mind that δ^* is a vector of $I\!R^p$, whereas $(\vec{z},\delta)$ is the identity map in $I\!R^{2d+p}$. The transformations $\vec{A}_0$ and $\vec{A}_0^{-1}$ are therefore

$$\vec{A}_0 = \vec{z} - \vec{z}_{fix} \circ \delta\ ,\quad \vec{A}_0^{-1} = \vec{z} + \vec{z}_{fix} \circ \delta\ , \tag{1.168}$$

which are symplectic maps.

1.9 General Normal Form Theory

If a map is not order n symplectic or if its linear eigenvalues are degenerate, one can still try to transform it in such a way that its Taylor map to a given order has a simpler form, meaning that it has less non-vanishing coefficients. Such a transformation can be obtained from the general normal form procedure which will be lined out.

Definition 1.9.1 *Let a map $\vec{M} : \mathbb{C}^d \rightarrow \mathbb{C}^d$ be given and let its Jacobian at the origin be diagonalizable. The successive performance of the following n steps produces the general n^{th} order normal form transformation $\vec{A}$ of $\vec{M}$.*

1. *Find a linear map $\vec{A}_1$ such that the Jacobian of $\vec{A}_1 \circ \vec{M} \circ \vec{A}_1^{-1}$ is diagonal.*

2. *From $\vec{N}_{m-1} = \vec{A}_{m-1} \circ \ldots \circ \vec{A}_1 \circ \vec{M} \circ \vec{A}_1^{-1} \circ \ldots \circ \vec{A}_{m-1}^{-1,n}$, find $\vec{A}_m$ with the help of $\vec{T}_m$, which is given analogously to equation (1.20) by*

$$(T_{m,l}|\vec{k}) = \begin{cases} (N_{m-1,l}|\vec{k})/D_l(\vec{k}) & \text{if } D_l(\vec{k}) \neq 0 \\ 0 & \text{if } D_l(\vec{k}) = 0 \end{cases}\ , \tag{1.169}$$

where the previously used notation for Taylor coefficients is applied. $\vec{A}_m$ is given by

$$\vec{A}_m =_m \exp(\vec{T}_m^T\vec{\partial})\vec{z}\ ,\quad \vec{A}_m^{-1,n} =_m \exp(-\vec{T}_m^T\vec{\partial})\vec{z}\ . \tag{1.170}$$

where the exponential Lie operator is defined by the power expansion of the exp *function. To order m this yields*

$$\vec{A}_m =_m \vec{z} + \vec{T}_m\ ,\quad \vec{A}_m^{-1,n} =_m \vec{z} - \vec{T}_m\ . \tag{1.171}$$

As shown in section (1.3), equations (1.170) and (1.171) guarantee that $\vec{A}_m$ changes $\vec{N}_{m-1}$ in a suitable fashion to eliminate the highest possible number of

m^{th} order Taylor coefficients in $\vec{A}_m \vec{N}_{m-1} \vec{A}_m^{-1,n}$. Use this iteration from $m = 2$ to $m = n$.

In general this method leads to an n^{th} order polynomial map $\vec{A} =_n \vec{A}_n \circ \ldots \circ \vec{A}_1$ which simplifies the Taylor expansion of $\vec{M}$ by $\vec{N} =_n \vec{A} \circ \vec{M} \circ \vec{A}^{-1,n}$. For two special cases, we will specify further properties.

Definition 1.9.2 (General Resonance of Order m) *The d eigenvalues of a diagonalizable $d \times d$ matrix are said to be in general resonance of order m if there is a set of d integers with $\sum_{i=1}^{d} |k_i| = m + 1$ and $\prod_{i=1}^{d} \lambda_i^{k_i} = 1$.*

Following we will call a map diagonalizable when its Jacobian at the origin is diagonalizable.

Theorem 1.9.3 (Nonlinear Diagonalization) *If a diagonalizable map $\vec{M} : \mathbb{C}^d \to \mathbb{C}^d$ has linear eigenvalues which are not in general resonance to any order $m \leq n$, then there is a map and an order n inverse $\vec{A}$ and $\vec{A}^{-1,n}$ such that the polynomial map of order n with $\vec{N} =_n \vec{A} \circ \vec{M} \circ \vec{A}^{-1,n}$ is given by $N_l = \lambda_l z_l$.*

Proof: Due to the condition, there are no general resonances up to order n, and therefore all resonance denominators $D_l(\vec{k})$ do not vanish and the normal form process creates a map with no Taylor coefficients between order 2 and order n.

Theorem 1.9.4 *For a non-degenerate map $\vec{M} \in \mathcal{SP}_n^{2d}(\mathbb{R})$ with linear eigenvalues which are not in resonance to any order $m \leq n$, the formalism demonstrated in the proof of theorem (1.1.8) is equivalent to the general normal form transformation, if the linear matrix in step 1. of definition (1.9.1) is chosen to be symplectic and the eigenvalues are ordered such that $\lambda_{2j-1}\lambda_{2j} = 1$.*

Proof: The diagonalization with a symplectic matrix is identical to the diagonalization performed in section (1.2). To show that also step 2, the iteration to higher orders, is identical to the process in section (1.3), we have to show that

$$\exp(\vec{T}_m^T \vec{\partial}) \vec{z} = \exp(: t_m :) \vec{z} \tag{1.172}$$

with $\vec{\partial} t_m = J_{2d} \vec{T}_m$. This, however, is obvious, since the Poisson bracket is defined as $: t_m : f = \vec{\partial}^T t_m J_{2d} \vec{\partial} f = \vec{T}_m^T \vec{\partial} f$.

One can also restrict the formulated method to avoid small denominators when perturbations of order n symplectic maps are analyzed.

Definition 1.9.5 *Let a diagonalizable map $\vec{M} : \mathbb{R}^{2d} \to \mathbb{R}^{2d}$ have linear eigenvalues which are not in general resonance to any order $m \leq n$. The successive performance of the following n steps produces the restricted n^{th} order normal form transformation $\vec{A}$ of $\vec{M}$.*

1. *Find a linear map $\vec{A}_1$ such that the Jacobian of $\vec{A}_1 \circ \vec{M} \circ \vec{A}_1^{-1}$ is diagonal and $\lambda_{2j-1} = \lambda_{2j}^*$ for complex eigenvalues.*

2. *From $\vec{N}_{m-1} = \vec{A}_{m-1} \circ \ldots \circ \vec{A}_1 \circ \vec{M} \circ \vec{A}_1^{-1} \circ \ldots \circ \vec{A}_{m-1}^{-1,n}$, find $\vec{A}_m$ with the help of $\vec{T}_m$, which is given analogously to equation (1.20) by*

$$(T_{m,l}|\vec{k}) = \begin{cases} 0 & \text{if } k_{2j-1} - k_{2j} = \delta_{2j-1,l} \quad \text{for odd } l \\ 0 & \text{if } k_{2j} - k_{2j-1} = \delta_{2j,l} \quad \text{for even } l \\ (N_{m-1,l}|\vec{k})/D_l(\vec{k}) & \text{else} \end{cases} \tag{1.173}$$

and choose the maps $\vec{A}_m$ and $\vec{A}_m^{-1,n}$ as in equation (1.170).

This choice of $\vec{T}_m$ corresponds to the choice for order n symplectic maps given in equation (1.20), since here $(\vec{T}_m|\vec{k})$ is chosen 0 whenever $D_l(\vec{k})$ is 0 for an order n symplectic map. When the transformation procedure is performed successively up to

order n, the only Taylor coefficients which are not eliminated are such that $N_l = z_l(h_l \circ \vec{a})$ with $a_i = z_{2i-1}z_{2i}$. However, there are no special restrictions on the polynomials h_i of order $[(n-1)/2]$, since $\vec{M}$ was not assumed to be order n symplectic.

It is worthwhile to introduce a real restricted normal form. To do this, we first observe that $\vec{N} \in \mathcal{S}$ with the definition of $\mathcal{S}$ and $\mathcal{C}$ given in equation (1.80). The formal proof is lengthy and was already performed for order n symplectic maps when theorem 1.5.1 was proved. Therefore, it will only be mentioned that every step in that proof can be performed for the non-symplectic case, when the linear map $\vec{A}_1$ is chosen to be $I\!R^{2d} \to \mathcal{C}$. With the reasoning used for the order n symplectic case it follows also that $\vec{R} = \vec{C} \circ \vec{N} \circ \vec{C}^{-1}$ is a real map and we can write $\vec{R}$ with the structure

$$\begin{pmatrix} R_{2j-1} \\ R_{2j} \end{pmatrix} =_n (r \circ \vec{b}) \begin{pmatrix} \cos(\psi_j \circ \vec{b}) & -\sin(\psi_j \circ \vec{b}) \\ \sin(\psi_j \circ \vec{b}) & \cos(\psi_j \circ \vec{b}) \end{pmatrix} \begin{pmatrix} z_{2j-1} \\ z_{2j} \end{pmatrix} \tag{1.174}$$

for complex eigenvalues λ_{2j-1} and λ_{2j}, and

$$\begin{pmatrix} R_{2k-1} \\ R_{2k} \end{pmatrix} =_n r_k \circ \vec{b} \begin{pmatrix} g_k \circ \vec{b} & 0 \\ 0 & 1/(g_k \circ \vec{b}) \end{pmatrix} \begin{pmatrix} z_{2k-1} \\ z_{2k} \end{pmatrix} \tag{1.175}$$

for real eigenvalues. $\vec{b}$ again is given by $b_j = z_{2j-1}^2 + z_{2j}^2$ and $b_k = z_{2k-1}z_{2k}$.

Let $\vec{M} \in \mathcal{SP}_n^{2d}$ satisfy the conditions of theorem 1.5.4 on real symplectic normal forms and a perturbation of this map $\vec{M}_\epsilon$ be given. The restricted normal form procedure will obtain a normal form map $\vec{N}_\epsilon$ of $\vec{M}_\epsilon$ which is a perturbation of the order n symplectic normal form map $\vec{N}$. Then the r_j are close to one. In the case of complex eigenvalues, which have modulus one for $\vec{M}$, the motion described by $\vec{N}_\epsilon$ will not be on a circle but will slowly spiral away from the a circle.

Chapter 2

Long Term Estimates for Weakly Nonlinear Motion

Estimating the time of stable motion for planetary systems has first started the interest in the stability of weakly nonlinear mechanical systems. In accelerator physics this question became important with the introduction of storage rings. In large storage rings particles often have to be kept in the accelerator for up to a billion turns or more. The presented work contributes to the complex subject of stability analysis by providing a method which allows one to compute rigorous lower bounds on the time of stability in weakly nonlinear motion.

In the past, the question of long term stability in storage rings has been analyzed by various methods including kick tracking [Tal91], element by element tracking and one-turn map tracking [Ber88b, Yan91, KSZ92], symplectic long term generating function tracking [Ber88a, Ber91b, Yan93, Gja93], approximately symplectic tracking [KSYZ91], evaluation of Lyapunov exponents and tune shift analysis [Sch91], as well as Nekhoroshev estimates [Tur90]. The principle underlying the proof of the Nekhoroshev estimate [Nek77] was evaluated numerically to obtain lower bounds for the survival time. We will call this the pseudo invariant estimation (PIE) method [WR92]. Although some of these methods are useful analysis tools, they all fail to

give mathematically rigorous lower bounds on the time particles stay inside the accelerator when the motion is described by a nonlinear map. We will introduce the PIE method by using pseudo invariants of normal form theory. This method comes close to giving guaranteed lower bounds on the survival time. To make the bounds completely rigorous, an extension of the PIE method is introduced which can obtain such a rigorous bound on the turn number. The pseudo invariant needed for this method is computed via nonlinear normal form theory, which was described in detail in chapter (1). The bounds are made completely rigorous by performing the required optimizations with interval methods. The use of interval arithmetic seems imperative for any rigorous treatment of the stability problem, since any tracking method only tests a small part of phase space of measure zero. The functions that have to be optimized are far more complex than typical applications of interval optimization. Through the introduction of arithmetic on the new structure of interval chains (IC), one can exploit the special properties of the problem and enable interval optimization. Computations in this structure are performed by introducing a new data type into the FOXY language, which is the input language of COSY INFINITY [Ber90b, Ber92b, BZWH91, Ber93a, Ber94].

2.1 Introduction to the PIE Method

After a short review of stability analysis in weakly nonlinear systems, the PIE method will be introduced in detail. A section about normal form theory describes our choice of getting pseudo invariants. These nearly invariant functions of the one-turn map are essential for defining the beam region and for bounding the survival time. The importance of resonances and their influence on estimates of the survival time is discussed. Two refinements will be introduced which increase the obtainable bounds on long term stability. Up to that point, the PIE method assumes that the one-turn

map of the storage ring in question is well known. Since this is rarely the case, the theory has been extended to maps which depend on an unknown parameter.

The PIE method *hinges on efficient global optimization; when the required optimizations* are performed by scanning the relevant volumes in phase space, the method cannot be completely rigorous. An introduction into interval analysis and rigorous global optimization will be given, followed by the definition of interval chains. The concept of interval chains takes advantage of the special structure of the problem and is faster than conventional interval arithmetic optimization by many orders of magnitude for the special functions that have to be optimized.

Most of the demonstrated examples are described by polynomial maps. To analyze general weakly nonlinear motion, it is necessary to find a bound on the Taylor remainder of a weakly nonlinear system. We will estimate a bound on such remainders by comparing tracking and one-turn maps. Such an estimate, however, is not completely rigorous. Interval chains are a subcase of a method called differential algebra with remainder or RDA [BH94a]. Like DA, RDA enables computation of the Taylor expansion of a function, but in addition automatically gives a bound on the remainder of the Taylor expansion in a given interval of the function's domain. Toward the end, outlining possible improvements, it will be described how RDA can be used to also make the predictions for general maps completely rigorous.

2.1.1 History

The investigation of the stability of planetary motion has been an important question for over a century. After early attempts by Laplace and Lagrange to understand the stability of the solar system, Poincaré [Poi99], Birkhoff [Bir27], and Siegel [Sie52, Sie56], among others, investigated the problem in detail. Usually the problem of planetary motion was analyzed by considering it as a perturbation of a known and

solvable Hamiltonian system. Innovative investigations of this problem were achieved by Kolmogorov [Kol54], Arnol'd [Arn63], and Moser [Mos62]. Nekhoroshev formulated a theory which estimates the time of stability of a system with a perturbation strength proportional to ϵ by an exponential estimate. In reference [Nek77] the following theorem is proven: (citation from p. 4) "Suppose that H_0 satisfies certain steepness conditions, ... Then there are positive constants a, b, and ϵ_0 with the following property. Let $0 < \epsilon < \epsilon_0$. Then for every solution $I(t), \phi(t)$ of the system with the Hamiltonian $H_0(I) + \epsilon H_1(I, \phi)$, $|I(t) - I(0)| < \epsilon^b$ for all $t \in [0, T]$, where $T = \frac{1}{\epsilon} \exp(\frac{1}{\epsilon^a})$."

This theorem is proven by performing canonical transformations $(I, \phi) \rightarrow (J, \psi)$ in order to minimize the dependence of the Hamiltonian on ψ as much as possible, thus bringing the new coordinates J as close to invariants of motion as possible, which is called creating "almost integrals" in [Nek77] on page 21. The exponential estimate is established by a detailed analysis of this canonical transformation, which is performed in a perturbative way in respect to ϵ, and by finding the optimum order to which the transformation should be performed.

For certain problems concerned with general Hamiltonians, celestial mechanics, and also single particle motion in accelerators, the Nekhoroshev method of exponential estimates has been used by finding values a and b for the specific problem. Examples for accelerator physics can be found in [Tur90].

The idea of the proof of the Nekhoroshev estimate has prompted an analysis of stability of the nonlinear motion in particle accelerators by analyzing it in normal form space, a space in which the Hamiltonian has as little dependence on ψ as possible. In this space the change of the "almost integrals" or pseudo invariants is not estimated by bounding the series of canonical transformations but by performing the canonical transformations on the computer and then evaluating their effect on

the pseudo invariants. This possibility was first mentioned and programed by R. L. Warnock for maps obtained by interpolation of individual tracking points. Later it was realized that Hamiltonians are not needed when the one-turn map or Poincaré map of a storage ring is known [WRGE89, WR89]. One only has to find the maximum change δ of the nearly invariant function during one application of the transfer map of the accelerator. This maximum change over the relevant regions of phase space bounds the change of the pseudo invariant for the entire particle motion in this region. Several other improvements on the method of pseudo invariants were made; they include using maps which describe many turns in the accelerator and different means of finding canonical transformations to the pseudo invariant coordinates [WR91, War91]. Most of this work was done by R. L. Warnock and R. D. Ruth in the Stanford Linear Accelerator Center, the fullest account is found in reference [WR92].

Following, our approach to the PIE method will be described in detail and applied to several examples, thereafter it will be shown how the predictions can be made completely rigorous and examples will demonstrate the applicability of the method. Our approach was described in [HB92b, HB93a, HB93b, BH94b].

2.2 Pseudo Invariant Estimation (PIE)

Storage rings are designed to hold particles for a long time. For example, the Large Hadron Collider (LHC) at CERN will have to allow particles to circle the 27 km long tunnel for one day at one millionth of a percent less than the speed of light in order to make effective high energy physics experiments; this corresponds to 10^9 orbits around the ring. It was pointed out in [WR92] that, if one considers the effect of every magnet as a perturbation comparable to perturbations encountered during one year of planetary motion, then this stability requirement corresponds to 10^{12} years of

stability in the solar system, far more than the estimated age of the universe.

To ensure that the machine design is capable of holding the required numbers of particles for such a long time, it is important to develop methods which find out how long a particle with a given initial condition will remain inside the ring. This could be done by tracking the orbits of particles through 10^8 turns, which is far too time consuming with today's computing power to be performed accurately. Another disadvantage of this approach is that the stability of motion can only be checked for a limited number of particles. Furthermore, the computational inaccuracies can build up to an untolerable amount. There are, however, some programs available which follow this approach using kick approximations for the optical elements to speed up the computation [Tal91, Sch91].

Other approaches look at the one turn transfer map that relates initial phase-space coordinates $\vec{z}_i$ to final coordinates after one turn $\vec{z}_f = \vec{M}(\vec{z}_i)$. This one-turn map contains all information about particle motion after many turns, since many turns are described by successive action of the one-turn map. The transfer map can be approximated in different ways. Recently an appropriate choice of B-spline functions and Fourier series has been applied [BWRF93]. More commonly the Taylor expansion of the function is used. This has been done for light optics by Hamilton [Pra33] and was used for charged particle optics since the 1930s. TRANSPORT and many other more recent computer codes follow this concept. In [Ber87] it was recognized that Taylor arithmetic in a DA framework allows to do this to arbitrary order. For the theory behind the DA technique, please refer to the references [Ber92a, Ber91a, Ber90a, Ber89, Ber87, Ral81], and for different DA programs, refer to the references [Ber94, Mic94, Yan94b, vZ94]. Time considerations often restrict calculations to about order 12 [Yan94a]. The accuracy of the Taylor map approach increases with proximity to the closed orbit. Once the one turn map is obtained,

particles can be tracked through the map to find out how long they stay inside the accelerator. Applying high order maps the required number of turns can still be very time consuming and, as in the case of element by element tracking, the stability can only be checked for a very limited number of particles.

The PIE method analyzes the one-turn map directly without tracking through it several times, which in particular avoids computational inaccuracies. Furthermore this method does not only test single particles but provides information about all particles in a given region of phase space.

We assume that there is a closed orbit in the ring. Particles with phase space coordinates near the closed orbit will not be lost, particles which are too far away from the closed orbit will be lost during their motion around the ring. We therefore divide the phase space $\mathcal{P}$ into the allowed region $\mathcal{A}$ and the forbidden region $\mathcal{P}\backslash\mathcal{A}$.

The question we want to answer is: How many turns does a particle which originates in a given region of phase space $\mathcal{O}$ circle the ring without leaving the accelerator. We therefore look for the number

$$N_{\max} = \max\{n | \vec{M}^n(\mathcal{O}) \subseteq \mathcal{A}\} \ , \tag{2.1}$$

where $\vec{M}^n(\mathcal{O}) = \{\vec{M}^n(\vec{z}) | \vec{z} \in \mathcal{O}\}$, and $\vec{M}^n(\vec{z})$ stands for n applications of $\vec{M}$. The different regions are shown in figure (2.1a). With the following method we will find a strict lower bound N for $N_{\max}$.

If we find a real valued test function f that does not have common values in $\mathcal{O}$ and in $\mathcal{P}\backslash\mathcal{A}$, then successive action of the map must bridge a gap Δf as shown in figure (2.1b) in order to map a $\vec{z} \in \mathcal{O}$ into $\mathcal{P}\backslash\mathcal{A}$. Particles start to bridge this gap by entering the phase-space region $\mathcal{S}_i = \vec{M}(\mathcal{O})\backslash\mathcal{O}$. The gap is bridged when a particle has reached the region $\mathcal{S}_f = \vec{M}(\mathcal{A})\backslash\mathcal{A}$. If $\mathcal{S}_i$ or $\mathcal{S}_f$ are empty, particles in $\mathcal{O}$ will never leave $\mathcal{A}$. If they are not empty, the gap goes from f_i to f_f with $f_i = \max\{f(\vec{z}) | \vec{z} \in \mathcal{S}_i\}$

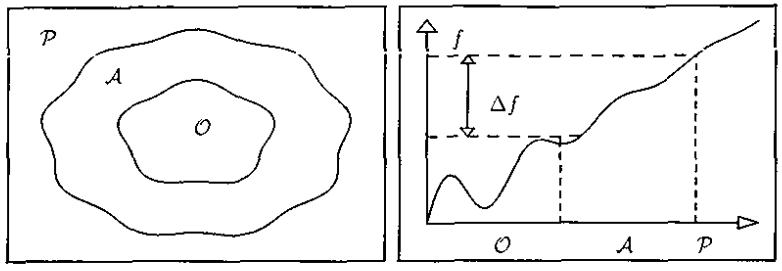

Figure 2.1: a) The initial region $\mathcal{O}$ and the allowed region $\mathcal{A}$ of phase space $\mathcal{P}$ with $\mathcal{O} \subset \mathcal{A} \subset \mathcal{P}$. b) The gap Δf that has to be bridged.

and $f_f = \min\{f(\vec{z}) | \vec{z} \in \mathcal{S}_f\}$. The function

$$d_f = f(\vec{M}) - f \tag{2.2}$$

describes how much f deviates from being an invariant of the map $\vec{M}$; d_f is called deviation function. When a phase space point $\vec{z}$ is mapped through $\vec{M}$ once, the gap Δf is diminished by $d_f(\vec{z})$. If we assume $f_f \geq f_i$, the step from f_i towards f_f is always smaller or equal to

$$\delta = \max\{d_f(\vec{z}) | \vec{z} \in (\mathcal{A} \backslash \mathcal{O})\} \quad . \tag{2.3}$$

A particle that starts in $\mathcal{O}$ therefore survives at least N turns, where

$$N = [\frac{f_f - f_i}{\delta}] \leq N_{max} \quad . \tag{2.4}$$

We are thus left with four problems:

1. finding a suitable test function f such that N becomes favorable,
2. finding f_i, the maximum of f on $\mathcal{S}_i$,
3. finding f_f, the minimum of f on $\mathcal{S}_f$,

4. finding δ, the maximum of the deviation function in the appropriate region.

To make the desired estimate as large as possible, we should find a function f which increases between the allowed and the forbidden region and should, at the same time, be close to an invariant of the one-turn map to make δ as small as possible.

The remaining three problems are concerned with finding maxima. These maxima can be found in a mathematically rigorous way using interval arithmetic, which will be explained in chapter (4). Doing this would, together with equation (2.4), give a mathematically rigorous estimate for the survival time of particles propagated by the given one turn Taylor map; this will be described in a later section. First we have to choose a suitable pseudo invariant f, and we are faced with the problem of describing the phase space regions $\mathcal{O}$ and $\mathcal{A}$ in a sensible way. We will use nonlinear normal form theory on Taylor maps to solve both problems.

2.3 Normal Form Transformations and Pseudo Invariants

Normal form theory for general order n symplectic maps is treated in detail in chapter (1). In the context of the PIE method we are only interested in the special case of stable linear motion, which means that all linear eigenvalues have modulus one. The phases of the linear eigenvalues are the tunes of the system, with $\lambda_{2j-1} = \exp(i2\pi\nu_j)$, $j \in \{1, \ldots, d\}$ for d degrees of freedom. For this special case, the definition (1.1.5) of resonances reduces to the well known resonance conditions for the tunes.

Definition 2.3.1 (Resonance of Order m for linearly stable systems)
The d tunes ν_i of a non degenerate stable symplectic $2d \times 2d$ matrix, are said to be in resonance of order m if there is a set of d integers k_i with $\sum_{i=1}^{d} |k_i| = m + 1$ and $\sum_{i=1}^{d} k_i \nu_i = 0 \pmod 1$.

Theorem 2.3.2 (Normal Forms for Linearly Stable Maps)

A non-degenerate linearly stable map $\vec{M} \in \mathcal{SP}_n^{2d}(\mathbb{R})$ *with tunes which are not in resonance to any order* $\leq n$ *can be transformed by a transformation* $\vec{B} \in \mathcal{SP}_n^{2d}(\mathbb{R})$ *to* $\vec{R} =_n \vec{B} \circ \vec{M} \circ \vec{B}^{-1,n} \in \mathcal{SP}_n^{2d}(\mathbb{R})$ *and*

$$\begin{pmatrix} R_{2j-1} \\ R_{2j} \end{pmatrix} =_n \begin{pmatrix} \cos\{\psi_j(\vec{b})\} & -\sin\{\psi_j(\vec{b})\} \\ \sin\{\psi_j(\vec{b})\} & \cos\{\psi_j(\vec{b})\} \end{pmatrix} \begin{pmatrix} z_{2j-1} \\ z_{2j} \end{pmatrix} . \tag{2.5}$$

The map $\vec{b} : \mathbb{R}^d \to \mathbb{R}^d$ *is given by* $b_j = z_{2j-1}^2 + z_{2j}^2$. *These functions* b_j *are order* $n+1$ *invariants of the map* $\vec{R}$ *and the polynomial of order* $n+1$ *given by* $I_j =_{n+1} b_j(\vec{B})$ *are order* $n+1$ *invariants of the map* $\vec{M}$.

Please refer to the section on symplectic normal forms for the proof of this theorem, which is just a restricted form of theorem (1.5.4). It can immediately be seen that

$$b_j(\vec{R}) =_{n+1} b_j , \tag{2.6}$$

which means that the functions b_j are order $n+1$ invariants of $\vec{R}$. In a similar vain we write

$$I_j(\vec{M}) =_{n+1} b_j \circ \vec{B} \circ \vec{M} =_{n+1} b_j \circ \vec{R} \circ \vec{B} =_{n+1} b_j \circ \vec{B} =_{n+1} I_j . \tag{2.7}$$

Up to order n, the motion in normal form coordinates is described by rotations. The amplitudes of these rotations are invariant up to order $n+1$. The proof given in chapter (1) demonstrates a method which allows direct computation of the normal form maps. During the calculations, Taylor terms of M_l have to be divided by the resonance denominators $D_l(\vec{k})$ with

$$D_l(\vec{k}) = \exp(i2\pi\nu_l) - \exp(i2\pi \sum_{i=1}^{d} k_i\nu_i) . \tag{2.8}$$

Since the resonance denominators vanish at resonances below order $n+1$, the theorem on symplectic normal forms excludes tune resonances. However, it can be shown that

there is no problem with resonances of the linear eigenvalues when the map $\vec{M}$ is the Taylor map of a system which has d exact invariants of motion.

To illustrate the normal form transformation, the motion in phase space for 2000 turns in a typical accelerator is shown in the left part of figure (2.2). For each turn, the horizontal position x as well as its canonical conjugate momentum a is displayed. The finite width and the irregular structure of the band is a result of nonlinear effects and of coupling to the other degree of freedom, the motion in vertical direction. From the picture one can see that the particle positions are bounded for the number of turns shown. However, it is very difficult to estimate if particles are on average moving away from the origin or not and what would happen if the number of turns were increased. The right picture in figure (2.2) shows the same motion after transformation by the normal form map. The motion now has nearly circular shape, which will make it *much easier to estimate the long term stability.*

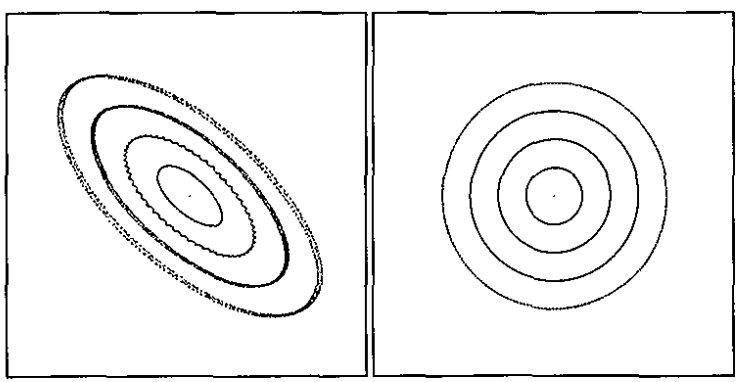

Figure 2.2: Phase Diagram for 2000 turns in an accelerator for four initial conditions. The left picture shows the motion displayed in standard particle optical coordinates x and a, and the right picture shows the same motion in normal form coordinates.

2.4 Maps to Test the Method

We will use six different maps to test the normal form invariants and the PIE method with and without interval optimization. Two of these example maps have one degree of freedom and four have two degrees of freedom. One map on two and one on four dimensional phase space is known to have completely stable motion; these maps are suitable to check what PIE yields for systems where infinite survival times can be guaranteed by analytic calculations.

2.4.1 The Physical Pendulum

A pendulum of length l and mass m in an uniform acceleration g is used as a model for stable motion in two dimensional phase space. The chosen position coordinate x is the arc length of the pendulum's elongation. The Hamiltonian is given by

$$H = \frac{p^2}{2m} - mgl\cos(\frac{x}{l}) . \tag{2.9}$$

In order to compare this motion to motion in an accelerator, we transform from the time t to a length s as independent variable, p_{max} is the maximum momentum for bound motion,

$$s = t\frac{p_{max}}{m} = 2t\sqrt{gl} . \tag{2.10}$$

Furthermore, we introduce the dimensionless canonical momentum $a = p/p_{max}$. With these coordinates and the independent variable s, the motion is canonical for the new Hamiltonian

$$G = \frac{m}{p_{max}^2}H(x, ap_{max}) = \frac{a^2}{2} - \frac{1}{4}\cos(\frac{x}{l}) . \tag{2.11}$$

The motion is governed by Hamilton's equations

$$\frac{d}{ds}x = \partial_a G , \quad \frac{d}{ds}a = -\partial_x G , \tag{2.12}$$

and the linear map becomes

$$\begin{pmatrix} x_f \\ a_f \end{pmatrix} = \begin{pmatrix} \cos(2\pi\nu) & 2l\sin(2\pi\nu) \\ -\frac{1}{2l}\sin(2\pi\nu) & \cos(2\pi\nu) \end{pmatrix} \begin{pmatrix} x_i \\ a_i \end{pmatrix} , \quad \nu = \frac{s}{4\pi l} . \tag{2.13}$$

The phase ν corresponds to the tune in an accelerator and the invariant ellipse of linear motion is given by

$$I_1(x, a) = \frac{x^2}{2l} + 2la^2 = \epsilon . \tag{2.14}$$

when the emittance is $\epsilon\pi$. This invariant of the linear map agrees up to order 2 with the order $n+1$ invariant I_1 of the n^{th} order map. In the examples to follow, we chose an emittance of $\epsilon = 10{,}000$ mm mrad and a tune of $\nu = 0.379$ if not stated specifically. The nonlinear map is computed by evaluating the exponential Poisson-bracket operator acting on the identity up to order n:

$$\vec{M} = \exp(- : 4\pi\nu l G :)\vec{z} . \tag{2.15}$$

As introduced in theorem (1.3.4), $: f : g$ denotes the Poisson bracket between f and g. If not specifically stated, we will use order 8 in the examples.

2.4.2 Henon Map for One Degree of Freedom

The Henon map [LL83] is a standard test case for the analysis of nonlinear motion, because it exhibits many phenomena encountered in Hamiltonian nonlinear dynamics. These include stable and unstable regions, chaotic motion, and elliptic fixed points. The Henon map can even serve as a very simplistic model of an accelerator under the presence of sextupoles for chromaticity correction. The figures (2.3a,b) show typical tracking pictures for the Henon map

$$\begin{pmatrix} x_f \\ a_f \end{pmatrix} = \begin{pmatrix} x \\ a + kx^2 \end{pmatrix} \circ \begin{pmatrix} \cos(2\pi\nu)x_i + \sin(2\pi\nu)a_i \\ -\sin(2\pi\nu)x_i + \cos(2\pi\nu)a_i \end{pmatrix} , \tag{2.16}$$

which is a composition of a kick map and a rotation.

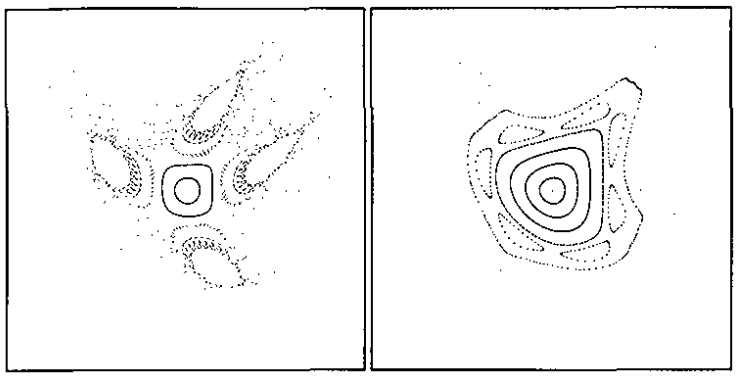

Figure 2.3: 9 particles tracked for 500 turns through the Henon map. The starting conditions were $x = 0.1 \cdot j$, $j \in \{1, \ldots, 9\}$ and the kick strength was 1.1. The tune in figure a) is 0.255 and in figure b) 0.29.

Since kicks and rotations are symplectic, the Henon map is symplectic. One can find Hamiltonians which have the Henon map as time step one map, for example,

$$H = \pi\nu\{x^2 + a^2 - 2(tk)ax^2 + (tk)^2x^4\} - \frac{1}{3}kx^3 \,. \tag{2.17}$$

However, it is not possible to find a time independent Hamiltonian, since in general the Henon map does not have an invariant of motion. To compare with accelerators, the tune corresponds to ν and the linear invariant ellipse for emittance $\epsilon\pi$ is $I_1(x, a) =_2 x^2 + a^2 = \epsilon$. In the examples the emittance will be chosen to be 10,000mm mrad and the tune will be $\nu = 0.379$ if nothing different is stated specifically.

2.4.3 Coupled Pendulum

Coupling two pendulums is not very suitable for comparison with an accelerator, since in linear approximation the motion does not decouple for a natural choice of coordinates, whereas in accelerators the linear motion in horizontal and vertical direction typically decouples. We therefore choose a physical pendulum with an elastic string,

a bungee jumping point mass, so to say, which behaves corresponding to mid–plane symmetry. The figure (2.4a) shows typical tracking pictures for this pendulum. The motion must be bound for small enough amplitudes, since the energy is a Lyapunov function [Lya92].

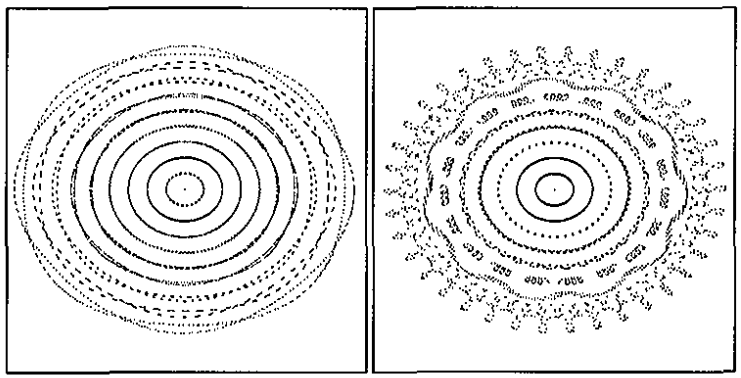

Figure 2.4: 9 particles tracked for 500 turns through the coupled pendulum. The starting conditions were angles $x/l_0 = 0.01 \cdot j$ for $j \in \{1, \ldots, 9\}$. This corresponds to a maximum emittance of 4050mm mrad. The horizontal and vertical tunes in figure a) are 0.36 and 0.78, and in figure b) 0.37 and 0.78.

The pendulum has a relaxation length $\tilde{l}_0$ and is elongated at rest by Δ to the rest length $l_0 = \tilde{l}_0 + \Delta$. The canonical positions are x, the angle times l_0, and y, the elongation from the rest length. Lagrange's formalism leads to the conjugated momenta $p_x = m\dot{x}(1 + y/l_0)^2$ and $p_y = m\dot{y}$. The Hamiltonian is given by

$$H = \frac{1}{2m}(p_y^2 + \frac{p_x^2}{(1 + y/l_0)^2}) - mg(l_0 + y)\cos(\frac{x}{l_0}) + \frac{mg}{2\Delta}(y + \Delta)^2 \,. \tag{2.18}$$

The frequencies of linear motion are $\omega_x = \sqrt{g/l_0}$ and $\omega_y = \sqrt{g/\Delta}$. Like for the physical pendulum in subsection (2.4.1), normalized coordinates will be introduced. The maximum momentum for bound motion is $p_{max} = 2m\sqrt{gl_0}$ and

$$s = t\frac{p_{max}}{m} \,, \quad a = \frac{p_x}{p_{max}} \,, \quad b = \frac{p_y}{p_{max}} \,, \quad G = \frac{m}{p_{max}^2}H \,. \tag{2.19}$$

The new Hamiltonian is

$$G = \frac{1}{2}(a^2 \frac{1}{(1+y/l_0)^2} + b^2) - \frac{1+y/l_0}{4}\cos(\frac{x}{l_0}) + \frac{(y+\Delta)^2}{8\Delta l_0} . \quad (2.20)$$

As in equation (2.15), the Taylor map is computed by $\vec{M} =_n \exp(-:sG:)\vec{z}$. In linear approximation, the map is given by

$$\begin{pmatrix} x_f \\ a_f \end{pmatrix} = \begin{pmatrix} \cos(2\pi\nu_x) & 2l_0\sin(2\pi\nu_x) \\ -\frac{1}{2l_0}\sin(2\pi\nu_x) & \cos(2\pi\nu_x) \end{pmatrix} \begin{pmatrix} x_i \\ a_i \end{pmatrix} , \quad (2.21)$$

$$\begin{pmatrix} y_f \\ b_f \end{pmatrix} = \begin{pmatrix} \cos(2\pi\nu_y) & 2\sqrt{l_0\Delta}\sin(2\pi\nu_y) \\ -\frac{1}{2\sqrt{l_0\Delta}}\sin(2\pi\nu_y) & \cos(2\pi\nu_y) \end{pmatrix} \begin{pmatrix} x_i \\ a_i \\ y_i \\ b_i \end{pmatrix} . \quad (2.22)$$

The tunes depend on the independent parameters and their ratio depends on the parameter of the pendulum,

$$\nu_x = \frac{s}{4\pi l_0} , \quad \nu_y = \nu_x\sqrt{\frac{l_0}{\Delta}} . \quad (2.23)$$

The invariant ellipses corresponding to the emittances $\epsilon_x\pi$ and $\epsilon_y\pi$ are

$$\frac{x^2}{2l_0} + 2l_0a^2 = \epsilon_x, \quad \frac{y^2}{2\sqrt{l_0\Delta}} + 2\sqrt{l_0\Delta}b^2 = \epsilon_y . \quad (2.24)$$

If not mentioned differently, the pendulum will have length $l_0 = 1m$, tunes $\nu_x = 0.17$, $\nu_y = 0.91$, emittances of 3000πmm mrad, and its map will be evaluated up to order 8.

2.4.4 The IUCF Ring

As an example storage ring, we used the ring of the Indiana University Cyclotron Facility (IUCF). The electron cooling device and the RF system were not used, since we want to compute the stability of motion when no such devices are present. The device is usually used for emittances of 0.3π mm mrad, which are made so small by electron cooling. Since we want to analyze operation without cooling, we assumed

$\epsilon_x = 3.7\pi$mm mrad and $\epsilon_y = 2.2\pi$mm mrad if not otherwise stated. The uncertainty of the first magnet's strength is assumed to be 0.01% and the linear tunes are chosen to be $\nu_x = 0.7727$ and $\nu_y = 0.6650$ in the examples shown.

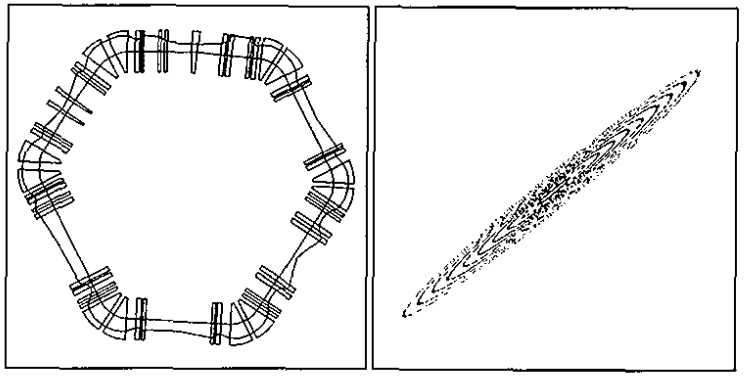

Figure 2.5: a) Layout of the IUCF ring, only dipoles and quadrupoles are shown. b) x-p_x phase space positions for 500 turns. The initial conditions are $(x = 5j, y = 5)\cdot 10^{-4}$ with $j \in \{1, \ldots, 10\}$.

2.4.5 The PSR II Ring

A second example storage ring is the PSR II, which was designed as a possible upgrade of PSR at the Los Alamos Meson Physics Facility (LAMPF). This device was analyzed for emittances of 40πmm mrad and for a uncertainty in the strength of the first magnet of 0.01%. The linear tunes are chosen to be $\nu_x = 0.2313$ and $\nu_y = 0.2705$.

2.4.6 The Demo Ring

The third storage ring which will be analyzed is a simple example ring. It consists of three identical cells. Every cell is mirror symmetric in the elements which influence the first order. The dispersion also is symmetric, which makes each cell an achromat.

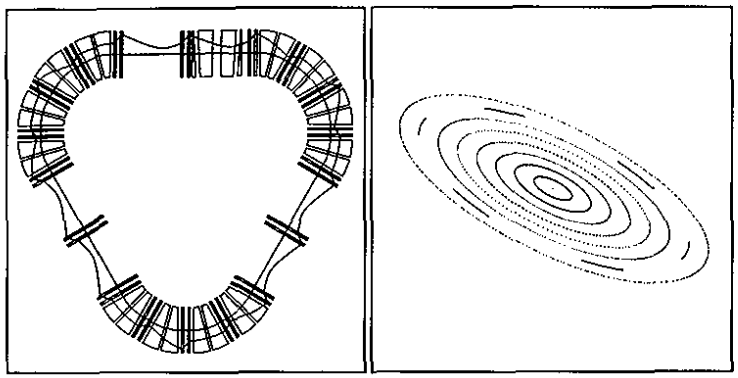

Figure 2.6: a) Layout of the PSR II ring, only dipoles and quadrupoles are shown. b) x–p_x phase space positions for 500 turns. The initial conditions are $(x = 5 \cdot j, y = 5 \cdot j) \cdot 10^{-3}$ with $j \in \{1, \ldots, 8\}$.

The chromaticities, which describe the linear dependence of the tunes on energy, are canceled by two hexapoles and the effect of nonlinear resonances is reduced by two further hexapoles. These hexapoles are adjusted by reducing the nonlinear resonance strength which can be computed by the normal form method. The 12 hexapoles are not shown in figure (2.7). This device was analyzed for emittances of $\epsilon_x = 5\pi$ mm mrad $\epsilon_y = 7\pi$ mm mrad and for an uncertainty in the first quadrupole of 0.01%. The linear tunes are $\nu_x = 0.37$ and $\nu_y = 0.67$. If not otherwise stated, the transfer map of the Demo ring will be evaluated to 8^{th} order.

2.5 The Pseudo Invariant and How to Parameterize Regions

Describing the initial region and the allowed region is essential to finding $\mathcal{S}_i$ and $\mathcal{S}_f$ and therefore to finding a function that changes substantially between those two regions. Accelerators, usually have mid-plane symmetry, which implies that the linear map

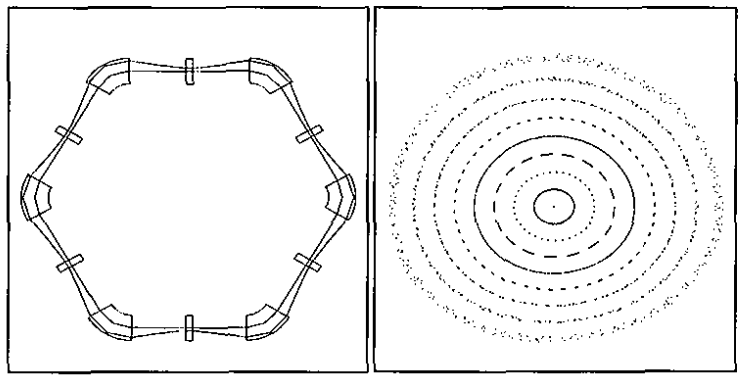

Figure 2.7: a) Layout of the Demo ring, only dipoles and quadrupoles are shown. b) x–p_x phase space positions for 500 turns. The initial conditions are $(x = 5 \cdot j, y = 5 \cdot j) \cdot 10^{-3}$ with $j \in \{1, \ldots, 8\}$.

does not couple the x–p_x and y–p_y component of motion. The projection of the linear motion of beam particles in the x–p_x subspace lies on invariant ellipses. The area of these ellipses is called the x and y emittances of the beam. Since the product of two ellipses is topologically a torus, the linear motion is said to lie on an invariant torus. The allowed region for a beam in a storage ring is typically given by the acceptance in the x–p_x phase space and the y–p_y phase space.

The x and y acceptances are defined as the largest invariant ellipses that can be transported through the accelerator in the horizontal and vertical plane respectively. The reason for giving the acceptance as an invariant ellipse is described as a peel-off effect. After every turn, a particle is on the same invariant ellipse in the x and y section of phase space. Turn by turn the particle's position rotates around these ellipses. The angles of these rotations, which are 2π times the tunes, are chosen not to be a fraction of 2π to avoid resonances. If some obstacle in the beamline touches an ellipse, sooner or later all particles on this ellipse will hit this obstacle and get lost.

Any obstacle therefore peels off particles lying outside an invariant ellipse.

The rotations in nonlinear normal form theory correspond to the concept of rotations on the invariant ellipses. It is therefore natural and follows from the same argument that in a nonlinear theory the allowed region or nonlinear acceptance $\mathcal{A}$ should be given by a nonlinear invariant of the map, which can be computed by normal form theory. According to theorem (1.4.4), normal form theory gives, one invariant circle for each of the d degrees of freedom.

The pictures a) and b) in figure (2.8) describe the nonlinear invariants which specify the boundary of the allowed region. Since the linear contribution in the map dominates, they are close to invariant ellipses of linear motion.

There are many different invariant surfaces which can be described by the d nonlinear invariants I_i. The two most suitable ways will be discussed here:

$$\mathcal{A}_\circ = \{\vec{z}|\sum_{i=1}^{d} I_i(\vec{z})/\epsilon_i \leq 1\} , \tag{2.25}$$

$$\mathcal{A}_\square = \{\vec{z}|I_i(\vec{z}) \leq \epsilon_i,\ \forall i \in \{1,\ldots,d\}\} . \tag{2.26}$$

The corresponding beam shape is expressed in figure (2.8c) by drawing the biggest allowed x and y coordinates. Elliptic beam shapes correspond to $\mathcal{A}_\circ$ and rectangular beam shapes correspond to $\mathcal{A}_\square$. To keep the notation simple, we describe the initial region $\mathcal{O}$ in a similar way with nonlinear emittances $\alpha\epsilon_i\pi$, where $\alpha < 1$. The boundaries are most easily described when a norm is introduced which measures the distance from the closed orbit according to the invariant torus on which the particle moves in n^{th} order approximation. If we want to represent the beam by a round shape, we choose $||\vec{z}||_\circ$, while if we want to describe it by a rectangle, we choose $||\vec{z}||_\square$, where

$$||\vec{z}||_\circ = \sum_{i=1}^{d} \frac{I_i(\vec{z})}{\epsilon_i} , \quad ||\vec{z}||_\square = \max\{\frac{I_i(\vec{z})}{\epsilon_i}, i \in \{1,\ldots,d\}\} . \tag{2.27}$$

In real normal form space, to which the transformation $\vec{B}$ in theorem (2.3.2) leads, the beam region can be suitably represented by a set of invariant tori. These tori can be transformed into phase space by the order n inverse $\vec{B}^{-1,n}$. We parameterize such a curve by the emittances ϵ_i which describe the torus in normal form space by writing

$$\mathcal{T}(\vec{\epsilon}) = \{\vec{B}^{-1,n}(\vec{z})|\begin{pmatrix} z_{2i-1} \\ z_{2i} \end{pmatrix} = \sqrt{\epsilon_i}\begin{pmatrix} \cos(\phi_i) \\ \sin(\phi_i) \end{pmatrix}, \phi_i \in [0,2\pi], \forall i \in \{1,\ldots,d\}\} , \tag{2.28}$$

With this notation, we can introduce regions in phase space which can describe the initial region and the allowed region. Let

$$\mathcal{F}_\circ(\xi,\zeta) = \{\vec{z}|\vec{z} \in \mathcal{T}(\vec{\eta}), \xi \leq \sum_{i=1}^{d} \frac{\eta_i}{\epsilon_i} \leq \zeta\} , \tag{2.29}$$

$$\mathcal{F}_\square(\xi,\zeta) = \{\vec{z}|\vec{z} \in \mathcal{T}(\vec{\eta}), \xi \leq \frac{\eta_i}{\epsilon_i} \leq \zeta, \forall i \in \{1,\ldots,d\}\} , \tag{2.30}$$

then the regions of interest are given by

$$\mathcal{O}_s = \mathcal{F}_s(0,\alpha) , \quad \mathcal{A}_s = \mathcal{F}_s(0,1) , \quad s \in \{\circ,\square\} . \tag{2.31}$$

Since $\vec{B}^{-1,n}$ is an order n inverse of $\vec{B}$, this definition is approximately the same as $||\vec{z}||_s \leq \zeta$ or $||\vec{z}||_s \leq \zeta$ with $\zeta \in \{\alpha,1\}$: therefore, the pseudo invariant $||\vec{z}||_s$ fluctuates very little on the surfaces of $\mathcal{O}_s$ and $\mathcal{A}_s$. Phase space points in the regions of interest are easily parameterized by the choice of the ϕ_i and η_i.

It is worthwhile to note that the first order inverse $\vec{B}^{-1,1}$ is the exact inverse of the first order of $\vec{B}$. $\vec{B}^{-1,1}$ transforms circles into invariant ellipses of linear motion. Therefore, when $n = 1$ is chosen in equation (2.28), then the conventional definition of the acceptance is obtained. Since the polynomial map $\vec{B}^{-1,n}$ is continuous, it maps closed regions of normal form space into closed regions of phase space. Therefore, this definition of the acceptance is meaningful: particles can never leave the region of $\mathcal{F}_s(0,\zeta)$ without crossing the surface $\mathcal{F}_s(\zeta,\zeta)$.

To make the desired estimate as large as possible, we should find a function f which tends to increase when the norm increases and should at the same time be close to an invariant to make δ in equation (2.3) as small as possible. The appropriate choice is $f_\circ(\vec{z}) = ||\vec{z}||_\circ$ and $f_\square(\vec{z}) = ||\vec{z}||_\square$.

There are three reasons which suggest the use of $f_\circ$. First, for d degrees of freedom, evaluating $f_\square$ takes d times longer than evaluating $f_\circ$, since d pseudo invariants have to be evaluated, whereas for $f_\circ$, the polynomials I_i/ϵ_i can be summed before evaluation. Second, since the beamline is generally circular, it seems more appropriate to choose this notation. A third reason comes from a somewhat heuristic argument. The figures (2.9) shows that the average invariant defects $I_i(\vec{M}) - I_i$ are of the same order of magnitude on the surface of $\mathcal{A}_\circ$, whereas they fluctuate substantially on the surface of $\mathcal{A}_\square$. If one accepts the heuristic view that bad pseudo invariants in the normal form picture are an indication of a low live time of beam particles, then it is more appropriate to specify the beam shape by $||\vec{z}||_\circ$. Following, the quantities with the circular subscript will be used and the subscript will be dropped.

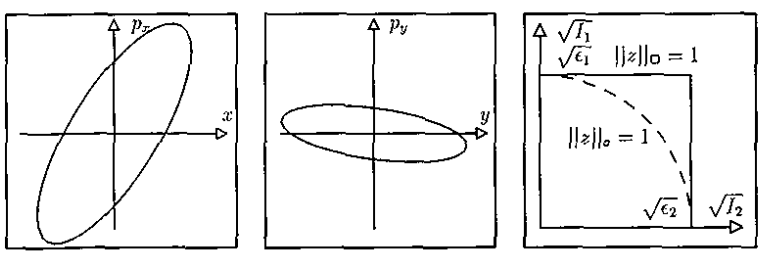

Figure 2.8: The motion on nonlinear invariants in the phase space section x-p_x in figure a) and y-p_y in figure b). The allowed and the forbidden region and the definition of $||\vec{z}||$ is depicted in figure c).

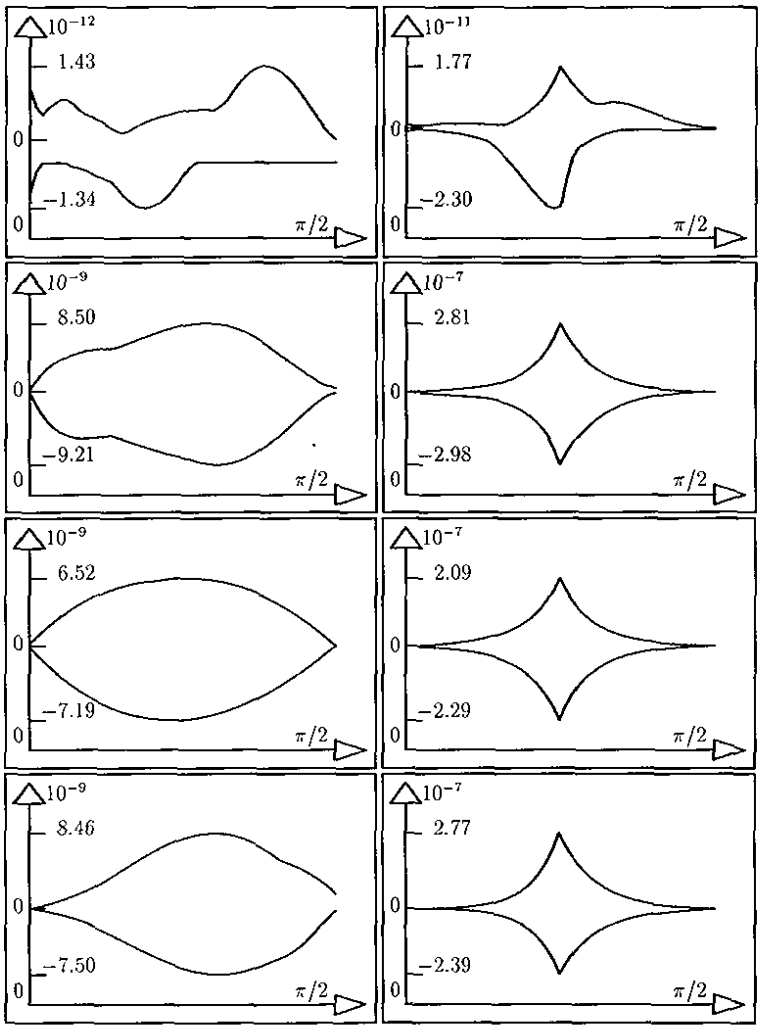

Figure 2.9: Fluctuation of the pseudo invariant on the surface of the allowed region. Elliptic beam shapes ($s = \circ$) and rectangular beam shapes ($s = \square$) were used for the left and the right picture respectively. The four cases and the emittances used are the coupled pendulum ($\epsilon_1 = 0.6\epsilon, \epsilon_2 = 0.4\epsilon$), the IUCF ring ($\epsilon_1 = 0.3\epsilon, \epsilon_2 = 0.7\epsilon$), the PSR II ($\epsilon_1 = 0.05\epsilon, \epsilon_2 = 0.95\epsilon$), and the Demo ring ($\epsilon_1 = 0.4\epsilon, \epsilon_2 = 0.6\epsilon$).

2.6 Analysis of Pseudo Invariants

The PIE method relies on the choice of the function f, which should be as close as possible to invariant under application of the map $\vec{M}$. In order to get a sense how well the order $n+1$ invariants of the normal form transformation are invariant under $\vec{M}$, typical cases were tested. These cases are the six systems described in section (2.4).

In figure (2.10) the invariant defect is shown for the physical pendulum. The deviation function $d_f = f(\vec{M}) - f$ with the pseudo invariant f was plotted over the region in phase space parameterized with equation (2.29).

The coordinate axes in the picture are polar coordinates $\sqrt{\epsilon}$ and ϕ. In high orders the invariants are extremely accurate. This accuracy is only possible because the physical pendulum has an exact invariant, the new Hamiltonian G of equation (2.11).

In table (2.1) the smallest resonance denominators in every order up to order 10 are displayed for the Physical pendulum and the Henon map. The denominators are equivalent for these two examples, since we chose $\nu = 0.379$ for both. All resonance denominators have absolute values which are sufficiently big to avoid divisions by dangerously small numbers. However, the normal form transformation requires successive divisions by these denominators and after multiple divisions, very big and inaccurate coefficients can occur in the normal form map. This fact however will not have an influence on the reliability of predictions given by the PIE method, since no exact invariants are required.

Also for depicting the invariant defect for the Henon map, polar coordinates $\sqrt{\epsilon}$ and ϕ were used. The accuracy of the pseudo invariants is less than for the pendulum, since no exact invariants exist.

Order	k	$e^{i2\pi\nu} - e^{i2\pi k\nu}$
2	2	0.9028227
3	3	0.5087166
4	4	0.8742662
5	5	1.2475892
6	6	1.5756998
7	7	1.8120295
8	8	1.9230358
9	9	1.8929639
10	10	1.7260816

Table 2.1: Smallest resonance denominators for the physical pendulum and the Henon map with a tune of 0.379.

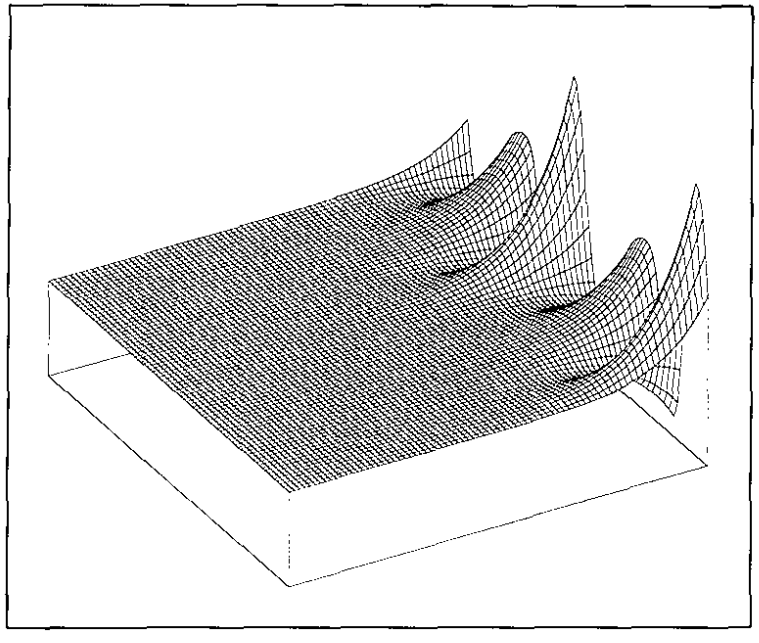

Figure 2.10: Invariant defect for the physical pendulum on an invariant ellipse. The coordinates are 0 to ϵ from left to right and 0 to 2π from front to back. The range of the depicted function is $[-2.36 \cdot 10^{-12}, 5.63 \cdot 10^{-12}]$.

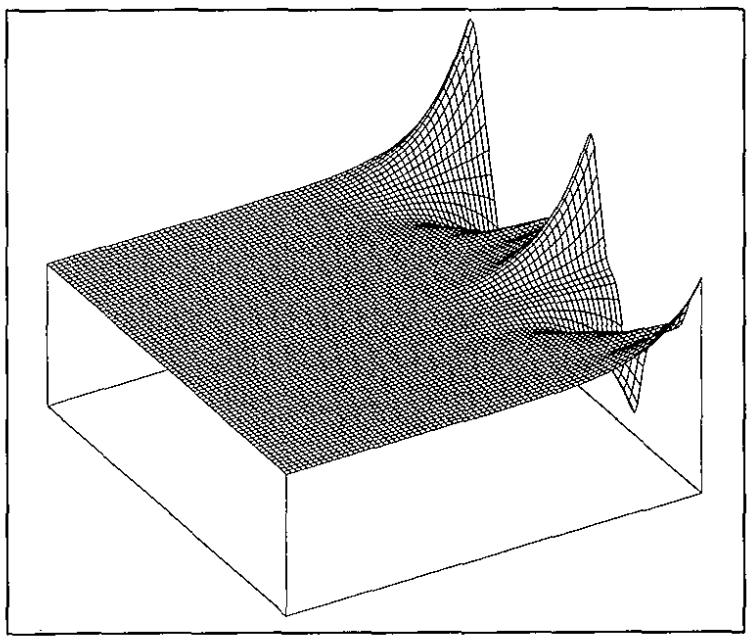

Figure 2.11: Invariant defect for the Henon map on an invariant ellipse. The coordinates are 0 to ϵ from left to right and 0 to 2π from front to back. The range of the depicted function is $[-5.59 \cdot 10^{-8}, 5.56 \cdot 10^{-8}]$.

The other four examples are systems for four dimensional phase space. We will therefore depict the invariant defect on a torus $\mathcal{T}(\vec{\epsilon})$. The coordinates in the figures are the angles ϕ_1 and ϕ_2 which parameterize this surface. In figure (2.12) the invariant defect is shown for the coupled pendulum. In high orders (here eight) the invariants are extremely accurate. When comparing the accuracy of the coupled pendulum to the other systems, it should be noted, that the emittance of the pendulum is about 1000 times bigger. This accuracy is only possible, because the physical pendulum has an exact invariant, the new Hamiltonian G of equation (2.20). In table (2.2) the resonance denominators up to order 10 are displayed. In figure (2.13), the invariant defect is shown for the IUCF ring. The invariants cannot reach the accuracy of the coupled pendulum, since no exact invariants of motion exist. In table (2.3) the resonance denominators up to order 10 are displayed. The tables (2.4) and (2.5) show the smallest resonance denominators for every order for the PSR II and the Demo ring; the figures (2.14) and (2.15) show the invariant defects for these systems.

Order	l	k_1	k_2	$e^{i2\pi\nu_l} - e^{i2\pi(k_1\nu_1+k_2\nu_2)}$
2	1	2	0	0.42830104E-01
3	1	3	0	0.11284027
4	1	3	−1	0.64523782E-01
5	1	4	−1	0.11918375E-01
6	1	5	−1	0.12615773E-01
7	1	6	−1	0.83713329E-02
8	1	1	−7	0.10957355E-01
9	1	2	−7	0.17465246E-01
10	1	4	6	0.41817583E-02

Table 2.2: Resonance denominators for the map of the coupled pendulum.

2.7 Influence of Resonances

In the chapter about normal form theory it was mentioned that in general a normal form transformation is only possible if no resonance condition up to order n is

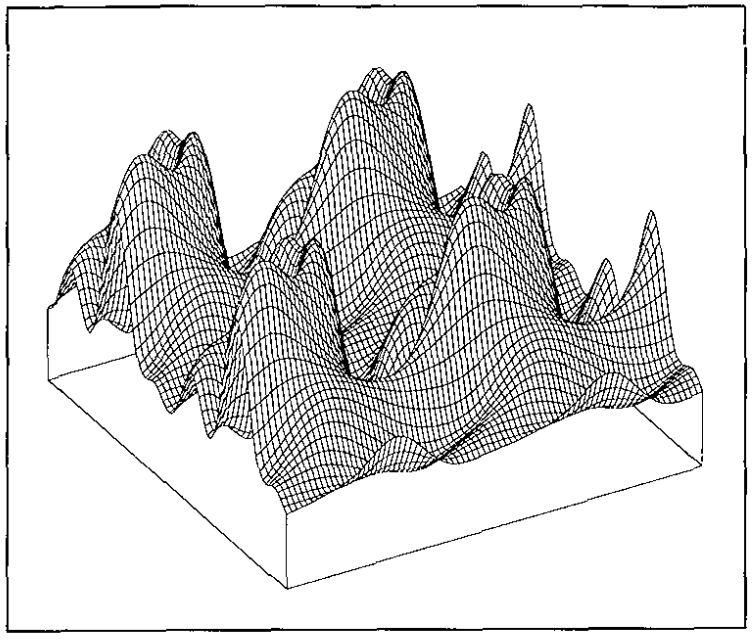

Figure 2.12: Invariant defect for the coupled pendulum on a pseudo invariant torus. The coordinates are in $[0, 2\pi] \times [0, 2\pi]$. The range of the depicted function is $[-2.55 \cdot 10^{-13}, 7.36 \cdot 10^{-13}]$.

Order	l	k_1	k_2	$e^{i2\pi\nu_l} - e^{i2\pi(k_1\nu_1 + k_2\nu_2)}$
2	2	1	−1	0.20728920
3	2	−1	2	0.61769437E-01
4	2	2	−2	0.18997422
5	2	−2	3	0.11370423
6	2	3	−3	0.16133895
7	1	−7	0	0.74483076E-01
8	2	−3	−5	0.15128203E-01
9	2	9	0	0.37879416E-02
10	2	3	7	0.15616662E-01

Table 2.3: Resonance denominators for the map of the IUCF ring.

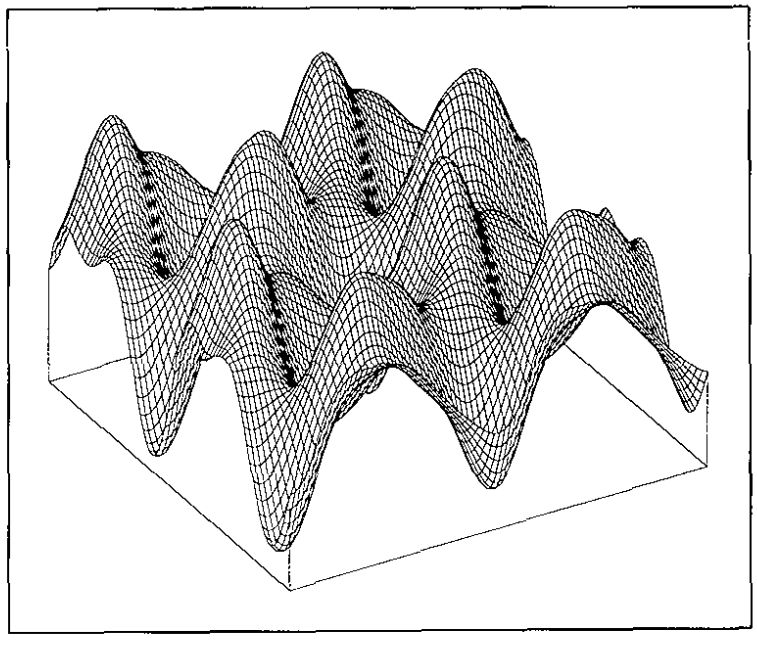

Figure 2.13: Invariant defect for the map of the IUCF ring on a pseudo invariant torus. The coordinates are in $[0, 2\pi] \times [0, 2\pi]$. The range of the depicted function is $[-6.84 \cdot 10^{-9}, 6.00 \cdot 10^{-9}]$.

Order	l	k_1	k_2	$e^{i2\pi\nu_l} - e^{i2\pi(k_1\nu_1 + k_2\nu_2)}$
2	1	1	-1	0.25862576E-01
3	1	2	-1	0.82362671E-02
4	1	2	-2	0.23559090E-01
5	1	3	-2	0.14964352E-01
6	1	3	-3	0.19723880E-01
7	1	4	-3	0.20173918E-01
8	1	4	-4	0.14362837E-01
9	1	5	-4	0.23856960E-01
10	1	5	-5	0.74841996E-02

Table 2.4: Resonance denominators for the map of the PSR II ring.

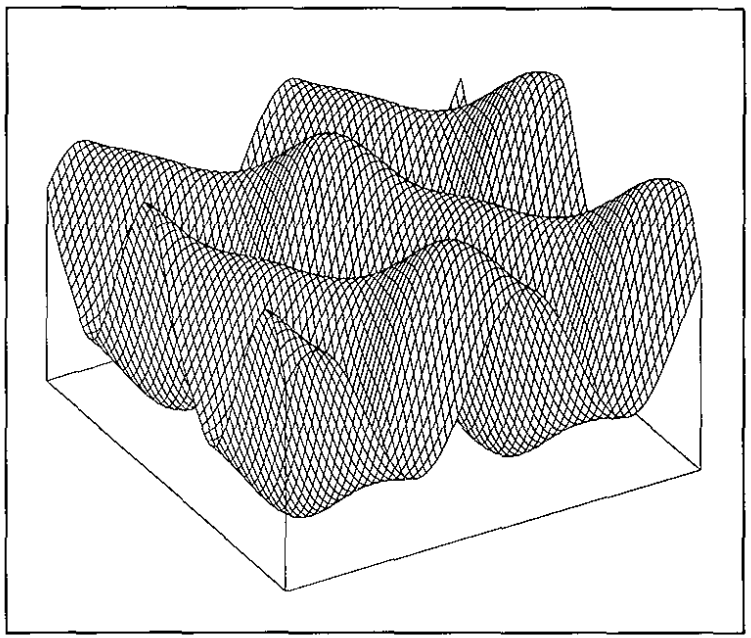

Figure 2.14: Invariant defect for the map of the PSR II ring on a pseudo invariant torus. The coordinates are in $[0, 2\pi] \times [0, 2\pi]$. The range of the depicted function is $[-1.76 \cdot 10^{-9}, 1.65 \cdot 10^{-9}]$.

Order	l	k_1	k_2	$e^{i2\pi\nu_l} - e^{i2\pi(k_1\nu_1+k_2\nu_2)}$
2	1	1	-1	0.25862576E-01
3	1	2	-1	0.82362671E-02
4	1	2	-2	0.23559090E-01
5	1	3	-2	0.14964352E-01
6	1	3	-3	0.19723880E-01
7	1	4	-3	0.20173918E-01
8	1	4	-4	0.14362837E-01
9	1	5	-4	0.23856960E-01
10	1	5	-5	0.74841996E-02

Table 2.5: Resonance denominators for the map of the Demo ring.

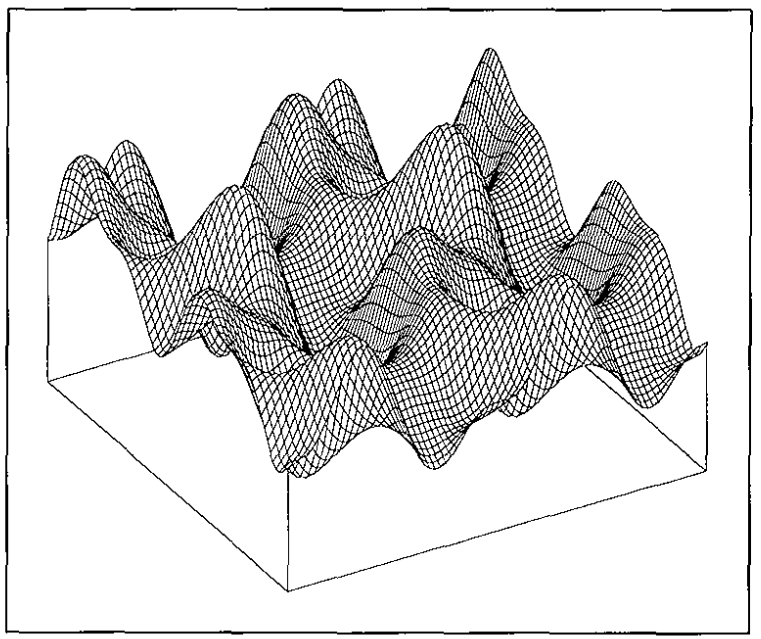

Figure 2.15: Invariant defect for the map of the Demo ring on a pseudo invariant torus. The coordinates are in $[0, 2\pi] \times [0, 2\pi]$. The range of the depicted function is $[-7.22 \cdot 10^{-9}, 6.95 \cdot 10^{-9}]$.

satisfied. It was also mentioned that this transformation can always be performed, even when resonances are present, if the motion is integrable, meaning there are as many invariants of motion as degrees of freedom. In general this is not the case, since probably most real systems are non-integrable. We therefore have to face the fact that resonances up to evaluation order have to be avoided in order to perform the normal form transformations needed for the PIE method. The figures (2.16) show the tune space for two degrees of freedom. In an accelerator these freedoms are the motion in vertical and in horizontal direction. The resonance conditions create lines in tune space on which the tunes are not allowed to lie. These lines are shown in figure (2.16a) for resonances up to order 6 and in (2.16b) for resonances up to order 12. Similar graphs are shown in most elementary accelerator physics text books and elementary papers [CS58, ES93]. In these graphs the tunes vary between 0 and 1/2. This quadrant of the complete tune space is depicted, since the set of resonance lines is mirror symmetric in respect to the lines $\nu_1 = 1/2$ and $\nu_y = 1/2$. If the tunes lie close to a line, small denominators $D_l(\vec{k})$ occur in the normal form calculation, the transformation becomes inaccurate and the quality of the pseudo invariants decrease. The reason for this fact is not only a computational problem but there are physical reasons, since at resonances, good pseudo invariants do not exist.

To analyze this fact, we computed the effect of the tune on the pseudo invariants and thus on the long term estimates of the PIE method. For the Henon map, we scanned the tune in 200 steps from 0 to 1. The variation of the deviation function is recorded in figure (2.17a), where a logarithmic scale was used. The rapidly increased deviation from invariance and thus the rapidly decreased survival times close to tune resonances can be clearly seen for every single resonance up to order 8, which was the evaluation order of the normal form transformation. This figure suggests the well known fact that it is advisable to keep the tune of storage rings out of "resonance

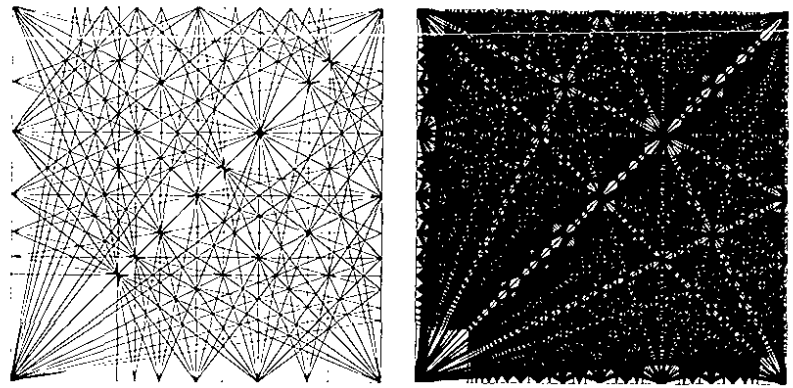

Figure 2.16: Regions of resonances for two degrees of freedom up to order a) 6, b) 12.

holes".

In figure 2.18 the tune of the physical pendulum was scanned from 0 to 1 in 200 steps and no resonance problem can be observed. Normal form theory is able to approximate the exact invariant given by the Hamiltonian in equation (2.11) even when the resonance denominators vanish. This also indicates that in the case of the Henon map, the problems at resonances are not only due to the resonance denominator problem.

In order to see if this effect is only of a computational nature or if the physical reason of non-existing pseudo invariants of good quality is important, we used the Henon map and performed only a fourth order normal form transformation. The result is depicted in figure (2.17b). The invariance defects tend to become larger, since now the invariant surfaces are only approximated to much lower order. However, resonances of orders higher than the evaluation order cannot be observed. If the decreased invariance of f were only due to physical reasons, such resonances should be

seen. It can also be observed that with higher orders the invariance decreases at resonances. *This is not too surprising, since nonlinear normal form transformations try* to approximate a non-existing invariant. We can therefore conclude that the normal form invariants are the Taylor expansion of true invariants if these exist, however we cannot conclude that they are the best possible pseudo invariants, especially close to resonances. The figures (2.17a) and (2.17b) also show that there is an optimum order for normal form transformations, which can be quite low if the system is close to low order resonances. For the example system we analyze, the tunes were sufficiently far away from resonances, such that this maximum order was not yet reached at order 8. This can be seen in the tables (3.1a–d).

Figure (2.19) shows a corresponding picture for the deviation function of the PSR II ring. Calculations were performed in order 8. The tunes ν_x and ν_y were scanned from 0 to 1 in 100 × 100 steps. In order to obtain comparable systems, the map of the PSR II was computed as discussed in section (2.4) and then composed with a linear map to obtain a symplectic map with the desired tunes. Again the figure is shown with a logarithmic scale. The boundary of the tune space has zero tune and is therefore excluded.

Resonance lines up to order 3 can be clearly seen. The lines which can be observed are one second order resonance line, $\nu_x+\nu_y = 1$, and four third order lines, $\nu_x+2\nu_y = 2$, $\nu_x - 2\nu_y = -1$, $\nu_x + 2\nu_y = 1$, and $\nu_x - 2\nu_y = 0$. Influences of other resonances cannot be observed. This indicates two things. First, not only the tune is responsible for the quality of pseudo invariants, and second, the increased deviation from invariance is not only an artifact of the normal form method but reflects properties of the system.

Figure (2.20) shows many more resonance lines. Resonances up to order 5 can be seen. Again it is apparent that not all resonances are observed. It can be imagined that survival time versus tune plots of this or similar kind can be helpful for machine

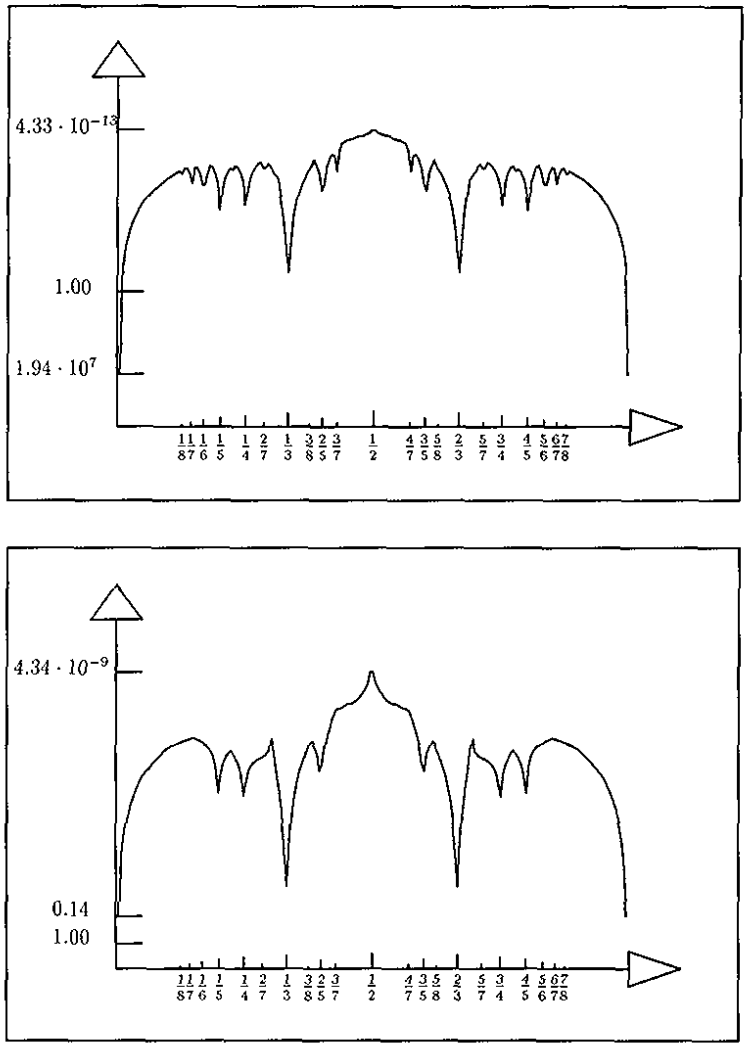

Figure 2.17: Variation of the maximum δ of the deviation function d_f with tune for the Henon map of a) order 8, b) order 4. The scale is logarithmic and inverted. Staying out of resonance holes yields long survival time predictions with the PIE.

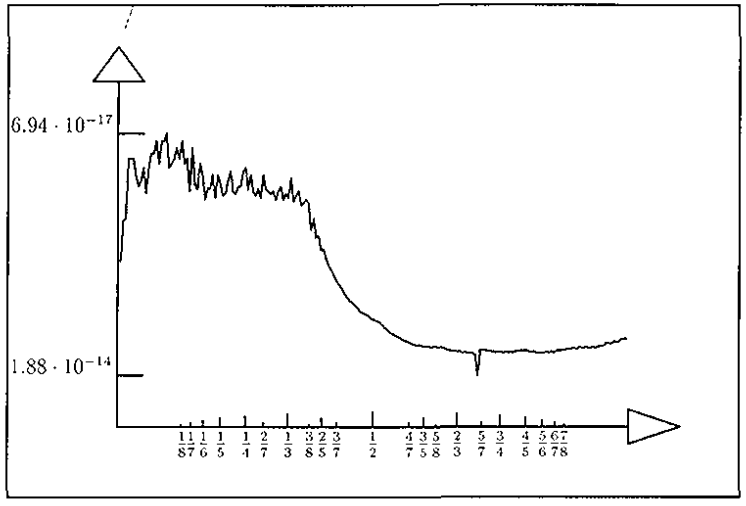

Figure 2.18: Variation of the maximum δ of the deviation function d_f with tune for the 8^{th} order map of the physical pendulum. The scale is logarithmic and inverted. Due to the existence of an invariant, resonance denominators do not cause a problem during normal form computation.

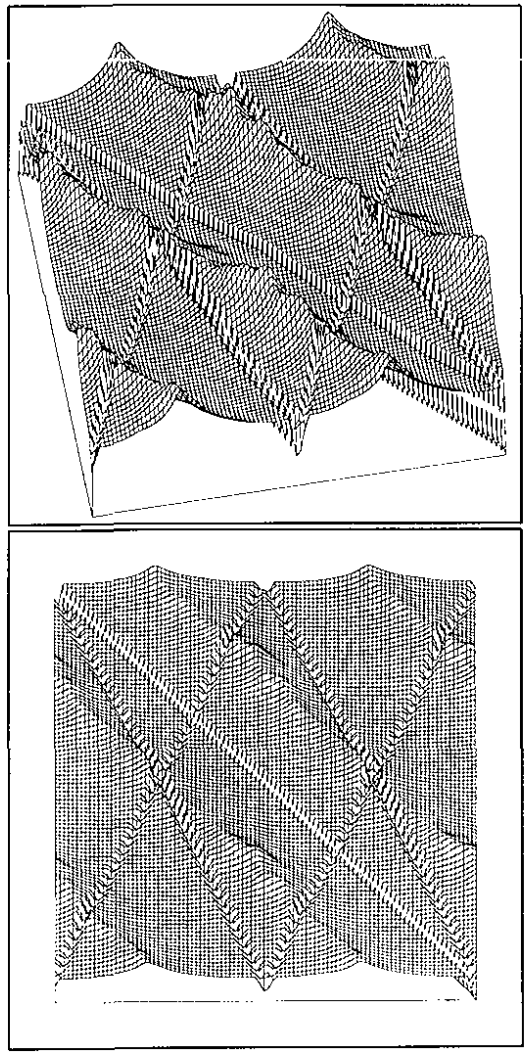

Figure 2.19: Variation of the maximum δ of the deviation function d_f with tune for the 8^{th} order map of the PSR II. The scale is logarithmic and inverted. The whole horizontal and vertical tune space is covered: $\nu_x \times \nu_y \in [0,1] \times [0,1]$. The range of d_f is from $2.2 \cdot 10^{-10}$ to $1.9 \cdot 10^{-7}$.

analysis and optimization. However, more experience with this technique is needed to make detailed predictions.

2.8 Symplectic Representations

The fact that the normal form method yields invariants hinges critically on order n symplecticity of the normal form map. This fact and also the notion that symplecticity guarantees area conservation in every $z_{2j-1} \times z_{2j}$ plane in phase space suggests to look for completely symplectic transfer maps to describe an accelerator.

This can be done by computing an order n generating function for the transfer map. The procedure for this computation was mentioned in the references [Ber88a, Ber91b, Ber90a]. The Taylor expansions of generating functions of symplectic map can be computed with DA based programs, generating functions give implicit definitions of symplectic maps, whereas the n^{th} order Taylor expansion of a symplectic map is only order n symplectic. The implicit definition of the transfer map by a generating function is usually inverted numerically with a Newton method. This method was implemented in COSY INFINITY. As mentioned in [Ber92b], six different modes of symplectic tracking are possible. The map can be represented by the four different generating functions F_1, F_2, F_3, and F_4, or the linear part of the map can be factored out of the map and the mixed variables generating functions F_2 or F_3 can be used to approximate the nonlinear part of the map by a completely symplectic transformation.

We used this procedure to check if it is reasonable to compute pseudo invariants by nonlinear normal form theory and to represent the map by a completely symplectic representation. The analysis revealed that the normal form invariants I_i of chapter (1) are not better pseudo invariants for a symplectic map generated by either of the six

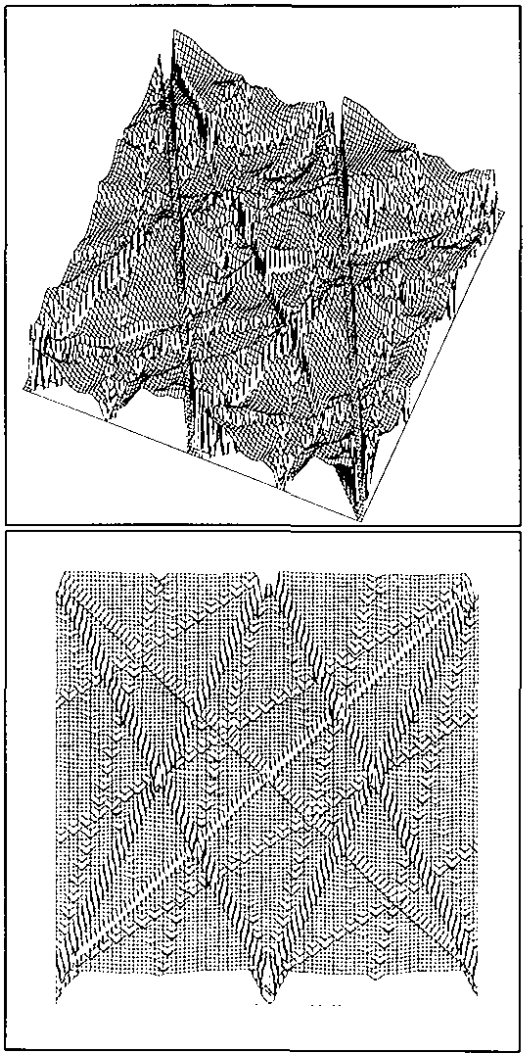

Figure 2.20: Variation of the maximum δ of the deviation function δy with time for the 8^{th} order map of the Duffing. The scale is logarithmic and inverted. The range of δy is from $1.3 \cdot 10^{-2}$ to $1.9 \cdot 10^{-1}$.

generating function. In fact, usually the normal form invariants are better invariants for the Taylor maps than for any of the symplectic representations.

We believe that the reason for this behaviour is the order $n+1$ invariance of the functions I_i under transformation of the Taylor map. The relation

$$I_j(\vec{M}) =_{n+1} I_j \tag{2.32}$$

only holds for the Taylor map, not for a symplectic map defined by a generating function, since the partial inversion by a Newton method changes all orders of the map, not only orders higher than n. The Taylor map $\vec{M}$ is the Taylor expansion of a symplectic map. Therefore, increasing the order of the expansion makes $\vec{M}$ become closer to a symplectic map. In table (2.6) the invariance defect of the coupled pendulum for the 9^{th} order polynomial f is shown for symplectification of the map by evaluating it to different orders. The quality of the invariants does not change substantially, since the first 9 orders cancel with and without this kind of symplectification.

Order	Coup. Pend. (10^{-13})	IUCF (10^{-9})	PSR II (10^{-9})	Demo (10^{-9})
8	5.858924	5.746786	1.597229	8.808577
9	9.721390	5.717355	1.599737	9.759362
10	9.677259	5.721978	1.599741	9.735593
11	9.744150	5.722880	1.599745	9.137200
12	9.745815	5.722909	1.599745	9.867690

Table 2.6: Maximum of the deviation function after symplectifying the map by adding higher orders.

In figure (2.21) the deviation function is given for the three example accelerators. For the emittances used, the different generating functions yielded graphs which differed less than printer resolution. Therefore, the generating function F_1 was used for all figures. The domain in phase space on which the deviation functions were evaluated is the same as in the figures (2.15,2.13,2.14, and 2.15). In all cases the

function f is a better pseudo invariant for the Taylor map than for the symplectic map represented by the generating function.

Even for many turns, where satisfying the symplectic condition could be superior, our calculations show that the normal form invariants are better invariants for the Taylor map, as can be seen in table (2.7).

	C. Pend. (10^{-14})		IUCF (10^{-11})		PSR II (10^{-10})		Demo (10^{-13})	
Turns	F_1	$\vec{M}$	F_1	$\vec{M}$	F_1	$\vec{M}$	F_1	$\vec{M}$
10	293	276	881	823	126	115	122581	129261
20	534	508	969	988	232	223	97341	87990
30	723	705	1191	1496	321	310	77279	67182
40	866	840	1091	1396	379	373	21238	36807
50	1002	949	1497	1219	462	449	43855	61792
60	1232	1214	1178	1334	571	561	128	125
70	1476	1444	1427	1028	674	666	162	153
80	1656	1637	1187	934	761	754	172	177
90	1803	1778	859	1134	820	814	194	186
100	1941	1890	1007	721	856	853	209	210

Table 2.7: The maximum of the deviation function as a function of the turns when the map is represented by a generating function.

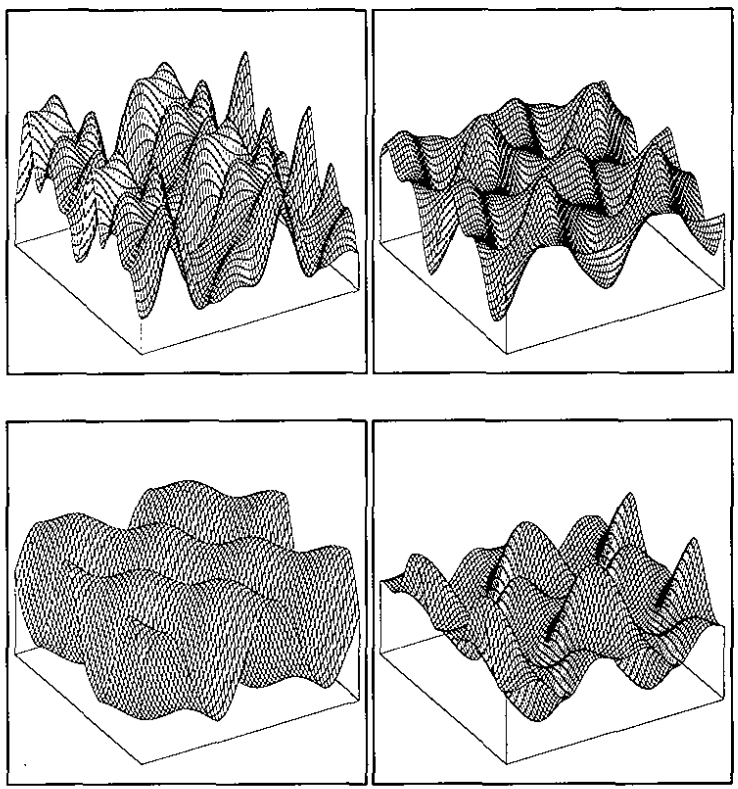

Figure 2.21: Quality of normal form invariants when the map is represented by a generating function for the four examples with two degrees of freedom: a) the coupled pendulum, the range of the displayed function is $[-2.15, 9.45] \cdot 10^{-13}$, b) IUCF: $[-1.16, 1.11] \cdot 10^{-8}$, c) PSR II: $[-2.63, 2.63] \cdot 10^{-9}$, d) Demo: $[-6.36, 8.49] \cdot 10^{-9}$. For the order 8 symplectic Taylor maps, the corresponding figures were displayed previously.

Chapter 3

Optimization by Scanning

On page (57) four problems were mentioned. The first problem, finding a suitable pseudo invariant f, has been discussed. The remaining three problems are connected to finding the minimum of f on $\mathcal{S}_f$, the maximum of f on $\mathcal{S}_i$, and the maximum of d_f on $\mathcal{A}\backslash\mathcal{O}$. The regions $\mathcal{S}_i = \bar{M}(\mathcal{O})\backslash\mathcal{O}$ and $\mathcal{S}_f = \bar{M}(\mathcal{A})\backslash\mathcal{A}$ cannot be represented as clearly as the regions $\mathcal{O} = \{\vec{z}|\alpha \geq ||\vec{z}||\}$ and $\mathcal{A} = \{\vec{z}|1 \geq ||\vec{z}||\}$. This does not lead to a problem when phase space regions are used which contain $\mathcal{S}_i$ and $\mathcal{S}_f$. When the maximum $\delta_\mathcal{O}$ of the deviation function on $\mathcal{O}$ and the maximum δ on $\mathcal{A}\backslash\mathcal{O}$ is known, it is sufficient to choose

$$\mathcal{S}_i = \mathcal{F}(\alpha, \alpha + \delta_\mathcal{O}) \ , \quad \mathcal{S}_f = \mathcal{F}(1, 1 + \delta) \tag{3.1}$$

with the phase space domain $\mathcal{F}(\xi, \zeta)$ defined in equation (2.29).

The functions f and d_f have some properties which allow to make sensible simplifications. Those properties will be demonstrated for the proposed PSR II. The evaluation order is 6 and the acceptances are $\epsilon_i = 100$mm mrad. As shown in figure (3.1a), the function $F(x) = \max\{f(\vec{z})|\mathcal{F}(x, x)\}$ is typically growing monotonously with x so that the maximum of $f(\vec{z})$ on $\mathcal{S}_i$ occurs on $\mathcal{F}(\alpha + \delta_\mathcal{O}, \alpha + \delta_\mathcal{O})$, which is approximately described by $||\vec{z}|| = \alpha$; and the minimum of $f(\vec{z})$ on $\mathcal{S}_f$ occurs on $\mathcal{F}(1, 1)$, where $||\vec{z}||$ is approximately 1. The function $D(x) = \max\{d_f(\vec{z})|\mathcal{F}(x, x)\}$ is

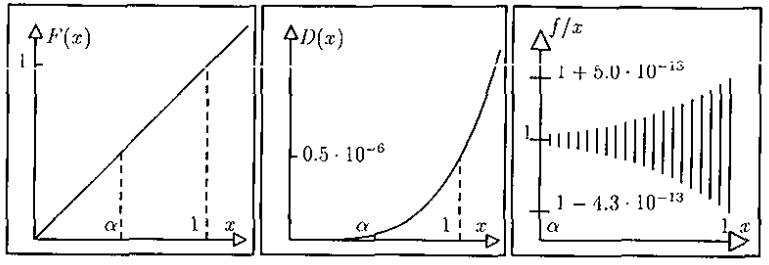

Figure 3.1: Figure a) depicts $F(x)$ and figure b) $D(x)$ in the allowed region. The variation of the pseudo invariant relative to $||\vec{z}||$ is shown in figure c).

also typically growing monotonously as shown in figure (3.1b). Therefore, the maximum δ occurs also at the border of the allowed region, where $||\vec{z}||$ is approximately 1. Furthermore, figure (3.1c) shows that the variation of $f(\vec{z})$ on $\mathcal{S}_i$ and $\mathcal{S}_f$ is much smaller than $\Delta f = f_f - f_i$ which therefore is close to $1 - \alpha$. We obtain the estimate

$$N = \frac{1-\alpha}{\max\{d_f(\vec{z})|\mathcal{F}(1,1)\}}\,, \tag{3.2}$$

which involves finding only one maximum on a subspace with nearly constant $||\vec{z}||$. The figure in section (2.6) show the range of the functions d_f on the border of the allowed region $\mathcal{A}$ for all the example systems. The function d_f does not have sharp maxima so that sampling with 20 steps in each direction gives a good approximation of the maximum value. Table (3.1) displays N for different systems and for different evaluation orders for $\alpha = 1/2$. Due to energy conservation, the pendulum and the coupled pendulums are stable for all times. The quality of our estimate is shown by the big numbers N which we obtain for those cases, in spite of the fact that the emittances are chosen to be extremely large and nonlinearities quite important.

The evaluation of the functions f and d_f, using interval arithmetic to find the maximum values and therefore establishing a mathematically strict lower bound for the turn number N_{max} will be analyzed in a later section. First we want to demonstrate

Order	Pendulum	Henon Map	Coupled Pendulums
2	434	6	43
3	434	41	915
4	1,039,578	1,109	85,907
5	1,039,578	7,149	2,577,221
6	455,537,706	27,556	61,418,923
7	455,537,706	176,827	1,535,527,685
8	92,114,163,553	1,474,124	29,750,319,370
9	92,114,163,553	9,133,037	357,584,630,384
Order	IUCF	PSR II	Demo
2	9	806	6
3	321	831	129
4	1,288	252,893	1,220
5	19,995	235,650	25,657
6	370,294	6,977,545	84,087
7	3,265,268	8,255,710	1,320,751
8	11,277,884	65,472,668	4,554,994
9	65,731,218	76,092,850	55,548,695

Table 3.1: Minimum number of turns required to move from the initial region to the forbidden region. The initial emittance was chosen to be half the acceptance. The maps were evaluated in order eight, whereas the pseudo invariants were computed to the indicated order. Scanning was performed with 20^k points for k relevant dimensions.

some possibilities of improving the obtained estimates.

3.1 Refinements and Examples

Two methods will be introduced that increase the quality of the bounds on long term stability. One is connected to separating phase space in appropriate regions, the other involves multi-turn maps. Furthermore, unknown parameters of the system will be included in the estimates. The results for the six example maps are accumulated in table (3.3). In this table the guaranteed number of turns for the assumed acceptance $\epsilon\pi$, which is given in section (2.4) for each example, and an initial beam with emittance $\epsilon\pi/2$ is given. For the coupled pendulum and for the IUCF ring, the emittance for which a beam can be guaranteed to survive 10^8 turns is also shown. To limit the computation time, we evaluated 10^k points for k relevant phase space dimensions. The parameter interval was also covered by 10 points.

3.1.1 Dividing Phase Space

Because of the rapid increase of δ with increasing $||\vec{z}||$, it is appropriate to separate the regions between $||\vec{z}|| = \alpha$ and $||\vec{z}|| = 1$ by surfaces $\mathcal{F}(\alpha_i, \alpha_i)$, $i \in \{0, \ldots, k\}$, where $\alpha_0 = \alpha$ and $\alpha_k = 1$. With $u_i = \max\{f(\vec{z}) | \vec{z} \in \mathcal{F}(\alpha_i, \alpha_i)\}$ and $l_i = \min\{f(\vec{z}) | \vec{z} \in \mathcal{F}(\alpha_i, \alpha_i)\}$, the lower bound on the number of turns becomes

$$N = \sum_{i=1}^{k} \frac{l_i - u_{i-1}}{\delta_i} \text{ with } \delta_i = \max\{d_f(\vec{z}) | \mathcal{F}(\alpha_i, \alpha_i)\} \; . \tag{3.3}$$

The turn numbers obtained from this technique and the transportable emittances are given in table (3.3) in the third line. In our experience, this separation of phase space can improve the estimate by up to a factor of 10.

The potential of this approach can be seen when using

$$D(x) = \max\{d(\vec{z}) | f(\vec{z}) = x\} \; . \tag{3.4}$$

We estimate the change that occurs in x by k map applications as $x(n+k) - x(n) = D(x(n+k)) \cdot k$ and approximate for big turn numbers N as

$$N(x) = \int_0^x \frac{d\tilde{x}}{D(\tilde{x})} \; . \tag{3.5}$$

In figure (3.2) $n(x)$ corresponds to the area under the curve. The PIE method without dividing phase space, however, only gives the area in the rectangle as guaranteed survival time.

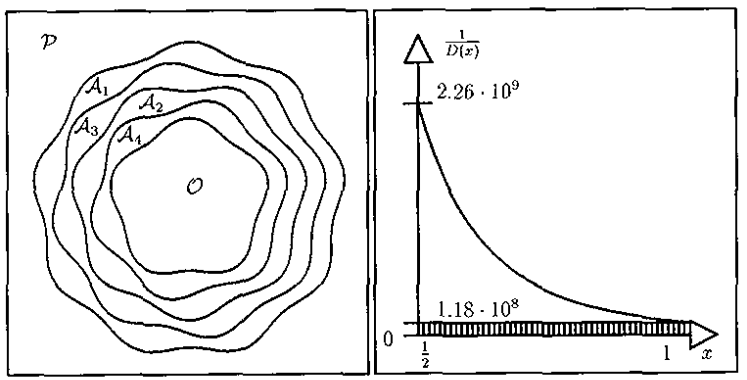

Figure 3.2: Dividing phase space approximates the area under the displayed curve by several rectangles to obtain the bound on the survival time. Without this improvement, the PIE method would only give the area of the drawn rectangle.

3.1.2 Time Evaluation

Figure (3.3a) shows how close the pseudo invariants are to invariants of motion. Over many turns the quantity of f changes but it always oscillates around a mean which grows very slowly. The normal form method, however, bounds the growth of the pseudo invariant by considering the largest growth that can happen in one application of the map. As demonstrated in figure (3.3b), the biggest change that can

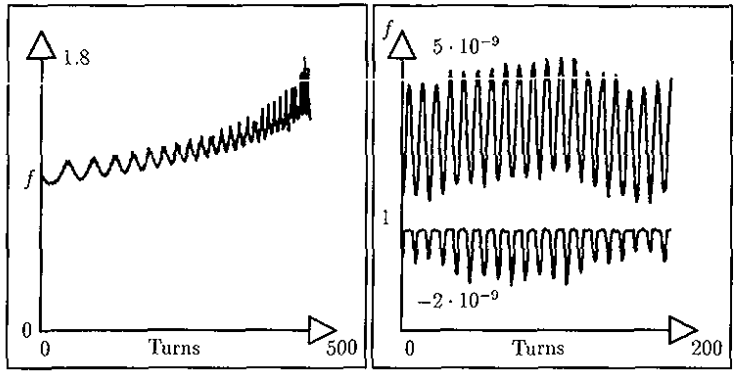

Figure 3.3: a) slow increase of the pseudo invariant over many turns, b) periodic change of the pseudo invariant after relatively few turns.

be generated by N applications of the map is usually much smaller than N times the largest growth that can happen during a single turn. Therefore, it is advantageous to consider the maximum growth that can occur when the map is applied several times.

In order to find the optimum number of map applications, the maximum and minimum of $d(\vec{z})$ over the allowed region $\mathcal{A}$ was plotted for many turns. The figures (3.4a–f) display the variation of $d(\vec{z})$ for our examples. For the improvements illustrated in table (3.3), the number of map applications used are displayed in table (3.2).

Pend.	Henon	Coup. Pend.	IUCF	PSR II	DEMO
14	37	6	89	247	100

Table 3.2: Number of map applications used for improving the estimation.

3.1.3 Parameter Dependence

So far, the normal form method assumes that the one-turn map of the storage ring in question is well known. Since this is rarely the case, the theory has been extended

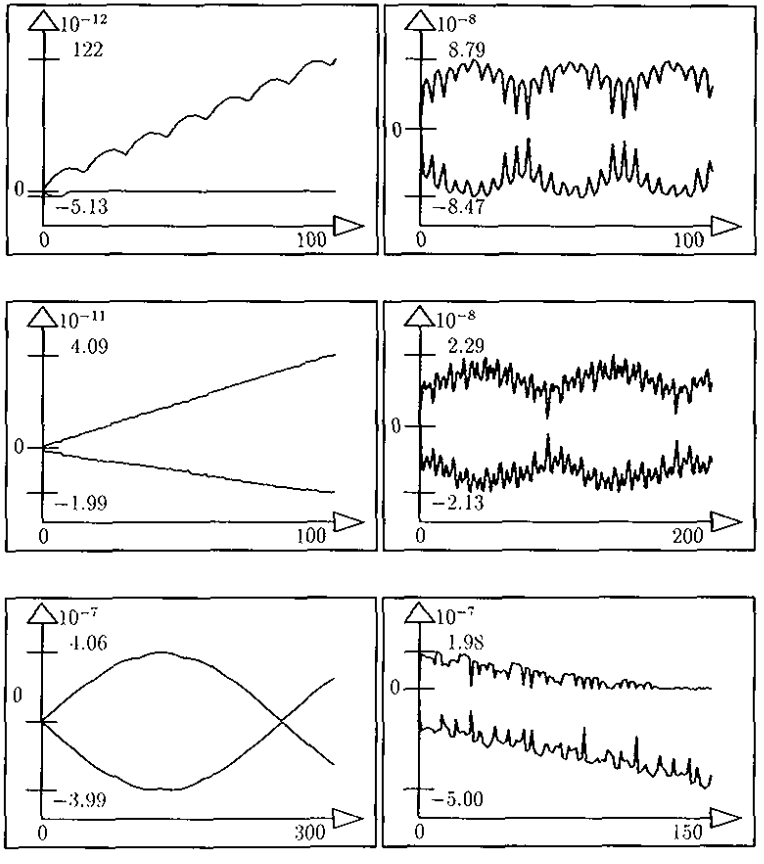

Figure 3.4: The figures display the variation of the deviation function in the allowed region for the six examples. From top left to bottom right these are a) Pendulum, b) Henon map, c) Coupled pendulum, d) IUCF, e) PSR II, f) Demo.

to maps which depend on an unknown parameter. Neither particle energy nor the magnet parameters are known exactly and have to be treated as parameters which can not be accurately specified. We computed the map as a function of a parameter of interest and then scanned not only through the interesting region of phase space, but also through the interval in which the parameter could lie in reality. The unknown parameter for each example is mentioned in section (2.4), where the examples are introduced.

If the map $\vec{M}$ is a function of a parameter, then the nonlinear normal form transformation $\vec{B}$ also depends on a parameter. Using DA programs allows, as mentioned in chapter (1), to compute the Taylor expansion of this parameter dependent map $\vec{B}$. The pseudo invariant f then also depends on the parameter. Changing the parameter changes the transfer map and the pseudo invariant simultaneously, such that f stays a good pseudo invariant for a wide range of the parameter. This is apparent when one considers that

$$f \circ \vec{M} - f =_{n+1} 0 \tag{3.6}$$

*also holds for parameter dependent normal form transformations, where partial deriva*tives in respect to the parameter and in respect to the coordinates are considered when equating with "$=_n$".

We belive that the described method usually gives a very reliable lower bound on the number of stable turns. However, to make completely rigorous statements about guaranteed bounds, several steps have to be performed in a more rigorous way. In particular, it will not be sufficient to approximate the maximum of δ by scanning. Interval arithmetic methods which guarantee a global maximum have to be used. Utilizing this guaranteed optimization requires a short introduction into interval arithmetic.

Lower bound for	**Pendulum**	**Henon map**
Simplest application	92,114,163,553	9,133,037
Length and Strength uncertainty 1%	23,556,300,993	8,167,533
Divided phase space	452,868,876,965	44,999,781
Multi-turn maps	388,804,862,856	1,456,171,297
Both	1,895,348,117,634	4,779,711,057
Lower bound for	**PSR II**	**Demo**
Simplest application	76,092,850	55,548,695
Quad field uncertainty 0.01%	47,166,060	51,963,620
Divided phase space	373,642,327	284,008,517
Multi-turn maps	21,172,838,624	1,042,575,616
Both	18,731,455,785	5,121,716,506
Coup. Pendulum	predicted turns	stable emittance
Simplest application	357,584,630,384	$5.00 \times 5.00\pi$m mrad
Length uncertainty 1%	144,173,434,143	$3.40 \times 3.40\pi$m mrad
Divided phase space	1,765,031,547,898	$11.3 \times 11.3\pi$m mrad
Multi-turn maps	1,029,815,934,687	$6.00 \times 6.00\pi$m mrad
Both	5,087,629,041,331	$14.5 \times 14.5\pi$m mrad
IUCF ring	predicted turns	stable emittance
Simplest application	65,734,218	$3.3 \times 2.0\pi$mm mrad
Quad field uncertainty 0.01%	18,535,102	$2.9 \times 1.7\pi$mm mrad
Divided phase space	335,420,083	$4.8 \times 2.9\pi$mm mrad
Multi-turn maps	5,804,832,818	$8.1 \times 4.8\pi$mm mrad
Both	27,745,480,680	$13 \times 7.7\pi$mm mrad

Table 3.3: Lower bounds on the turns of particles for initial emittance of one half the acceptance and lower bounds on the stable emittances for 10^8 turns obtained by various variations of the PIE method.

Chapter 4

Rigorous PIE with Interval Arithmetic

The introduced method of pseudo invariant optimization has the potential to be completely rigorous. Equation (2.4) is a strict inequality, if all the maxima and minima can be strictly bounded. In the field of numerical analysis with automatic result verification, a number of methods have been developed which lead to rigorous bounds on the extrema of functions. Below, the basics of interval arithmetic will be introduced and it will be explained how interval arithmetic can lead to rigorous bounds on extrema. In preparation of the presented work, several methods of standard interval optimization have been used. However, for the complicated function d_f involved, which is a multidimensional polynomial of order $n(n+1)$ when n is the evaluation order of the normal form transformation, conventional techniques turned out to be fair to slow to be useful at current computer speed. Therefore, these standard methods will only be shortly mentioned and the reader is referred to the references. In the weakly nonlinear systems of interest, the inefficiency of the conventional methods is mainly due to the low order contributions in the polynomial d_f. In order to take advantage of the special structure exhibited by the deviation function, namely

$$d_f = f(\vec{M}) - f =_{n+1} 0 \,, \tag{4.1}$$

we introduced an innovative concept which we shall call interval chains. Interval chains allow one to bound the contribution to a polynomial of order higher than $n+1$. Using interval chains therefore completely eliminates the inefficiencies caused by low order contributions. After this concept is introduced, several examples will be presented. The example maps used are the same as those of the previous chapter and the refinements used correspond to those in section (3.1).

4.1 Interval Arithmetic

Interval arithmetic was developed because of the fact that the set of numbers which can be expressed on a computer is finite. Therefore, computers cannot store accurate information about a real number, except that it is located within an interval of width equal to or greater than the computer accuracy. Thus, if completely accurate arithmetic should be performed on a computer, an arithmetic for intervals has to be developed. Such an arithmetic is also necessary to formulate accurate statements using results of measurements, because measurements usually do not yield real numbers but intervals, often denoted by error bars [AHS3, Kul89, May89, Moo66, Moo79, Moo88].

Following, intervals will be symbolized by capitol letters and real numbers will be denoted by small letters. The upper and the lower bound of an interval will be denoted by underscore and overscore respectively.

$$X = [\underline{X}, \overline{X}] = \{x | \underline{X} \leq x \leq \overline{X}\} \,. \tag{4.2}$$

If $f : \mathbb{R} \mapsto \mathbb{R}$ then $f(X)$ is defined as the set of possible results for all elements of the interval X.

$$f(X) = \{a | a = f(x), x \in X\} \,. \tag{4.3}$$

It will be our goal to describe a method to find an interval which contains all possible results. Such an interval that encloses $f(X)$ will be denoted by $F(X) \supseteq f(X)$.

Elementary Operations

If we are concerned with functions which can be constructed by a finite number of elementary operations, it is sufficient to ensure that the result of every elementary *operation on intervals is an interval containing all possible results. If this is true* for any elementary operation, it will infallibly be true for the result of the complete function evaluation. This thought leads us to the need of establishing the result of elementary operations between intervals. The required property of an elementary operation between n numbers, described by the function $e: \mathbb{R}^n \mapsto \mathbb{R}$, is given by

$$E(X_1, \ldots, X_n) \supseteq e(X_1, \ldots, X_n) \,. \tag{4.4}$$

In order to achieve results $F(X)$ which approximate $f(X)$ as closely as possible, one tries to define the elementary operations such that the equality holds in equation (4.4).

At first we choose addition, subtraction, multiplication, and division as elementary operations:

$$X + Y = [\underline{X} + \underline{Y}, \overline{X} + \overline{Y}] \,, \tag{4.5}$$

$$X - Y = [\underline{X}, \overline{X}] + [-\overline{Y}, -\underline{Y}] \,, \tag{4.6}$$

$$X \cdot Y = [\min\{\underline{X}\overline{Y}, \underline{X}\overline{Y}, \overline{X}\underline{Y}, \overline{X}\overline{Y}\}, \max\{\underline{X}\underline{Y}, \underline{X}\overline{Y}, \overline{X}\underline{Y}, \overline{X}\overline{Y}\}] \,, \tag{4.7}$$

$$X/Y = [\underline{X}, \overline{X}] \cdot [1/\overline{Y}, 1/\underline{Y}] \text{ for } 0 \notin Y \,. \tag{4.8}$$

The addition and the multiplication are commutative and associative. It is important to note that intervals with addition do not form a group, since there is no inverse of addition, which follows immediately from equation (4.10). In particular, $-X = [-\overline{X}, -\underline{X}]$ is not the additive inverse of X, because $X - X = [\underline{X} - \overline{X}, \underline{X} - \overline{X}] \neq 0$. There is also no distributivity law, but subdistributivity

$$X \cdot (Y + Z) \subseteq X \cdot Y + X \cdot Z \,. \tag{4.9}$$

The diameter of an interval is defined as $d(X) = \overline{X} - \underline{X}$, and the absolute value is defined as $|X| = \max\{|\underline{X}|, |\overline{X}|\}$. It is helpful to know the diameter and absolute value of results of elementary operations

$$d(X \pm Y) = d(X) + d(Y) \,, \tag{4.10}$$

$$d(X \cdot Y) \leq d(X) \cdot |Y| + d(Y) \cdot |X| \,, \tag{4.11}$$

$$|X + Y| \leq |X| + |Y| \,, \tag{4.12}$$

$$|X \cdot Y| = |X| \cdot |Y| \,. \tag{4.13}$$

If more complicated functions have to be evaluated, which cannot be established by a finite number of those four operations, then further elementary functions have to be defined. Examples are sine and cosine functions of intervals.

Interval Blow-up

The function $f: x \mapsto x - x$ yields $f(X) = 0$ and $F(X) = X - X = [\underline{X} - \overline{X}, \overline{X} - \underline{X}]$. This readily establishes that interval computations, albeit yielding all possible results, can overestimate the set of possible results substantially. In this example the set of possible results $\{0\}$ is contained in $F(X)$, which is however a great overestimation. The blow-up occurs because the constructed arithmetic treats the two intervals X to the right and to the left of the operator $-$ as two unrelated intervals. Another example is $f: x \mapsto x * x$. The results for an interval $X = [-a, a]$ can be in the interval $f(X) = [0, a^2]$, whereas the arithmetic yields a bigger interval $F(X) = [-a^2, a^2]$.

There are three major ways to minimize blow-up:

i) Reduction of the number of elementary operations. This can be achieved by restructuring the evaluation of the function. For example, $f(x) = x - x$ can be restructured to $f(x) = 0$. Because of the subdistributive property of interval

arithmetic (4.9), a reduction of the number of multiplications by restructuring parenthesis will always be useful.

ii) Introduction of new elementary operations. For example, $e(x) = x^2$ can be introduced as new elementary operation which is evaluated such that $E(X) = e(X)$ by $E(X) = [\max\{0, \underline{(X \cdot X)}\}, \overline{(X \cdot X)}]$.

iii) Decreasing the absolute value of intervals involved in a multiplication decreases the resulting diameter according to equation (4.11). Therefore, it is sometimes helpful to use a so-called centered form, which can be obtained from the intermediate value theorem. The intermediate value theorem states for differentiable functions on X:

$$\forall x, c \in X \ \exists \xi \text{ between } x \text{ and } c \text{ such that } f(x) = f(c) + f'(\xi) \cdot (x - c) \ . \quad (4.14)$$

Any value $f(x)$ with $x \in X$ is in the interval $f(c) + F'(X) \cdot (x - c)$. Therefore, we can write the centered form $F^c(X) \supseteq f(X)$ as

$$F^c(X) = f(c) + F'(X) \cdot (X - c) \quad (4.15)$$

and have achieved a multiplication with an interval $X - c$, which has the smallest absolute value when c is chosen to be the center of X. The center of an interval X is defined as $m(X) = (\overline{X} + \underline{X})/2$.

The possibility of computing an interval

$$F(X) \supseteq f(X) \quad (4.16)$$

in a straight forward way for complicated functions f implies the possibility of finding upper bounds on f in the interval X. $\overline{F}(X)$ is such an upper bound. If $\overline{F}(X)$ overestimates the maximum of f on X substantially, the interval X can be subdivided

in several subintervals X_i with $\cup_i X_i = X$ and a better bound can be found by

$$f(x) \leq f_m = \max(\overline{F}(X_i)) \ . \quad (4.17)$$

When the width of X_i is made small, the bound will become tight, due to decreased blow up. This interval rastering method automatically gives a measure for the overestimation

$$f_m - f \leq \max(\overline{F}(X_i)) - \max(\underline{F}(X_i)) \ . \quad (4.18)$$

The series of graphs in figure (4.1) shows how the blow-up reduces when the region of interest is covered with smaller intervals.

For further refinement of global optimization with intervals see [Jan91, JK92, Jan92a, Jan92b, Han79, Han80, RR88, WHS85, Rat92, Cse91, Eri91, Han88, IF79, MR88, Moh90]. One important refinement is the successive decrease of the width of the subintervals X_i after exclusion of subintervals X_k which certainly do not contain the maximum due to

$$\overline{F}(X_k) < \max(\underline{F}(X_i)) \ . \quad (4.19)$$

Conventional local optimization can find intervals X_i with big $\underline{F}(X_i)$, which will effectively exclude many intervals X_k by criterion (4.19).

4.2 Interval Chains and Optimization

The deviation function

$$d_f = f(\vec{M}) - f = \sum_{i=1}^{l} \frac{I_i(\vec{M}) - I_i}{\epsilon_i} = 0 \ , \quad (4.20)$$

with $I_i = B_{2i-1}^2 + B_{2i}^2$, is a polynomial with coefficients that cancel up to order n if the map $\vec{M}$ and the normal form transformation $\vec{B}$ were computed to order $n - 1$. This fact is established by theorem (1.1.4). Since the functions I_i are polynomials of order n and the Taylor map $\vec{M}$ has order $n - 1$, the deviation function is a polynomial of

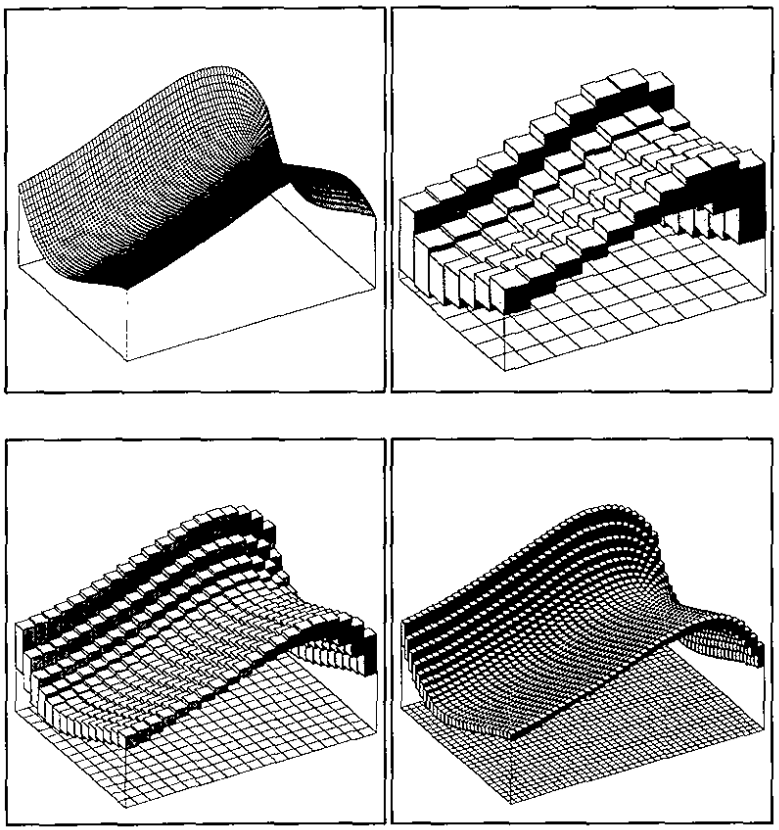

Figure 4.1: Top left: The function of which an upper bound should be found. Others: Covering the region of interest with smaller intervals reduces the overestimation of the maximum.

order $n(n-1)$, where all contributions in the first n orders cancel out. Conventional interval arithmetic evaluates d with intolerable blow-up, due to this cancellation. To obtain reasonable estimates at all, one would have to cover $\mathcal{A}$ by about 10^{24} volumes described by 4 intervals for systems with 2 degrees of freedom. Evaluating d_f 10^{24} times in interval arithmetic is certainly out of the question for current and near future computer speed. If we found a method to bound only the contributions to a polynomial of order higher than n, we could evaluate the deviation function by bounding only the relevant orders. The cancellation of lower orders would not influence this result and thus all blow-up due to cancellations would be avoided. The concept of interval chains will achieve this goal.

Definition 4.2.1 (Interval Chains, IC) *An interval chain I_c consists of a finite sequence of intervals I_i, $i \in \{0, \ldots, n+1\}$:*

$$I_c = (I_0, I_1, I_2, \ldots, I_{n+1}) \tag{4.21}$$

where I_i is called the i^{th} order of the interval chain.

For interval chains, we define the elementary operations addition, scalar multiplication, and multiplication. The results of those operations are interval chains with the following elements:

$$\begin{aligned}
(I_c + J_c)_i &= I_i + J_i,\ 0 \le i \le n+1, \\
(rI_c)_i &= rI_i,\ 0 \le i \le n+1,\ r \in I\!R, \\
(I_c \cdot J_c)_i &= \sum_{j=0}^{i} I_j J_{i-j},\ 0 \le i \le n, \\
(I_c \cdot J_c)_{n+1} &= \sum_{i=0}^{n+1} (I_i \sum_{j=n+1-i}^{n+1} J_j).
\end{aligned} \tag{4.22}$$

For convenience of notation, we denote the i^{th} order contribution of an m^{th} order polynomial p by p_i. Then $p : \mathbb{R}^k \to \mathbb{R}$ can be written as $p: \ p(\vec{x}) = \sum_{i=0}^{m} p_i(\vec{x})$. For i greater than m, p_i is chosen to be zero.

Definition 4.2.2 *Call an interval chain $P(A^k) = (P_0, \ldots, P_{n+1})$ an interval chain (IC) evaluation of a polynomial p of order m on the interval box $A^k = A_1 \times \ldots \times A_k$ if $P_i \supseteq \{p_i(\vec{x}) | \vec{x} \in A^k\}$, $0 \le i \le n$ and $P_{n+1} \supseteq \{\sum_{i=n+1}^{m} p_i(\vec{x}) | \vec{x} \in A^k\}$.*

Thus P_{n+1} bounds all contributions to the polynomial of order higher than n.

Theorem 4.2.3 *If $F(A^k)$ is an IC evaluation of a polynomial f on A^k and $G(A^k)$ is an IC evaluation of a polynomial g on A^k, then $F(A^k) + G(A^k)$, $F(A^k) \cdot G(A^k)$, and $rF(A^k)$, $r \in \mathbb{R}$ are IC evaluations of $f + g$, $f \cdot g$, and rf on A^k, respectively.*

Proof: Given the polynomials $f : f(\vec{x}) = \sum_{i=0}^{\alpha} f_i(\vec{x})$ and $g : g(\vec{x}) = \sum_{i=0}^{\beta} g_i(\vec{x})$, then by definition

$$\begin{aligned} F_i \supseteq \{f_i(\vec{x}) | \vec{x} \in A^k\} \quad , \quad G_i \supseteq \{g_i(\vec{x}) | \vec{x} \in A^k\}, \ 0 \le i \le n, \\ F_{n+1} \supseteq \{ \sum_{i=n+1}^{\alpha} f_i(\vec{x}) | \vec{x} \in A^k\} \quad , \quad G_{n+1} \supseteq \{ \sum_{i=n+1}^{\beta} g_i(\vec{x}) | \vec{x} \in A^k\}, \end{aligned} \tag{4.23}$$

from this we infer

$$\begin{aligned} (F(A^k) + G(A^k))_i &= F_i + G_i \supseteq \{(f+g)_i(\vec{x}) | \vec{x} \in A^k\}, \ 0 \le i \le n+1, \\ (rF(A^k))_i &= rF_i \supseteq \{(rf)_i(\vec{x}) | \vec{x} \in A^k\}, \ 0 \le i \le n+1, \\ (F(A^k) \cdot G(A^k))_i &= \sum_{j=0}^{i} F_j G_{i-j} \supseteq \{\sum_{j=0}^{i} f_j(\vec{x}) g_{i-j}(\vec{x}) | \vec{x} \in A^k\} \\ &= \{(fg)_i(\vec{x}) | \vec{x} \in A^k\}, \ 0 \le i \le n, \end{aligned}$$

$$(F(A^k) \cdot G(A^k))_{n+1} = \sum_{i=0}^{n+1} (F_i \sum_{j=n+1-i}^{n+1} G_j)$$

$$\begin{aligned} &= \sum_{i=0}^{n} [F_i(\sum_{j=n+1-i}^{n} G_j + G_{n+1})] + F_{n+1}(\sum_{j=0}^{n} G_j + G_{n+1}) \\ &\supseteq [\sum_{i=0}^{n} [f_i(\sum_{j=n+1-i}^{n} g_j + \sum_{j=n+1}^{\beta} g_j)] + (\sum_{i=n+1}^{\alpha} f_i)(\sum_{j=0}^{n} g_j + \sum_{j=n+1}^{\beta} g_j)](A^k) \\ &= [\sum_{i=0}^{\alpha} (f_i \sum_{j=\max(n+1-i,0)}^{\beta} g_j)](A^k) \\ &= [\sum_{i=n+1}^{\alpha+\beta} (\sum_{j=0}^{\beta} f_{i-j} g_j)](A^k) = \{ \sum_{i=n+1}^{\alpha+\beta} (fg)_i(\vec{x}) | \vec{x} \in A^k\}. \end{aligned} \tag{4.24}$$

The expression in the fourth line from the bottom contains the expression in the next line, since it is an interval evaluation of the function in the third line from the bottom.

Some notations will become useful: Let I be an interval, then $[I; k]$ is an interval chain with the k^{th} order being I and all other orders being 0. We will only use

$$[I; n+1] = (0, \ldots, 0, I) \text{ and } [I; 1] = (0, I, 0 \ldots, 0) \ . \tag{4.25}$$

Given an IC by $I_c = (I_0, I_1, \ldots, I_{n+1})$, then the interval $[I_c]_k = I_k$ is the k^{th} order of I_c.

Theorem 4.2.4 *Let now $\mathcal{A}$ be any algorithm based on addition, scalar multiplication, and multiplication that evaluates a polynomial p at $\vec{x} = (x_1, \ldots, x_k)$. Then performing $\mathcal{A}$ on*

$$\vec{I}_c = [(0, A_1, 0, \ldots, 0), \ldots, (0, A_k, 0, \ldots, 0)] = [A^k; 1] \ . \tag{4.26}$$

a vector of interval chains, yields an IC evaluation of p on A^k.

Proof: For all $l \in \{1, \ldots, k\}$, the interval chain $(0, A_l, 0, \ldots, 0)$ is an IC evaluation of the identity polynomial $i_l : \ i_l(\vec{x}) = x_l$ and $P(A^k)$ is the result of finitely many elementary operations which evaluate p and therefore, using theorem (4.2.3), we infer that $P(A^k)$ is an IC evaluation of p on A^k.

Bearing this in mind, it is easy to see that for an IC evaluation $D(A^k)$ of the deviation function d_f on A^k it holds that $\{d_f(\vec{x})|\vec{x} \in A^k\} \subseteq D_{n+1}$, since d_f is known to have no contributions with orders lower than $n+1$ if the map and the normal form transformation are evaluated to order $n-1$. In this approach cancellations up to order n do not contribute and blow-up caused by such cancellations is completely avoided. In fact, subtraction of f is not necessary at all any more, since

$$D_{n+1} = [d(\vec{I}_c)]_{n+1} = [f \circ \vec{M}(\vec{I}_c)]_{n+1} - [f(\vec{I}_c)]_{n+1} = [f \circ \vec{M}(\vec{I}_c)]_{n+1} \ , \qquad (4.27)$$

with the polynomial f of order n.

But even with these simplifications, the resulting objective functions have a tendency to exhibit interval blow-up because of complexity, while the bounds of the function have to be determined rather tightly in order to guarantee many turns. Furthermore, the functions have a large number of local maxima. All these effects make the exclusion of intervals rather difficult and not practically possible unless in the order of 10^4 intervals per dimension are used. These large numbers make bookkeeping of intervals for later exclusion rather cumbersome if not impossible.

Because of this situation, the conventional methods discussed in subsection (4.1), which are based on disposing of intervals that can be excluded and halving of the remaining ones combined with occasional local optimization in real arithmetic, are not directly applicable. For this reason, we restricted ourselves to a mere rastering of the objective function with a large number of intervals of equal size. The results in the next section were obtained by choosing 630 intervals for the examples with one degree of freedom and 1,000,188 for the example with two degrees of freedom. Because of limitations in computation time, it was still assumed that the maximum of the deviation function occurs on the surface of the allowed region. *Without the concept* of interval chains a realization of the described method was virtually impossible. For

examples with two degrees of freedom approximately 10^{12} times more intervals would *have been needed for similar results.*

4.3 Parameterizing Regions for the IC–PIE Method

To avoid interval blow-up, it is advisable to perform as few operations as possible. This fact becomes obvious when subdistributivity in equation (4.9) is considered. We therefore try to minimize the computations required to represent the initial and the allowed region. Previously the invariant tori of order n were represented by equation (2.28). The conventional emittance and acceptance of linear motion is given by the invariant tori of first order motion, which are given by $n = 1$ in equation (2.28), and by construction of the sets $\mathcal{F}(\xi, \zeta)$ in equation (2.29). We now write the tori in linear normal form space as

$$\mathcal{T}_{NF}(\vec{\epsilon}) = \{\vec{z}|\begin{pmatrix} z_{2i-1} \\ z_{2i} \end{pmatrix} = \sqrt{\epsilon_i}\begin{pmatrix} cos(\phi_i) \\ \sin(\phi_i) \end{pmatrix}, \phi_i \in [0, 2\pi], \forall i \in \{1, \ldots, d\}\} \qquad (4.28)$$

and the regions in linear normal form space as

$$\mathcal{F}_{NF}(\xi, \zeta) = \{\vec{z}|\vec{z} \in \mathcal{T}_{NF}(\vec{\eta}), \xi \leq \sum_{i=1}^{d} \frac{\eta_i}{\epsilon_i} \leq \zeta\} \ . \qquad (4.29)$$

Then the relevant phase space regions are given by

$$\mathcal{F}(\xi, \zeta) = \{\vec{B}_1^{-1}(\vec{z})|\vec{z} \in \mathcal{F}_{NF}(\xi, \zeta)\} \ , \qquad (4.30)$$

where $\vec{B}_1^{-1}$ is the linear part of the inverse normal form transformation $\vec{B}^{-1}$.

To find the maximum deviation function δ on the surface of the acceptance, we have to find

$$\begin{aligned} \delta &= \max\{(f \circ \vec{M} - f) \circ \vec{B}_1^{-1}|\mathcal{F}_{NF}(1,1)\} \qquad (4.31) \\ &= \max\{f \circ \vec{B}_1^{-1} \circ \vec{B}_1 \circ \vec{M} \circ \vec{B}_1^{-1} - f \circ \vec{B}_1^{-1}|\mathcal{F}_{NF}(1,1)\} \ . \end{aligned}$$

The map $\vec{B}_1 \circ \vec{M} \circ \vec{B}_1^{-1}$ is the transfer map in the first order normal form space and is to first order a rotation in every $z_{2i-1} \times z_{2i}$ plane in phase space. Call this linear rotation map $\vec{R}$ and let $\vec{N} = \vec{B}_1 \circ \vec{M} \circ \vec{B}_1^{-1} \circ \vec{R}^{-1}$; $\vec{N}$ is the identity to first order. Write $g = f \circ \vec{B}_1^{-1}$ to get

$$\delta = \max\{g \circ \vec{N} \circ \vec{R} - g|\mathcal{F}_{NF}(1,1)\} \ . \tag{4.32}$$

g is a polynomial of order n if the evaluation order for $\vec{M}$ is $n-1$. g therefore does not contribute to the order $n+1$ of the interval chain which is used to bound d_f and the second appearance of g in equation (4.32) can be omitted. The rotation $\vec{R}$ leaves the tori invariant and can therefore be avoided; we finally get the simple interval evaluation of

$$\delta = \max\{g \circ \vec{N}|\mathcal{F}_{NF}(1,1)\} \ . \tag{4.33}$$

Now the intervals $[0, 2\pi]$ in the definition of $\mathcal{T}_{NF}$ in equation (4.28) have to be covered by many small intervals. The maximum upper bound of the intervals $[g \circ \vec{N}|_{I_c}]_{n+1}$ has to be found for all interval chains I_c that cover $\mathcal{F}_{NF}(1,1)$. This yields a rigorous upper bound for δ. All blow up due to linear transformations is avoided in this way.

4.4 Comparison Between Intervals and Interval Chains

Several nonlinear systems were studied using the interval chain rastering methods to provide upper bounds for the invariant defects. In order to get a sense for the quality of these upper bounds, the numbers were compared with approximations for the maximal invariant defects obtained by a rather tight rastering in real arithmetic. Because of the large number of local maxima, this method proved to be the most robust non-interval approach to estimate the absolute maxima of the functions involved. Lower

Order of Invariant	Interval Bounding (guaranteed)	Interval Chains (guaranteed)	Conventional Rastering (optimistic)
3	11,252	743,667	849,195
4	11,252	743,667	849,195
5	11,306	876,059,284	982,129,435
6	11,306	876,059,284	982,129,435
7	11,306	432,158,877,713	636,501,641,854
8	11,306	432,158,877,713	636,501,641,854

Table 4.1: Predictions of the number of stable turns as a function of the order of the polynomials describing the normal form transformation for the physical pendulum with a maximum elongation of 1/10 rad. Because of energy conservation, the map is known to be permanently stable.

bounds on the number of stable turns obtained by conventional intervals are given in the tables (4.1), (4.2), and (4.3) in order to illustrate the usefulness of interval chains. When conventional intervals were used, the deviation function was simplified as much as possible by accounting for cancellations up to second order analytically. The number of conventional intervals and the number of interval chains used in the bounding are equivalent.

As the first example to check the method, we used a one-dimensional physical pendulum. This is a good test case, since energy conservation requires the nonlinear motion to be stable. Table (4.1) shows the results of the stability analysis for this case. As is to be expected, the number of stable turns predicted increases with the order and hence accuracy of the approximate invariants. While the approximate scanning method can take full advantage of this increased accuracy, the interval bounding method shows a saturation at 11,306 turns. This asymptotic behavior is connected to the size of the intervals because of the unavoidable blow-up of intervals in the process of cancellation of large terms. The blow-up in third order dominates the calculation, causing the higher order improvements to not materialize. The method of interval

chains takes care of all the cancellations up to evaluation order and consequently the estimate is much better.

Order of Invariant	Interval Bounding (guaranteed)	Interval Chains (guaranteed)	Conventional Rastering (optimistic)
2	895	891	1,086
3	1,736	9,926	11,450
4	1,668	54,016	65,667
5	1,674	678,725	809,612
6	1,670	3,389,641	4,351,679
7	1,671	42,640,927	52,474,387
8	1,671	192,650,961	263,904,035

Table 4.2: Predictions of the number of stable turns for the Henon map at tune 0.13, strength parameter 1.1, and starting position $(x, a) = (0.01, 0)$ as a function of the order of the normal form transformation.

As another example, we chose the Henon map described in section (2.4). The results of these calculations are shown in table (4.2). Similar to the previous case, the number of predicted turns increases with order. In the case of interval bounding, the number of guaranteed turns shows asymptotic behavior limited by blow-up. Again the superiority of strict bounding with interval chains is obvious.

Order of Invariant	Interval Bounding (guaranteed)	Interval Chains (guaranteed)	Conventional Rastering (optimistic)
3	179	16,137	38,385
4	179	18,197	38,857
5	173	309,356	560,309
6	173	347,312	613,135
7	171	925,531	2,184,998
8	171	1,004,387	2,248,621

Table 4.3: Predictions of the number of stable turns as a function of the order of the approximate invariant for the Los Alamos PSR II storage ring for the motion in a phase space of 100 mm mrad.

In the final example, we study a realistic accelerator, the Los Alamos PSR II

already described above. The same data are shown as for the two previous, more academic examples. To limit the calculation time, the intervals used for the optimization were 5 times as wide as the intervals used for the previous two tables. The results are shown in table (4.3).

4.5 Refinement of the Rigorous Estimates

In section (3.1) the long term estimation by pseudo invariants was improved by three methods:

1. analysis of multi-turn maps,
2. separation of phase space,
3. consideration of random parameters.

The improvements obtained by separating phase space in smaller regions can increase the bound on the survival time by about a factor of ten. With interval arithmetic this method becomes impracticable. As observed, using arithmetic with interval chains, one can bound the maximum of the deviation function d_f rigorously and rather tightly. This is only possible, since all low order contributions to the deviation function vanish. When separate phase space regions are used, one has to find several maxima and minima $u_i = \max\{f(\vec{z}) | \vec{z} \in \mathcal{F}(\alpha_i, \alpha_i)\}$ and $l_i = \min\{f(\vec{z}) | \vec{z} \in \mathcal{F}(\alpha_i, \alpha_i)\}$ as mentioned in equation (3.3). The polynomial f does not have the property that low orders vanish and therefore the advantages of ICs do not materialize. At current computer speed, these maxima and minima can therefore not be bounded rigorously with the required tightness.

In order to minimize interval blow-up, it is desirable to minimize the number of operations needed. For the rigorous computation with intervals, we chose therefore

the first order acceptances to describe the allowed and the initial region, and we performed all first order transformations analytically without blow-up, as already described in section (4.3).

Therefore $n = 1$ was used in equation (2.28) when representing $\mathcal{F}(\zeta, \zeta)$ by equation (2.30). For optimization by scanning, it was necessary to use the nonlinear acceptance to make $l_i - u_{i-1}$ as big as possible when separation of phase space was used.

Because of the described problems with finding extrema of f, it is not possible at current computer speed to find the required maximum on $\mathcal{S}_i$ and minimum on $\mathcal{S}_f$ rigorously. In the examples given below we performed these optimizations by scanning. The more critical deviation function d_f however was bounded rigorously. As mentioned before, the introduction of interval chains improved the computation time at least by a factor of 10^{12}. However, even after this reduction of CPU time, at current computer speed the needed computations take very long. In the examples a restriction to the surface of the allowed region was necessary when d_f was optimized with interval chains.

One can try to use multi-turn maps and random parameters to refine the IC-PIE method. For the simple application of PIE, the surface of the allowed region was completely covered in order to rigorously bound the maximum of the deviation function. In the case of two dimensional phase space, the surface was covered by 800 intervals; for four dimensional phase space, 8,000,000 intervals were used. For the parameter dependent case, these numbers were 160,000 and 50,000,000, respectively.

4.5.1 Analysis of Multi–Turn Maps

It was discussed in section (3.1) and displayed in figure (3.3) that the quality of the pseudo invariants fluctuates depending on how often the transfer map is applied. One

can try to use multi-turn maps for rigorous estimation with the use of ICs.

Usually the map has to be applied k times for every phase space interval, in order to evaluate the k-turn map. Computing the n^{th} order Taylor approximation of the k-turn map would only take approximately $[\log_2(k)]$ Taylor map compositions and would save a lot of CPU time, however, using this approach would not be rigorous, since the orders higher than the evaluation order n, which are created by the compositions, would be neglected. Interval chains allow one to take advantage of the speed increase achieved by Taylor map compositions. This is due to the fact that we can bound the high order contributions of map compositions by applying ICs.

In the subsequent section (4.6), Taylor maps with remainder intervals will be used to describe non-polynomial maps rigorously. For this we denote the map by $\vec{M}$ and its n^{th} order Taylor map by $\{\vec{M}\}_n$. The remainder only has contributions of orders higher than n. An interval bound on the remainder of $\{\vec{M}\}_n$ over a phase space region A will be denoted by the vector of intervals $\vec{R}_1(A)$, and then

$$\vec{M}(\vec{z}) \in \{\vec{M}\}_n(\vec{z}) + \vec{R}_1(A) \quad \forall \vec{z} \in A \,. \tag{4.34}$$

With interval chains, a remainder of the two-turn map $\vec{M}^2$ can be computed if a region B_1 of phase space can be found with $B_1 \supseteq \vec{M}(A)$. One way to find such a region is the interval evaluation of $\vec{M}_n$ by

$$B_1 = \{\vec{M}\}_n(A) + \vec{R}_1(A) \supseteq \vec{M}(A) \,. \tag{4.35}$$

Let $\vec{R}_1(B_1)$ be the remainder of the Taylor map in the region B_1. Then the Taylor expansion of the two-turn map is bounded by

$$\begin{aligned} \vec{M}^2(\vec{z}) &\in \{\vec{M}\}_n(\{\vec{M}\}_n(\vec{z}) + \vec{R}_1(A)) + \vec{R}_1(B_1) \\ &\in \{\vec{M}^2\}_n(\vec{z}) + [\{\vec{M}\}_n(\{\vec{M}\}_n([A;1]) + [\vec{R}_1(A); n+1])]_{n+1} + \vec{R}_1(B_1) \\ &= \{\vec{M}^2\}_n(\vec{z}) + \vec{R}_2(A) \,, \end{aligned} \tag{4.36}$$

and one is left with an interval remainder for the n^{th} order expansion of the two-turn map. $[\vec{R}_1(A); n+1]$ could only be written because the remainder only has contributions of order higher than n. The necessity to know a bound on the region $\vec{M}(A)$ in order to compute $\vec{R}_2(A)$ can make computations very involved. This becomes apparent when a remainder interval for the 2^k-turn map is computed from a given 2^{k-1}-turn map with remainder interval. Let equation (4.34) be given and assume that from this information a bound on the 2^{k-1} turn map was computed with ICs to get

$$\vec{M}^{2^{k-1}}(\vec{z}) \in \{\vec{M}^{2^{k-1}}\}_n(\vec{z}) + \vec{R}_{2^{k-1}}(A) \quad \forall \vec{z} \in A \,. \tag{4.37}$$

The demonstrated method computes the remainder of the 2^k-turn map by

$$\vec{R}_{2^k}(A) = [\{\vec{M}^{2^{k-1}}\}_n(\{\vec{M}^{2^{k-1}}\}_n([A;1]) + [\vec{R}_{2^{k-1}}(A); n+1])]_{n+1} + \vec{R}_{2^{k-1}}(B_{2^{k-1}}) \tag{4.38}$$

with the region $B_{2^{k-1}} \supseteq \vec{M}^{2^{k-1}}(A)$, which can again be found by interval arithmetic evaluation of $\{\vec{M}^{2^{k-1}}\}_n(A) + \vec{R}_{2^{k-1}}(A)$. However, finding the remainder $\vec{R}_{2^{k-1}}(B_{2^{k-1}})$ requires to repeat all the procedure of obtaining bounds of compositions from $\vec{M}$ up to $\vec{M}^{2^{k-1}}$, now for $B_{2^{k-1}}$ instead of A.

This general problem can be overcome easily in case of the PIE method. The reason for the simplifications is that the simple application of the PIE method for the one-turn map gives bounds on all the needed regions B_i. If an interval remainder of the 2^l-turn map is desired, then let $B = \mathcal{F}(0,\gamma)$ and let the maximum δ of the deviation function in this region be given. Choose γ such that $A = \mathcal{F}(0, \gamma - 2^l \cdot \delta)$ is the phase space region for which remainder intervals are to be found. B therefore contains all regions $\vec{M}^i(A)$ for $i \in \{1, \ldots, 2^l\}$. We can compute all remainders over that region B to get bounds for map applications in the region A. The step from the 2^{k-1}-turn map to the 2^k-turn map simply reads

$$\vec{M}^{2^k}(\vec{z}) \in \{\vec{M}^{2^k}\}_n \tag{4.39}$$

$$+ \; [\{\vec{M}^{2^{k-1}}\}_n(\{\vec{M}^{2^{k-1}}\}_n([A;1]) + [\vec{R}_{2^{k-1}}(B); n+1])]_{n+1} + \vec{R}_{2^{k-1}}(B) \,.$$

There is now no need to go back to a lower turn number for obtaining bounds on a different region than B. All the required interval chain evaluations can be performed on a set of smaller intervals covering B. As before, the union of all remainders found on the subintervals is then used as an interval remainder.

The size of remainder intervals decreases drastically with the evaluation order used. This is shown in table (4.4), where the union of the remainder intervals for the different phase space coordinates is displayed. To allow comparison to the previously demonstrated calculations, we continue to use order 8. In table (4.5) the bounds on the remainder of the multi-turn maps for various turn numbers is displayed for four examples. For the Pendulum and the Henon map, 700 intervals were used to cover the region of interest. For the coupled pendulum, the number of intervals was 1,000. For the PSR II ring, 1,000,000 intervals were used to reduce blow-up.

The deviation function d_f is bounded by

$$d_f(\vec{z}) \in [f(\{\vec{M}^{2k}\}_n([A;1]) + [\vec{R}; n+1])]_{n+1} + \{f(\vec{M}^{2k})\}_n(\vec{z}) \tag{4.40}$$

$$= [f(\{\vec{M}^{2k}\}_n([A;1]) + [\vec{R}; n+1])]_{n+1}. \tag{4.41}$$

The term $\{f(\vec{M}^{2k})\}_n$ vanishes, since f is an order n invariant of $\vec{M}$ as well as of $\vec{M}^{2k}$.

The higher order Taylor coefficients of the composed map $\vec{M}^{2k}$ increase with k, and with the increased nonlinearities also the interval blow-up increases. This blow-up counteracts the advantages of applying multi-turn maps, which do not materialize with the current evaluations of intervals and at the evaluation order used. Increasing the evaluation order substantially, however, is not possible at current computer speed.

Order	Pendulum	Henon
6	$[-0.288, 0.288] \cdot 10^{-5}$	$[-0.450, 0.483] \cdot 10^{-4}$
7	$[-0.455, 0.455] \cdot 10^{-7}$	$[-0.997, 0.724] \cdot 10^{-5}$
8	$[-0.456, 0.456] \cdot 10^{-7}$	$[-0.189, 0.199] \cdot 10^{-5}$
9	$[-0.112, 0.112] \cdot 10^{-8}$	$[-0.600, 0.562] \cdot 10^{-6}$
10	$[-0.113, 0.113] \cdot 10^{-8}$	$[-0.182, 0.179] \cdot 10^{-6}$
11	$[-0.347, 0.347] \cdot 10^{-10}$	$[-0.450, 0.500] \cdot 10^{-7}$
12	$[-0.350, 0.350] \cdot 10^{-10}$	$[-0.145, 0.140] \cdot 10^{-7}$
13	$[-0.121, 0.121] \cdot 10^{-11}$	$[-0.433, 0.462] \cdot 10^{-8}$
14	$[-0.122, 0.122] \cdot 10^{-11}$	$[-0.142, 0.150] \cdot 10^{-8}$
15	$[-0.422, 0.422] \cdot 10^{-13}$	$[-0.481, 0.461] \cdot 10^{-9}$
16	$[-0.425, 0.425] \cdot 10^{-13}$	$[-0.152, 0.153] \cdot 10^{-9}$

Order	Coup. Pend.	PSR II ring
6	$[-0.401, 0.401] \cdot 10^{-5}$	$[-0.451, 0.451] \cdot 10^{-5}$
7	$[-0.499, 0.499] \cdot 10^{-6}$	$[-0.370, 0.370] \cdot 10^{-6}$
8	$[-0.113, 0.113] \cdot 10^{-6}$	$[-0.358, 0.358] \cdot 10^{-6}$
9	$[-0.152, 0.152] \cdot 10^{-7}$	$[-0.289, 0.289] \cdot 10^{-7}$
10	$[-0.332, 0.332] \cdot 10^{-8}$	$[-0.278, 0.278] \cdot 10^{-7}$
11	$[-0.482, 0.482] \cdot 10^{-9}$	$[-0.217, 0.217] \cdot 10^{-8}$
12	$[-0.982, 0.982] \cdot 10^{-10}$	$[-0.207, 0.207] \cdot 10^{-8}$

Table 4.4: Decreasing width of the remainder interval with evaluation order.

Turns	Pend.	Henon
2	$[-0.659, 0.659] \cdot 10^{-11}$	$[0.000, 0.000]$
4	$[-0.354, 0.354] \cdot 10^{-10}$	$[-0.128, 0.114] \cdot 10^{-8}$
8	$[-0.261, 0.261] \cdot 10^{-9}$	$[-0.732, 0.870] \cdot 10^{-7}$
16	$[-0.353, 0.353] \cdot 10^{-8}$	$[-0.296, 0.339] \cdot 10^{-6}$
32	$[-0.457, 0.457] \cdot 10^{-7}$	$[-0.190, 0.199] \cdot 10^{-5}$
64	$[-0.791, 0.791] \cdot 10^{-6}$	$[-0.221, 0.239] \cdot 10^{-4}$
128	$[-0.124, 0.124] \cdot 10^{-4}$	$[-0.214, 0.216] \cdot 10^{-3}$
256	$[-0.218, 0.218] \cdot 10^{-3}$	$[-0.361, 0.320] \cdot 10^{-2}$

Turns	Coup. Pend.	PSR II ring
2	$[-0.247, 0.247] \cdot 10^{-11}$	$[-0.367, 0.367] \cdot 10^{-11}$
4	$[-0.108, 0.108] \cdot 10^{-10}$	$[-0.144, 0.144] \cdot 10^{-9}$
8	$[-0.509, 0.517] \cdot 10^{-10}$	$[-0.212, 0.212] \cdot 10^{-8}$
16	$[-0.373, 0.374] \cdot 10^{-9}$	$[-0.240, 0.240] \cdot 10^{-7}$
32	$[-0.449, 0.449] \cdot 10^{-8}$	$[-0.441, 0.441] \cdot 10^{-6}$
64	$[-0.586, 0.592] \cdot 10^{-7}$	$[-0.789, 0.789] \cdot 10^{-5}$
128	$[-0.705, 0.705] \cdot 10^{-6}$	$[-0.932, 0.931] \cdot 10^{-4}$
256	$[-0.117, 0.115] \cdot 10^{-4}$	$[-0.880, 0.880] \cdot 10^{-2}$

Table 4.5: Remainder intervals for multi-turn maps.

4.5.2 Random Parameters

We want to find a lower bound on the survival time for a given accelerator including uncertainty of a parameter in a given tolerance. The same settings as in table (4.6) were used. Instead of the length or field strength, also other parameters could have been used, like the uncertainty of the particle's energy or uncertainty in the length of an element.

The pseudo invariants are computed by parameter dependent nonlinear normal *form theory*, which is described at the end of chapter (1). While a different parameter produced a different transfer map, it also produces a different pseudo invariant which changes very little during one application of that map. This is due to the fact that

$$f \circ \vec{M} - f =_{n+1} 0 \tag{4.42}$$

holds for parameter dependent map, when "$=_n$" equates *partial derivatives in respect* to parameters as well as in respect to coordinates, and $f(\vec{z}, \delta)$ as well as $\vec{M}(\vec{z}, \delta)$ are functions of the parameter δ.

Lower bound for	**Pendulum**	**Henon map**
Simplest application	52,366,096,777	5,830,904
Length and Strength uncertainty 1%	14,051,907,204	3,123,964
Lower bound for	**Coup. Pendulum**	**IUCF**
Simplest application	56,917,938,176	19,500,358
Length/Field uncertainty 1% / 0.01%	27,080,626,416	10,768,020
Lower bound for	**PSR II**	**Demo**
Simplest application	58,680,622	10,106,151
Length/Field uncertainty 1% / 0.01%	45,819,009	4,831,120

Table 4.6: Lower bounds on the turns of particles for an initial emittance of one half the acceptance, obtained by the IC–PIE method.

4.6 Using Taylor Maps with Remainder Bound

So far we were only concerned with nonlinear motion which is described by Taylor maps. The number of interest was the survival time of particles in an accelerator. This time was formulated as the number of map applications for which no phase space point of the initial beam distribution is mapped into a forbidden region. A method was presented with which rigorous lower bounds on this number can be obtained. In the phase space regions which we analyzed, the Taylor maps usually describe the accelerator well and the limits obtained are valuable for storage rings, however, strictly speaking they are not rigorous, since the transfer map of an accelerator is not a polynomial map.

This problem could be overcome if a bound on the remainder of the Taylor map would be known. The method of RDA, described in reference [BH94a], potentially provides a way of rigorously bounding the Taylor remainder of functions which can be evaluated with DA based programs. As on page (108) for ICs, also for this method elementary operations are introduced such that an operation between two Taylor maps with remainder intervals yields again a Taylor map with remainder interval. Furthermore, function evaluations on Taylor maps with remainders are introduced, as well as a derivative. With these operations, all functions which can be evaluated with DA programs to obtain their Taylor map, can also be evaluated with RDA programs to obtain their Taylor map and a bound on the remainder. The implementation of the rigorous RDA method is a bigger project and will be future work. Here we will estimate remainders by comparing the 8^{th} order map with the 19^{th} order map for the two dimensional case and with the 12^{th} order map for the cases of four dimensional phase space. The results for the examples are shown in table (4.7).

The long term analysis will be performed with the Taylor map and the remainder

Pendulum	Henon	Coup. Pend.
$[-0.517, 0.517] \cdot 10^{-12}$	$[\ 0.000, 0.000]$	$[-0.268, 0.268] \cdot 10^{-9}$
IUCF ring	PSR II	Demo ring
$[-0.248, 0.248] \cdot 10^{-13}$	$[-0.282, 0.282] \cdot 10^{-11}$	$[-0.727, 0.727] \cdot 10^{-8}$

Table 4.7: Maximum error of the Taylor map in the phase space region of interest.

term by evaluating

$$d_f(\vec{z}) \in \{f(\vec{M})\}_n + [f(\vec{M}([\Lambda; 1]) + [\vec{R}; n+1])]_{n+1} \tag{4.43}$$

$$= [f(\vec{M}([\Lambda; 1]) + [\vec{R}; n+1])]_{n+1} \tag{4.44}$$

with the remainder $\vec{R}$. Calculations equivalent to those of section (4.5) were performed with this complete map and the results are shown in table (4.8).

	Guaranteed Turns	With Unknown Parameter
Pendulum	21,517,254,240	10,064,641,158
Henon	5,831,178	3,123,964
Coup. Pend.	25,021,201	24,506,730
IUCF	19,441,816	10,749,711
PSR II	49,241,881	39,571,014

Table 4.8: Results of the IC-PIE bounds on the survival time of particle motion for *rigorous description of the systems by a Taylor map with remainder intervals.*

Chapter 5

Symplectic Scaling (SYSCA)

The map which relates coordinates $\vec{z}_i$ in the initial plane of an optical system to coordinates $\vec{z}_f$ in the final plane contains all information about optical properties. This map depends on the parameters of the system and is expressed by $\vec{M} : I\!R^{2d+p} \rightarrow I\!R^{2d}$ for d degrees of freedom and p system parameters δ_i, such that

$$\vec{z}_f = \vec{M}(\vec{z}_i, \vec{\delta}) \ . \tag{5.1}$$

It occurred first to Hamilton that optical systems could be analyzed by computing the Taylor expansion of their transfer map [Pra33]. He utilized what he called the characteristic function to compute this expansion to third order for rotationally symmetric optical systems. This concept was also used in charged particle optics. The motion of the particles is described by a set of ordinary differential equations

$$\frac{d}{ds}\vec{z} = \vec{f}(\vec{z}, \vec{\delta}, s) \ . \tag{5.2}$$

where s is the coordinate along the central trajectory and $\vec{z}$ describes the usual particle optical coordinates. *The general solution of this set of differential equations yields the* transfer map of the system. Starting from the 1930s, many references can be given which carried the computation of Taylor maps to higher orders. Some important contributions can be found in [BS34, BBB64, Wol65, PR71, Ros87]. The Taylor

coefficients are typically described as multiple integrals over powers of solutions of the linearized equation of motion. The kernels of these integrals can be computed with the program MOPS [Pre92] to an arbitrary order; above order seven the formulas tend to become very lengthy. If the fields involved do not change with s and consequently the equation of motion (5.2) is autonomous, then the linearized equation of motion can be solved in basic functions and also the integrations can be performed analytically. In this case the Taylor coefficients can be computed with the program COSY 5.0 up to fifth order [BHW87].

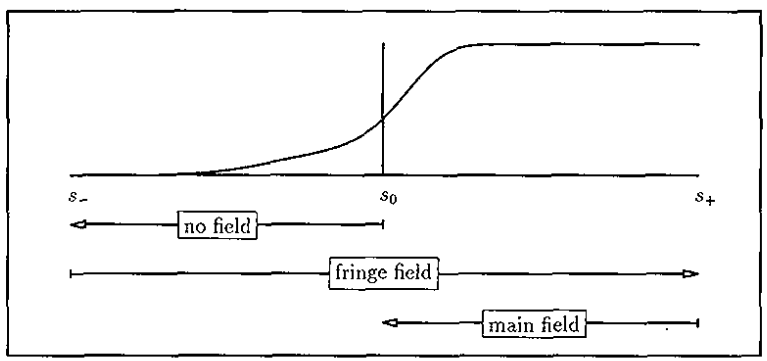

Figure 5.1: Definition of fringe-field and main-field maps.

Because of the simplifications involved in the regions where the field does not depend on s, traditionally the field of a particle optical device is separated into the main-field region and the fringe-field region as shown in figure (5.1). This figure also describes the definition of the fringe-field and the main-field map. To compute the main-field map $\vec{M}_{mf}$, one assumes that the field $\vec{B}(x,y,s)$ between the effective field boundaries does not change along the central trajectory and has the structure of the

field at the middle $s = s_m$ of the element. Outside the effective field boundary the field is assumed to vanish.

$$\vec{B}_{mf}(x,y,s) = \begin{cases} \vec{B}(x,y,s_m) & \text{for } s \text{ in the main field} \\ \vec{0} & \text{for } s \text{ outside the main field} \end{cases} \tag{5.3}$$

The abrupt change of the field violates the Laplace equation and can therefore not represent a physical system. To describe a realistic system, the main-field map has to be composed with fringe-field maps, which describe the connection of the main-field to the field-free region outside the element.

The fringe-field map $\vec{M}_{ff}$ can be decomposed into three maps. To illustrate this, let s_0 denote the effective field boundary at the entrance of the element, s_- be a position so far before the optical device that the field can be neglected, and let s_+ be a position so far inside the element that $\vec{B}(x,y,s)$ changes very little with s. The map $\vec{M}_{mf,s_0\to s_+}$ describes the particle motion through the main field given in equation (5.3) from the effective field boundary to s_+. The fringe-field map is constructed in such a way that a drift $\vec{D}_{s_-\to s_0}$ from s_- to the effective field boundary composed with $\vec{M}_{ff}$ and then with $\vec{M}_{mf,s_0\to s_+}$ yields the transfer map $\vec{M}_{s_-\to s_+}$ from s_- to s_+ by

$$\vec{M}_{s_-\to s_+} = \vec{M}_{mf,s_0\to s_+} \circ \vec{M}_{ff} \circ \vec{D}_{s_-\to s_0} \,. \tag{5.4}$$

This leaves the fringe-field map as

$$\vec{M}_{ff} = \vec{M}^{-1}_{mf,s_0\to s_+} \circ \vec{M}_{s_-\to s_+} \circ \vec{D}^{-1}_{s_-\to s_0} \,. \tag{5.5}$$

Computing fringe-field maps requires the computation of the map $\vec{M}_{s_-\to s_+}$ of a system where $\vec{B}(x,y,s)$ depends on s, and therefore the right hand side in the equation of motion (5.2) depends on s. For this, methods to find general solutions of non-autonomous differential equations are needed. The method of numerical integration in DA will be described, which yields Taylor maps to non-autonomous ordinary differential equations for an arbitrary expansion order.

5.1 Integration in DA

Since the theory of differential algebra (DA) and its applications is sufficiently discussed in the literature [Ber92a, Ber91a, Ber90a, Ber89, Ber87, Ral81], only the underlying idea will be lined out here. As mentioned previously, one can introduce the notion that functions agree up to order n as an equivalence relation. Equivalence is denoted by "$=_n$", which equates functions which have the same partial derivatives at the origin up to order n. In other words, "$=_n$" equates maps which have the same Taylor map up to order n. A differential algebra of the corresponding equivalence classes can be established. Since a Taylor expansion of any map in an equivalence class represents the whole class, this concept leads to a rigorous description of the manipulation of Taylor maps. Functions which can be represented by a computer consist of finitely many elementary operations and elementary function evaluations. The set of these functions is too big to be handled on a computer. The success which the DA concept experienced in the last 8 years is due to the fact that there is a homeomorphism from this set of functions into the differential algebra.

If f is a function of this set, then we symbolize the corresponding element in the differential algebra as $[f]_n$. Let $\mathcal{A}_f$ be an algorithm evaluating a function $f : \mathbb{R}^d \to \mathbb{R}$ then $\mathcal{A}_f\vec{x} = f(\vec{x})$ for all $\vec{x} \in \mathbb{R}^d$. When $\vec{z}$ is the identity function in $\mathbb{R}^d$, then $\mathcal{A}_f\vec{z} = f$. Due to the homeomorphism, we can evaluate the algorithm in the differential algebra via

$$\mathcal{A}_f\vec{z} = f \implies \mathcal{A}_f[\vec{z}]_n =_n [f]_n \,. \tag{5.6}$$

The equivalence class to "$=_n$" of the Taylor expansion of f is denoted by $[f]_n$. To obtain all partial derivatives of f up to order n, it is therefore sufficient to know the identity and to perform the elementary operations and the elementary function evaluations which contribute to $\mathcal{A}_f$ in the differential algebra. In the next section

we will deal with an algorithm which also contains derivatives. Under conditions explained in that section, also derivatives can be performed in the differential algebra.

Generally the equation of motion is solved by numerical integration. Starting with an initial coordinate $\vec{z}_i$ and a choice of parameters δ_i with $i \in \{1, \ldots, n_p\}$, the integration produces a final coordinate $\vec{z}_f$, which means that the combination of elementary numerical steps performed by the integrator define an algorithm $\mathcal{A}_{\vec{M}}$ which evaluates the transfer map $\vec{M}(\vec{z}, \vec{\delta})$. According to equation (5.6), evaluating the numerical integrator in the differential algebra yields the Taylor map to any order n. In our applications, the Taylor expansion is computed with respect to $\vec{z}$ as well as to $\vec{\delta}$. With the Taylor maps, all partial derivatives up to order n are computed. Because of this fact, the described function evaluation in DA is often called automatic differentiation of algorithms. In connection with this method, it is often referred to [Ral81], the basic idea, however, is much older.

5.2 Evaluating Propagators in DA

Let L_f denote the operator $\vec{\partial}^T\vec{f} + \partial_s f$. Then the equation of motion $d\vec{z}/ds = \vec{f}(\vec{z}, \vec{\delta}, s)$ allows one to compute all derivatives of $\vec{z}$ with respect to s by

$$\frac{d^2\vec{z}}{ds^2} = \vec{f}^T\vec{\partial}\vec{f} + \partial_s\vec{f} = L_f\vec{f}\,, \tag{5.7}$$

$$\frac{d^n\vec{z}}{ds^n} = (L_f)^{n-1}\vec{f} = (L_f)^n\vec{z}\,. \tag{5.8}$$

Let the central trajectory $\vec{z} = \vec{0}$ be a solution of the equation of motion for the system with parameters $\vec{\delta} = \vec{0}$, then $\vec{f}(\vec{0}, \vec{0}, s) = \vec{0}$. The Taylor expansion of $\vec{f}$ has no constant part and is known to order n, therefore $\vec{f}^T\vec{\partial}\vec{f}$ can be computed up to order n, in spite of the fact that $\vec{\partial}\vec{f}$ can only be computed up to order $n-1$. However, $\partial_s\vec{f}$ can only be known to order $n-1$. Therefore only maps to autonomous equations of motion, which have $\partial_s\vec{f} = \vec{0}$, can be evaluated in DA by the propagation operator, for which

we write

$$\vec{M} =_n \exp(L_{\vec{f}})\vec{z} = \sum_{i=1}^{\infty} \frac{1}{i!} L_{\vec{f}}^i \vec{z} = \sum_{i=1}^{\infty} \frac{1}{i!} (\vec{f}^T \vec{\partial})^i \vec{z} \,. \tag{5.9}$$

In writing this equation, we assume that all the involved sums converge. To use the propagator for non-autonomous differential equations, an extension of DA would have to be introduced, in which the coordinate s can be evaluated to orders higher than n.

In the main-field region the equation of motion is autonomous, and using the propagator in equation (5.9) to compute the map is very efficient. Figure (5.2) shows the time advantage as a function of the evaluation order for dipoles, quadrupoles, hexapoles, and octupoles.

Also the following table makes the time consumption of integration in DA apparent and shows the computation speed which is accomplished by the symplectic scaling approximation (SYSCA). It displays the time needed for fitting the multipole fields of the S800 beamline and the S800 Spectrograph, which are under construction at the NSCL, to satisfy 14 conditions on first order Taylor coefficients and 6 conditions on second order.

Only main fields with propagator	51 sec.
Fringe fields with DA integration	7 hours 10 min. 50 sec.
Fringe fields with SYSCA	6 min. 38 sec.

In order to analyze if the transfer map can be represented well by the main-field map, monomials are symbolized by $\vec{z}^{\vec{k}} = \prod_{i=1}^{2d} z_i^{k_i} \prod_{j=1}^{n_p} \delta_j^{k_{2d+j}}$ with natural numbers $k_j, j \in \{1, \ldots, 2d + n_p\}$. The order of such a monomial is given by $||\vec{k}|| = \sum_{j=1}^{2d+n_p} k_j$. Now the i^{th} component of the transfer map $\vec{M}$ can be written as

$$M_i = \sum_{m=1}^{n} \sum_{\vec{k}}^{||\vec{k}||=m} (M_i|\vec{z}^{\vec{k}})\vec{z}^{\vec{k}} \tag{5.10}$$

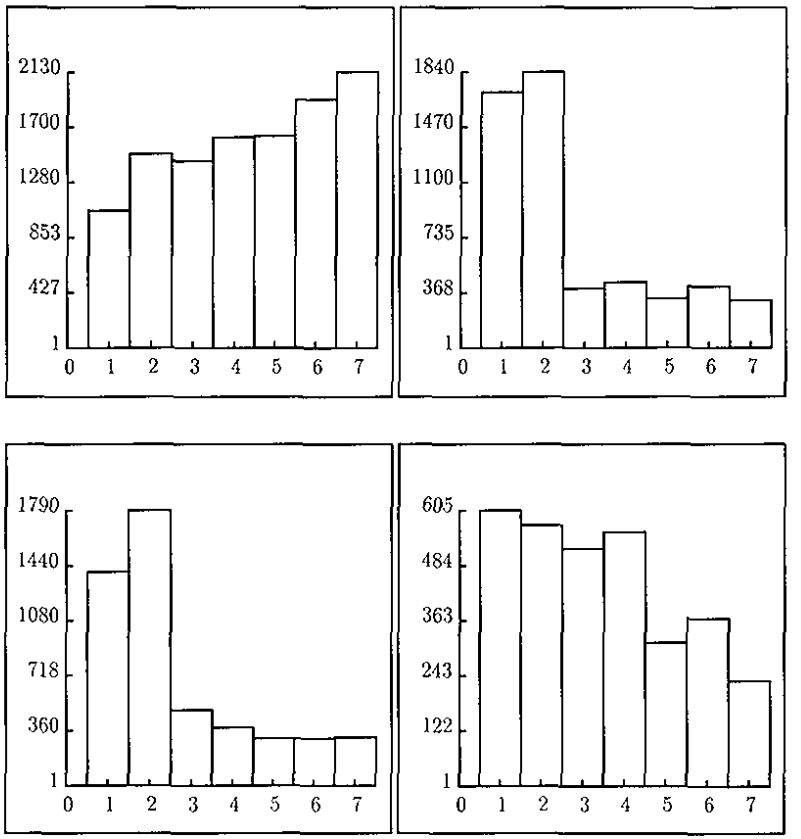

Figure 5.2: Time consumption of integration in DA relative to main-field map computation with the propagator for different expansion orders. From top left to bottom right: dipole, quadrupole, hexapole, octupole.

with symbols $(M_i|\vec{z}^{\vec{k}})$ for the Taylor coefficients. Figure (5.3) shows the normalized average deviation Δ_m between the Taylor coefficients of the transfer map and those of the main-field map in order m for four typical charged particle optics devices. The wedge dipole in the examples of this section has radius 2m, an angle of 30°, and an aperture of 2.54cm. All other multipoles have: length 41.9cm, a pole-tip field of 2T, and an aperture of 2.54cm. The chosen ion is $^{16}O^{3+}$ with an energy of 25MeV per nucleon. The fringe fields used are those of the Enge model [Ber92b, KE87, BS81]. Δ_m is computed by

$$\Delta_m = \frac{1}{\ln(2)} \sum_{i=1}^{2d} \sum_{\vec{k}}^{||\vec{k}||=m} \frac{|(M_i|\vec{z}^{\vec{k}}) - (M_{mf,i}|\vec{z}^{\vec{k}})|}{|(M_i|\vec{z}^{\vec{k}})| + |(M_{mf,i}|\vec{z}^{\vec{k}})|} \,. \tag{5.11}$$

If the coefficients $(M_i|\vec{z}^{\vec{k}})$ and $(M_{mf,i}|\vec{z}^{\vec{k}})$ are randomly chosen, then Δ_m is on average one. This can be seen by the following integration. If the coefficients are allowed to vary in an arbitrary interval between $-N$ and N, one can write

$$\ln(2) < \Delta_m > = \int_{-N}^{N}\int_{-N}^{N} \frac{|a-b|}{|a|+|b|}\frac{dadb}{4N^2} = \frac{1}{2} + 2\int_0^1\int_0^1 \frac{|a-b|}{a+b}\frac{dadb}{4} \tag{5.12}$$

$$= \frac{1}{2}(1 + \int_0^1 \int_{2b}^{1+b} \frac{a-2b}{a} dadb - \int_0^1 \int_b^{2b} \frac{a-2b}{a} dadb) \tag{5.13}$$

$$= \frac{1}{2}(1 + \int_0^1 \{1 - 2b - 2b\ln(\frac{1+b}{4b})\} db) \tag{5.14}$$

$$= \frac{1}{2}(1 - [b^2\ln(\frac{1+b}{4b})]_0^1 - \int_0^1 \frac{b}{1+b} db) \tag{5.15}$$

$$= \frac{1}{2}\{1 + \ln(2) - \int_0^1 (1 - \frac{1}{1+b}) db\} = \ln(2) \,. \tag{5.16}$$

Obviously, some trivial computational steps have been skipped.

Figure (5.3) shows that the so called "sharp cut off fringe field" (SCOFF) approximation, which replaces the transfer map by the main-field map, is very inaccurate for nonlinear coefficients. Some averages are even larger than one, and thus on average

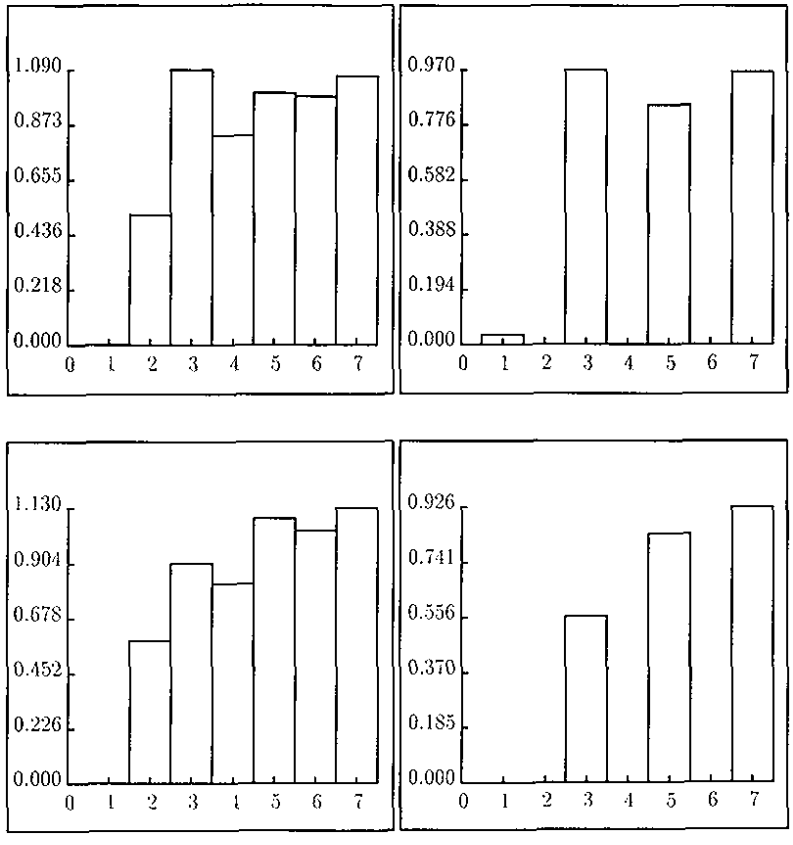

Figure 5.3: Accuracy of SCOFF for different orders, a random choice of Taylor coefficients would be close to one. From top left to bottom right: dipole, quadrupole, hexapole, octupole.

the approximation is worse than a random choice of coefficients. More examples of the insufficient accuracy of the SCOFF approximation will be demonstrated in section (5.5) where several examples are discussed.

These results show that the advantages of very quick DA evaluation of propagators can only be taken advantage of if an efficient fringe–field approximation can be found.

5.3 Desirable Properties of an Arbitrary Order Fringe–Field Approximation

After stating three properties which we consider desirable for a fringe–field approximation, the importance of each property will be explained in separate subsections. The approximation should:

1. lead to order n symplectic maps,
2. represent the fringe effect well for a wide range of apertures,
3. be usable for arbitrary orders.

The simplest approximation, as already described, is SCOFF, where fringe fields are simply ignored. As illustrated in section (5.2), this method strongly violates point 2. The impulse approximation [Hel63] used in the code TRANSPORT [BRCI77] violates the points 2 and 3 and the method of fringe–field integrals [HBW90, HIW93, Wol65] used in the computer code GIOS [WHB88, Wol92] violates the points 1 and 3.

5.3.1 Order n Symplecticity

The necessity for order n symplectic maps is especially apparent when long term behaviour in storage rings is to be analyzed. If the Taylor map does not approximate a symplectic map very well, then, according to theorem (1.6.4), the phase space area is not conserved in every $z_{2i-1} \times z_{2i}$ phase space section. This is the case for order n symplectic maps, when the evaluation order n is small. In [Yan91], for instance, it is illustrated that in case of the SSC lattice, expansion to 12^{th} order is needed to have a sufficient degree of symplecticity. If the fringe–field map is not computed to be order n symplectic, even very high evaluation orders can not lead to trustworthy predictions of long term behaviour.

In figure (5.4) the tracking picture of a 15° dipole for the horizontal plane is shown. On the left side the coordinates used are the conventional coordinates x–p_x, whereas on the right side the phase space points are displayed in normal form coordinates. Normal form coordinates are used since violation of the symplectic symmetry can most easily be seen in these coordinates, where the motion lies on circles if the map is symplectic.

The top two figures illustrate the action of the transfer map of the dipole. Since 24 applications of the map yield the identity, the motion is stable for all times. Approximating this map by a fifth order Taylor map does not approximate the symplectic transfer map sufficiently and the tracking points move further and further away from the origin, as if the motion were unstable. This is shown in the third and fourth figure in conventional and in normal form coordinates respectively.

To make the map completely symplectic, one can compute the Taylor expansion of a generating function from the Taylor map. The generating function can then be used for tracking particle coordinates through a completely symplectic approximation of

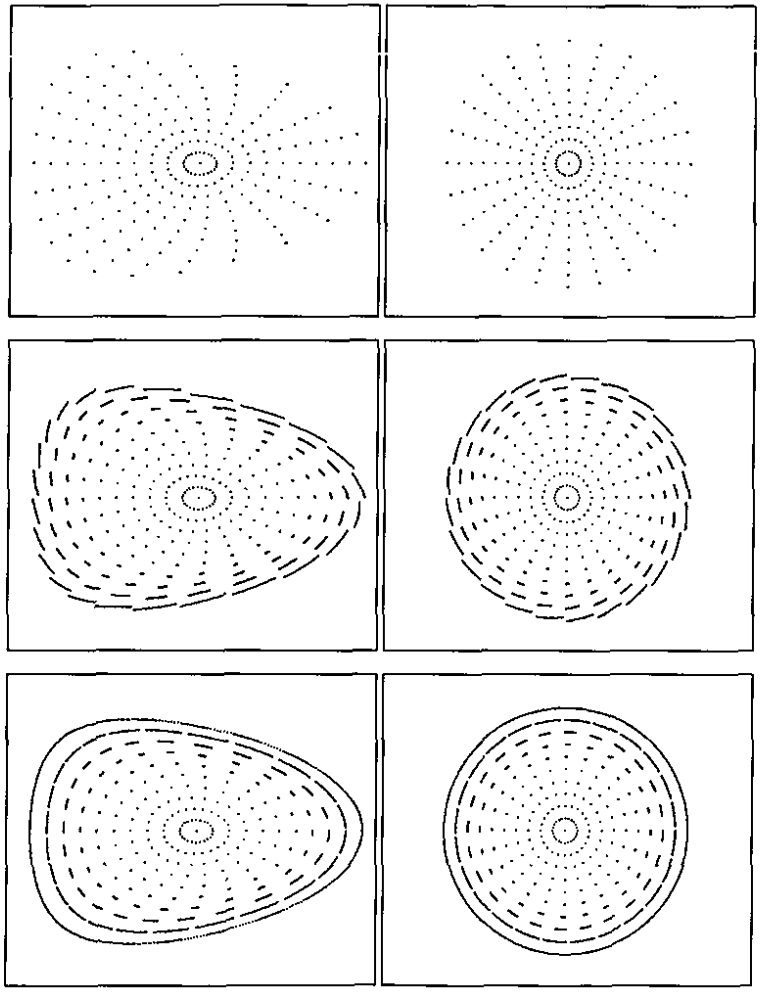

Figure 5.4: Tracking through a 15° dipole, displayed in conventional coordinates on the left and in normal form coordinates on the right. The figures on the top display accurate tracking data, those in the middle were created by the 5^{th} order Taylor map, and the bottom pictures were produced by 5^{th} order symplectic generating function tracking.

the transfer map. Strategies for symplectic tracking are discussed in [Ber88a, Ber91b, Yan93, Gja93]. This method relies on the order n symplecticity of the underlying map and therefore only a fringe-field approximation which leads to order n symplectic maps can be used for symplectic tracking. The two graphs on the bottom of figures (5.4) show tracking with the fifth order approximations of a generating function. Again the left involves conventional generating function tracking, whereas the right displays symplectic normal form tracking. It is apparent that the transfer map which creates the top two figures is only approximated by the generating function which creates the bottom two figures, but the permanent stability of motion is correctly represented due to the fact that the generating function represents a symplectic map.

Still another important reason for striving to find order n symplectic fringe-field maps is the interrelations between different Taylor coefficients which are imposed by symplecticity. Some systems rely on these interrelations to correct aberrations. Examples are the high order achromates described in the references [WGB93, WGB94] and the opening aberration correction for electron microscopes by means of hexapoles described in [Ros90, Hof91], to mention only a small sample of the wealth of systems which were designed with the symplectic condition in mind. All these systems can not be analyzed well if fringe-field maps are used which are not order n symplectic.

5.3.2 Accuracy for a Wide Range of Apertures

Designing spectrographs, simulating electron microscopes, and analyzing beamlines and high energy storage rings are all topics which rely on the same principle of calculating transfer maps from the equation of motion. It therefore seems highly desirable to formulate calculation methods which work equally well for all these subfields of particle optics. The effect of the fringe fields in these areas is of different importance. In high energy accelerators, fringe fields typically have less influence, however, also

in this field substantial influences can be observed. Most fringe-field approximations assume that the region of the fringe field is much shorter than the region of the main field. For large aperture spectrographs and for electron microscopes, this is typically not the case. Therefore, to compute fringe-field maps of general usefulness, this assumption has to be avoided.

5.3.3 Usability for Arbitrary Orders

With the described DA methods it became easily possible to compute Taylor maps to very high order. The limit is only given by computer memory and computation time. To allow the potentials of the DA approach to be used with fringe fields, the computation of fringe-field maps should work for arbitrary evaluation orders. Especially since an efficient way of computing fringe-field maps was sought for the arbitrary order code *COSY INFINITY*, this requirement was important for the development of symplectic scaling (SYSCA).

5.4 The Principles and Usefulness of SYSCA

At first the basic ideas of symplectic scaling will be outlined and it will be explained why one can expect that our approach will yield accurate fringe-field maps. This method was first outlined in [HB91, HB93c]. The accuracy and speed of the approximation will be illustrated on several examples including linear design, high order effects, and long term tracking. These examples are also analyzed in [HB92a, HB94]. All the steps needed for symplectic scaling will be described in detail; since they can not only be used for fringe-field maps, the scaling principles will be formulated for general maps.

Following, we will use geometric coordinates for the map which means the variables

of motion are the cartesian coordinates and slopes x, x', y, y', the path length l, and the momentum p. Those six quantities form the vector $\vec{z}_g = (x, x', y, y', l, p)$, which is transformed by a transfer map which depends on n_p parameters D_j,

$$\vec{z}_{g,f} = \vec{M}(\vec{z}_{g,i}, \vec{D}) \; . \tag{5.17}$$

Here and in the following sections, parentheses sometimes symbolize functional dependences and sometimes they symbolize function evaluations. For example, $\vec{M}(\vec{z}_g, \vec{D})$ is a map $I\!R^{2d+n_p} \rightarrow I\!R^{2d}$, whereas $\vec{M}(\vec{z}_{g,i}, \vec{D}) = \vec{M}(\vec{z}_g, \vec{D})|_{(\vec{z}_{g,i}, \vec{D})}$ in equation (5.17) is an element of $I\!R^{2d}$. Whether a map or a real vector is described will become clear from the context.

The parameters we want to consider here are the mass m and the charge q of the particle, the size A of the optical element, and the pole-tip field B. When the size A is changed, the length and the aperture of an element change simultaneously. Call $\vec{M}(\vec{z}_g, m, q, A, B) : I\!R^{2d} \times I\!R^4 \rightarrow I\!R^{2d}$ the general parameter dependent transfer map of an optical element with the vector of parameters $\vec{D} = (m, q, A, B)$. From now on we will restrict ourselves to magnetostatic elements, although parts of the procedure are applicable to electrostatic elements, too.

Well known scaling properties allow to compute the general parameter dependent map $\vec{M}(\vec{z}_g, m, q, A, B)$ from the specific transfer map $\vec{M}^{m^*,q^*,A^*,B^*}(\vec{z}_g) : I\!R^{2d} \rightarrow I\!R^{2d}$ for one particle type with mass m^* and charge q^* and one parameter setting for the optical element of size A^* and field B^*. This is due to the fact that maps in geometric coordinates observe two scaling properties. The bending radius of the path of a particle with momentum p at field B is

$$R = \frac{p}{qB_\perp} \tag{5.18}$$

where $B_\perp$ denotes the field component perpendicular to the momentum of the particle. All maps that describe particles with equivalent bending radii along their path are

identical. If the specific map $\vec{M}^{m^*,q^*,A^*,B^*}(\vec{z}_g)$ is known for geometric coordinates $\vec{z}_g = (x, x', y, y', l, p)$, then it is known for all kinds of particle momenta p. If the specific map for any other parameter vector (m, q, A^*, B) is desired, one only has to choose p appropriately to create a map which describes the trajectory that corresponds to this parameter setting by

$$\vec{M}^{m,q,A,B}(\vec{z}_g) = \vec{M}^{m^*,q^*,A^*,B^*}(x, x', y, y', l, p \cdot \frac{q^* B^*}{Bq}) \,. \tag{5.19}$$

This is just another way of saying that the map depends only on the ratio of field to magnetic rigidity. Therefore the first scaling property is called scaling with magnetic rigidity. Strictly speaking this property only holds if the field structure $B(x, y, s)/B$ does not change with the pole-tip field, which means that saturation effects are not important. However, even when saturation effects are important, SYSCA is very accurate over a substantial range of the field strength.

One can also compute the field dependent map $\vec{M}^{m^*,q^*,A^*}(\vec{z}_g, B) : \mathbb{R}^{2d} \times \mathbb{R} \to \mathbb{R}^{2d}$ from the specific map $\vec{M}^{m^*,q^*,A^*,B^*}(\vec{z}_g)$ by scaling with magnetic rigidity. This map will become important for geometric scaling.

From the field dependent map $\vec{M}^{m^*,q^*,A^*}(\vec{z}_g, B)$, we can compute the specific map for any different size A of the element. For that, let us consider two similar magnetostatic elements that differ only by a scaling factor α. If the bending radii also differ by a factor of α, the maps are similar. Equation (5.18) shows that this is the case whenever the increase in size by a factor α is accompanied by a decrease in the field strength by the same factor. After scaling the coordinates x, y, l, we obtain

$$\begin{pmatrix} \vec{M}_x^{m^*,q^*,A,B}(\vec{z}_g) \\ \vec{M}_{x'}^{m^*,q^*,A,B}(\vec{z}_g) \\ \vec{M}_y^{m^*,q^*,A,B}(\vec{z}_g) \\ \vec{M}_{y'}^{m^*,q^*,A,B}(\vec{z}_g) \\ \vec{M}_l^{m^*,q^*,A,B}(\vec{z}_g) \end{pmatrix}_{(x, x', l, p)} = \begin{pmatrix} \frac{A}{A^*} \vec{M}_x^{m^*,q^*,A^*}(\vec{z}_g, B\frac{A}{A^*}) \\ \vec{M}_{x'}^{m^*,q^*,A^*}(\vec{z}_g, B\frac{A}{A^*}) \\ \frac{A}{A^*} \vec{M}_y^{m^*,q^*,A^*}(\vec{z}_g, B\frac{A}{A^*}) \\ \vec{M}_{y'}^{m^*,q^*,A^*}(\vec{z}_g, B\frac{A}{A^*}) \\ \frac{A}{A^*} \vec{M}_l^{m^*,q^*,A^*}(\vec{z}_g, B\frac{A}{A^*}) \end{pmatrix}_{(x, \frac{A^*}{A} x', l \frac{A^*}{A}, p)} . \tag{5.20}$$

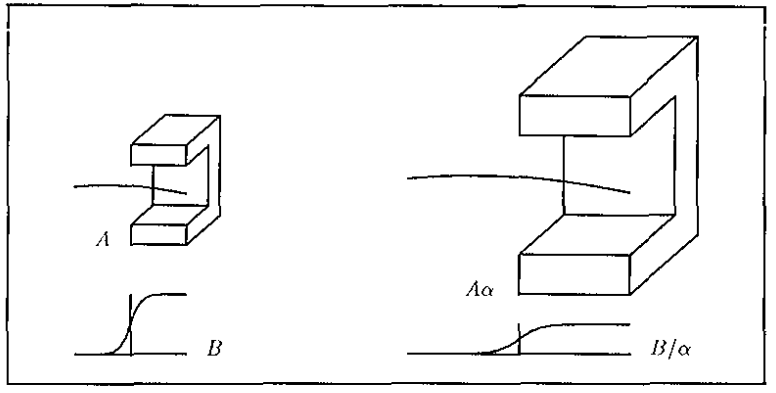

Figure 5.5: The coordinates of the particle trajectories in two elements scale with the factor α if the elements scale with the factor α and the fields scale with the factor $1/\alpha$.

Geometric scaling (5.20) and scaling with magnetic rigidity (5.19) together allow one to compute any specific map $\vec{M}^{m,q,A,B}(\vec{z}_g)$. Since this holds for any parameter vector $\vec{D} = (m, q, A, B)$, the general map $\vec{M}(\vec{z}_g, m, q, A, B)$ can be computed from a specific map $M^{m^*,q^*,A^*,B^*}(\vec{z}_g)$.

To conclude, we state that the knowledge of the transfer map $\vec{M}^{m^*,q^*,A^*}(\vec{z}_g, B)$ as a function of the field strength at the pole tip for particles with a specific magnetic rigidity and for an element with a specific aperture is sufficient to know all transfer maps of similar elements for all energies, masses, and charges. In fact the map does not even have to be known as a function of the field because the dependence on the field can be obtained by equation (5.19) from the dependence of the map on the momentum.

In accelerator physics, the phase space coordinates are often chosen to be $\vec{z}_p = (x, x', y, y', \delta_l, \delta_p)$. δ_l is the difference between the length of the particle's trajectory

and the reference particle's trajectory. δ_p is the relative deviation from the momentum p of the reference particle. It should be noted that in the literature the reference momentum is often denoted by p_0; this would lead to confusing notations in the formulas which are to follow and therefore p is used to describe the reference momentum. The particles momentum, which was called p in the geometric notation, is given by $p(1+\delta_p)$.

The coordinates $\vec{z}_p$ are introduced to ensure that particles which move close to the reference particle have small phase space coordinates. Then a Taylor expansion of the map is usable to describe the weakly nonlinear motion. Often this notation is called TRANSPORT notation [BRCI77], it can be transformed to the geometric notation and the scaling properties can be applied.

In general it is useful and customary to work with the canonical coordinates [Ber90a] $\vec{z}_E = (x, a, y, b, \tau, \delta_E)$, which are described in detail in subsection (5.8); δ_E is the relative deviation from the reference energy E. These coordinates are also small when the particle is close to the reference particle and Taylor expansions can be used. Maps in canonical notation have to be transformed to TRANSPORT notation before the two scaling laws can be applied.

If D is a parameter and the Taylor expansion around the reference parameter D^* is needed, we use $\delta_{D^*} = (D - D^*)/D^*$ as parameter. Given a reference pole-tip field B^*, then δ_{B^*} can be used to expand the field dependence of a map around B^*. COSY INFINITY readily computes the Taylor expansion of a field dependent map $\vec{M}^{m^*,q^*,A^*}(\vec{z}_{E^*}, \delta_{B^*})$ at reference values indicated by "$*$".

This Taylor map has to be stored to a file in order to compute maps of similar fields and all kind of beams by the previously mentioned scaling method. The accuracy with which the Taylor expansion approximates the field dependent map depends on

the chosen order of the expansion and on the difference between the reference field B^* and the field B_s to which one has to scale.

Unfortunately, the symplectic structure of the map would not be conserved in this process. While $\vec{M}^{m^*,q^*,A^*}(\vec{z}_{E^*}, \delta_{B^*})$ is symplectic for all δ_{B^*} and the corresponding Taylor map is order n symplectic, this is not the case for the Taylor map $\vec{M}^{m^*,q^*,A^*}(\vec{z}_{E^*}, \delta_{B^*})|_{\delta_B}$, which is $\mathbb{R}^{2d} \rightarrow \mathbb{R}^{2d}$ and is obtained when $\delta_B \in \mathbb{R}$ is inserted in the field dependence. Order n symplecticity, however, is an intrinsic symmetry of canonical motion that arises from the special structure of Hamilton's equations and should not be violated as mentioned in subsection (5.3.1).

This drawback can be eliminated by transforming the field dependent Taylor map $\vec{M}^{m^*,q^*,A^*}(\vec{z}_{E^*}, \delta_{B^*})$ to a symplectic representation, either in the form of a generating function, or in the form of a Lie exponent

$$\vec{M}^{m^*,q^*,A^*}(\vec{z}_{E^*}, \delta_{B^*}) = L(\delta_{B^*}) e^{:P(\vec{z}_{E^*}, \delta_{B^*}):} \vec{I} \tag{5.21}$$

with the identity map $\vec{I}$. In higher orders the representation via generating functions is slow, because a map inversion is required. The Lie representation has the disadvantage that the matrix $L(\delta_{B^*})|_{\delta_B}$ is not exactly symplectic. A combination of both methods is most efficient. We represent the nonlinear part by $P(\vec{z}_{E^*}, \delta_{B^*})$ and the linear part by the generating function $F(\delta_{B^*})$ that is most accurate for the given matrix $L(\delta_{B^*})$.

The left of figure (5.6) describes the procedure of computing the symplectic reference representation, which is stored in a reference file. First the Taylor map $\vec{M}^{m^*,q^*,A^*,B^*}(\vec{z}_{E^*})$ for a certain size of the optical element and for a certain particle is computed in canonical variables. In our implementation this is done with the code COSY INFINITY. Scaling with magnetic rigidity yields the field dependent map $\vec{M}^{m^*,q^*,A^*}(\vec{z}_{E^*}, \delta_{B^*})$. From this map the symplectic representations $F(\delta_{B^*})$ and $P(\vec{z}_{E^*}, \delta_{B^*})$ are computed and stored in a file [see subsections (5.6) and (5.7)].

The Taylor expansion of the general parameter dependent map $\vec{M}(\vec{z}_E, m, q, A, B)$ around $(m, q, A, B) \in \mathbb{R}^4$ is written as $\vec{M}(\vec{z}_E, \delta_m, \delta_q, \delta_A, \delta_B)$. The goal is to compute this Taylor map from the reference representation. The right side of figure (5.6) illustrates the procedure which will achieve this goal. After reading the reference file, the first step is to insert a value δ_{B^*} into the field dependence of the symplectic representation. δ_{B^*} is chosen in such a way that the symplectic representation describes particle motion which differs only by a scale in geometrical size from the trajectories of the desired map $\vec{M}^{m,q,A,B}(\vec{z}_E)$. If $A = A^*$, then equation (5.19) yields that $B_s = B\frac{p^*q}{pq^*}$. Then scaling with magnetic rigidity will create the map of a particle with p and q for the field B. If the desired element is bigger by a factor $\frac{A}{A^*}$, then the field B_s has to be chosen bigger by the same factor, due to equation (5.20). Then geometric scaling to size A will bring the field back to $B\frac{p^*q}{pq^*}$. Therefore

$$\delta_{B^*} = (B\frac{p^*qA}{pq^*A^*} - B^*)/B^* \tag{5.22}$$

has to be inserted.

From the so scaled symplectic representation one computes the order n symplectic Taylor map [see subsection (5.6) and (5.7)] which is then transformed to TRANSPORT coordinates [see subsection (5.8)]. The transformation map $\vec{T}(E, m)$ from canonical to transport coordinates depends on the properties of the particle which's motion the map describes:

$$\vec{M}(\vec{z}_p, \vec{\delta}) = \vec{T}(E, m) \circ \vec{M}(\vec{z}_E, \vec{\delta}) \circ \vec{T}^{-1}(E, m) \; . \tag{5.23}$$

The map in TRANSPORT coordinates $\vec{z}_p$ can then be scaled to the desired field by scaling with magnetic rigidity and to the correct size of the element by geometric scaling. As mentioned before, we can obtain the general parameter dependent map from the specific map by scaling. With DA this procedure automatically leads to the Taylor expansion with respect to all the parameters.

Finally one obtains the required general parameter dependent order n symplectic Taylor map $\vec{M}(\vec{z}_E, \delta_m, \delta_q, \delta_A, \delta_B)$ by transforming back to canonical coordinates [see subsection (5.8)].

Symplectic scaling can be applied to any map, but it is especially useful for fringe-field maps. The following examples show the accuracy and speed of obtaining fringe-field maps by symplectic scaling of a stored symplectic reference representation.

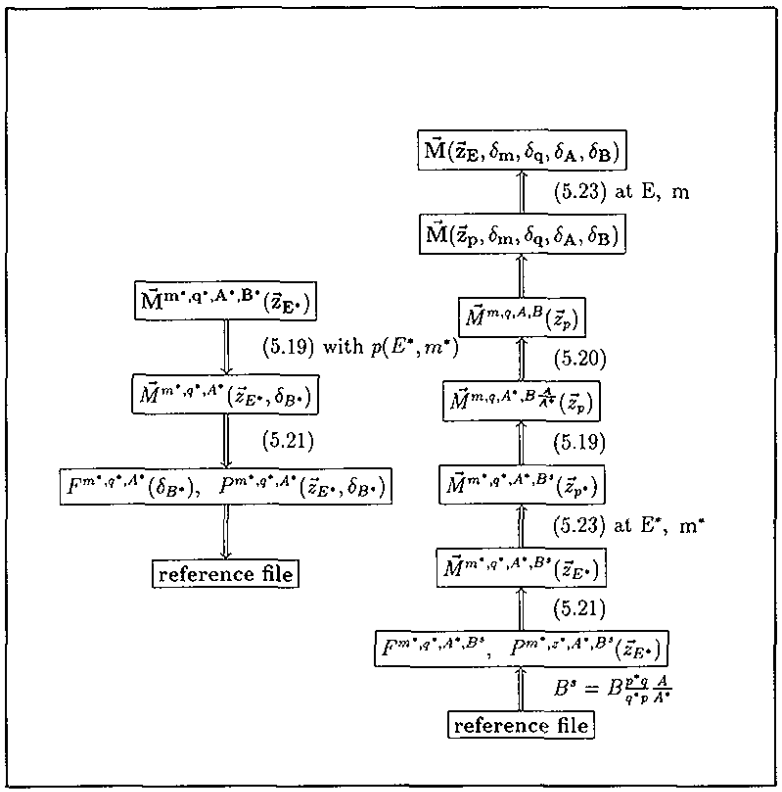

Figure 5.6: Schematic outline of the procedures leading to the reference representation and from the reference representation to the general transfer map.

5.5 Examples

In this section, we will illustrate the profitable use of the method with several examples. In order to evaluate speed and accuracy of the proposed approximation, we study a certain aberration coefficient of a quadrupole. Figure (5.7) shows the dependence of the expansion coefficient $(x|xxa)$ as a function of the field B at the pole tip. Because functions like this can be closely approximated by polynomials, symplectic scaling (SYSCA) is very accurate.

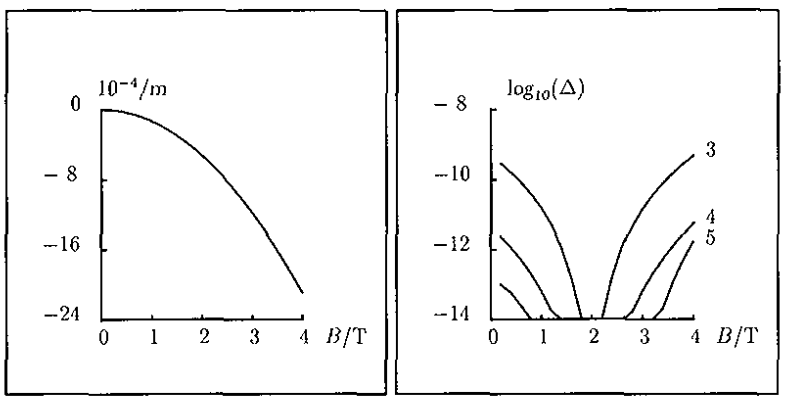

Figure 5.7: left: $(x|xxa)$ for a quadrupole as a function of the field at the pole tip. right: Error Δ of the approximation of $(x|xxa)$ with different expansion orders for the reference representation at B=2T.

Even at the border of the range in figure (5.7) the presented method is more accurate than the COSY standard integrator. Close to the value with which the reference file was produced, the accuracy increases drastically. The results in figure (5.7) were obtained by evaluating the symplectic reference representation to third, fourth, and fifth order. The accuracy can be further improved by increasing this

order which of course increases the computation time that has to be invested for creating the reference map in advance. This investment can be very much rewarding, especially when beamlines or spectrometers are being fitted or when system errors are analyzed so that maps of similar fringe fields are needed over and over again with only slightly different parameters.

The SYSCA approximation is especially helpful in the design of a realistic system after approximate parameters of the elements have been obtained by neglecting fringe fields. These values can be used to create a reference file for symplectic scaling. In this way, a very high accuracy almost equivalent to accurate but time intensive numerical integration can be obtained. The time advantage of this method is illustrated in figure (5.8).

Fringe fields do have noticeable effects already in first order. In the example of the A1200 [She92] isotope separator at the NSCL, the effect of the fringe fields on the calculated setting of the field strength is shown in figure (5.9). The fringe fields were described by Enge functions, and the Enge coefficients had been fitted to measured field data. Here the time advantage of the proposed approximation in the fit is three minutes versus two hours. As a measure of accuracy, we study the tilt angle Θ of the dispersive image plane and the opening aberration C_O for various approximation methods. In the discussed device the coefficient $(x|aa)$ vanishes because of symmetry of the axial ray and anti symmetry of the dipole fields; therefore $(x|aaa)$ is the relevant opening aberration.

$$\Theta = -\frac{(x|a\delta)}{(a|a)(x|\delta)} \quad , \quad C_O = (x|aaa) \; . \tag{5.24}$$

Table (5.1) shows Θ and C_O for various fringe-field models. The values of Θ with and without fringe fields differ by 0.5% for the first dispersive image plane in the A1200; the third order aberration, however, is completely wrong if fringe fields are

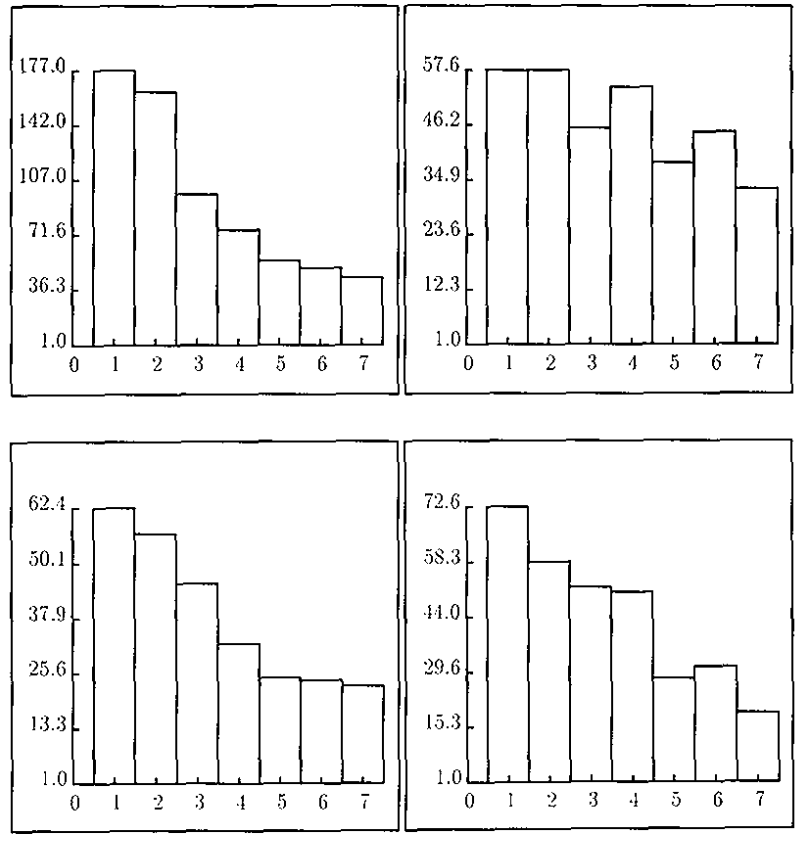

Figure 5.8: Factor of time advantage of SYSCA to numerical integration with accuracy of 10^{n-9} as a function of the expansion order. From top left to bottom right: dipole, quadrupole, hexapole, octupole.

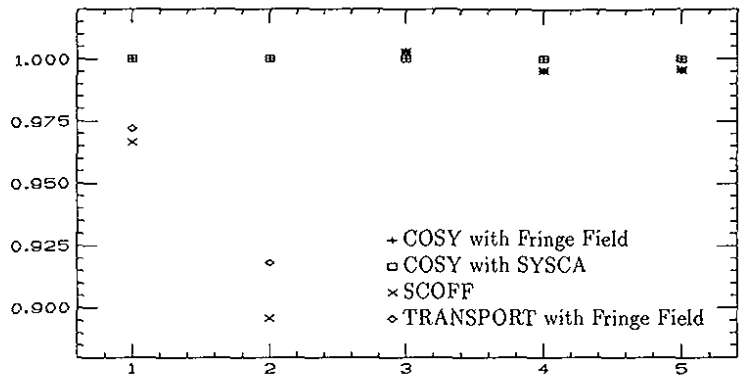

Figure 5.9: Relative deviation of predicted field settings with SCOFF and SYSCA from the correct settings for five quadrupoles. The standard fringe-field approximation of TRANSPORT is given as a reference; the deviation is mainly due to the neglect of quadrupole fringe fields.

Θ and C_O with SCOFF approximation	80.8840°	−65.96m
Θ and C_O with dipole fringe fields only	81.1696°	−65.96m
Θ and C_O with quad fringe fields only	81.2694°	−682.68m
Θ and C_O with SYSCA approximation	81.2701°	−687.10m
Θ and C_O with actual fringe fields	81.2702°	−687.10m

Table 5.1: Tilt angle and opening aberration for various fringe-field models.

disregarded. This comparison also shows that quadrupole fringe fields, although often disregarded, can have effects which dominate over dipole fringe fields. Nonlinear effects can be seen by sending a cone of particles through the 7^{th} order A1200 map. The images with SCOFF and SYSCA approximation are shown in figure (5.10). The maximum angle used is 15mrad. Note that due to the difference in scale, the beam spot computed with SCOFF is only one tenth as big. Trusting SCOFF would lead to a loss of most of the beam.

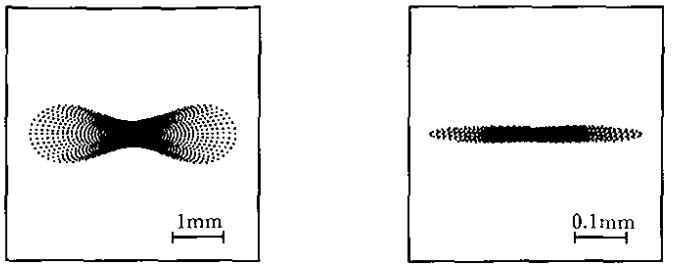

Figure 5.10: Beam spots with SYSCA (left) and SCOFF (right) approximation. The plot produced with the exact fringe fields can not be distinguished from the plot produced with SYSCA. Note the difference in scale.

Also for long term tracking in storage rings, fringe fields are influential. In figure 5.11 typical tracking pictures are displayed. An example storage ring for 1GeV protons was optimized for a big dynamical aperture. Eight particles were tracked with phase space coordinates which had x and y components in order not to avoid x–y coupling. The left picture was computed without fringe-field maps, whereas the right picture was computed with fringe-field maps. When fringe fields are neglected, one can often not trust the computed dynamical aperture.

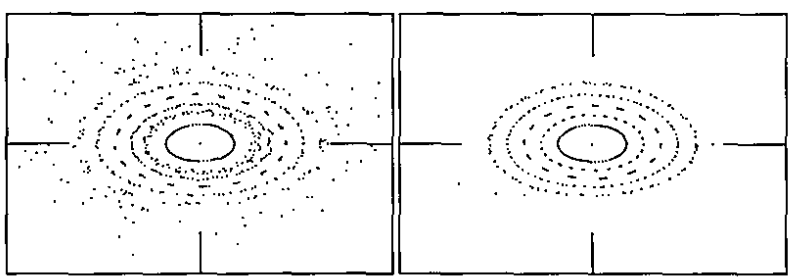

Figure 5.11: 500 turn tracking without (left) and with (right) fringe fields trough an 1Gev proton storage ring.

The effort involved in generating a symplectic approximation is rewarded when

repetitive tracking is being performed. The example lattice of choice is the proposed PSR II Ring. The 9^{th} order 5000 turn tracking pictures are displayed in figure (5.12).

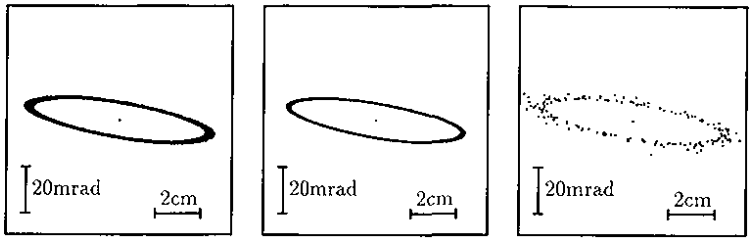

Figure 5.12: 5000 turn tracking with fringe fields obtained by numerical integration (left), SYSCA (middle), and a non -symplectic fringe-field approximation (right). The initial position of the particle is $(x, y) = (3\text{cm}, 3\text{cm})$ with no initial inclinations x' and y'.

The tracking was performed with the described standard numerical integration, SYSCA, and a non-symplectic fringe-field approximation obtained by low accuracy numerical integration. Non-symplectic tracking strongly violates the conservation of phase-space volumes. SYSCA yields more stable results than the numerical integration since the limited accuracy of the numerical integrator slightly violates symplecticity. The corresponding 9^{th} order maps were produced with the SYSCA mode in COSY INFINITY in 30 minutes, whereas the standard numerical integration took 15 hours, and the non symplectic approximation took 44 minutes on a VAX 4000 90 computer.

It is worthwhile mentioning that only maps of entrance fringe fields have to be saved. The exit fringe field of an element is described by the reversed map. A reversed map is computed by inverting a map and changing the signs of the incoming and the

outgoing momenta:

$$\vec{M}^{rev} = \begin{pmatrix} M_x^{-1} \\ -M_a^{-1} \\ M_y^{-1} \\ -M_b^{-1} \\ -M_\tau^{-1} \\ M_{\delta_E}^{-1} \end{pmatrix}_{(x,-a,y,-b,-\tau,\delta_E)} \tag{5.25}$$

Computing the inverse map $\vec{M}^{-1}$ from the SYSCA reference file is just as direct as computing the transfer map $\vec{M}$ itself. The generating function is a mixed function of initial and final variables. To compute the transfer map, it has to be partial inverted with respect to the initial variables. Partial inversion with respect to the final variables is a very similar process and leads to the inverse map. For the Lie exponent, $\exp(- : P :)$ acting on the identity $\vec{I}$ leads to the inverse of $\exp(: P :)\vec{I}$. If a representation approximates maps with pole-tip fields close to B then fields close to $-B$ can be approximated, also. The reason for this advantage is that the change of the sign in a multipole of symmetry C_ν corresponds to a rotation of that element by $\frac{180}{\nu}$ degrees.

5.6 The Lie Exponent

We search for a representation of the order n symplectic Taylor map $\vec{M} : I\!R^{2d} \to I\!R^{2d}$ of a Hamiltonian system in the form

$$\vec{M} =_n \vec{L} \circ (e^{:P^{(n+1)}:}\vec{z}) \tag{5.26}$$

where again "$=_n$" indicates that the right and left side agree up to order n. Also here we use the previously advocated notation of the identity map $\vec{z}$, not to be confused with a real vector. $\vec{L}$ is the linear map and the Lie exponent $P^{(n+1)}$ is a polynomial of orders from three to $n+1$. With the following induction, we will proof that the

Lie exponent always exists and the induction proof itself will reveal a methode to compute this exponent.

Since the Jacobi matrix L of $\vec{L}$ is symplectic, it has an inverse. As in chapter (1), we write N for the Jacobian of a map $\vec{N}$. The exponential has to satisfy

$$e^{:P^{(n+1)}:}\vec{z} =_n \vec{L}^{-1} \circ \vec{M} = \vec{z} + \vec{N} \tag{5.27}$$

with the nonlinear map $\vec{N}$. The right-hand side has a symplectic Jacobian $I + N$, where I symbolizes the identity matrix. Symplecticity requires

$$(I+N)^T J_{2d}(I+N) \quad =_{n-1} \quad J_{2d} \ , \tag{5.28}$$

$$J_{2d}N + N^T J_{2d} + N^T J_{2d} N \quad =_{n-1} \quad 0 \ . \tag{5.29}$$

The first order of this equation shows that $J_{2d}N_2$ is symmetric. The parts of exact order m of $\vec{N}$ and $P^{(n+1)}$ are denoted by $\vec{N}_m$ and P_m respectively. This implies that the potential problem given by the second order of equation (5.27)

$$: P_3 : \vec{z} = -J_{2d}\vec{\partial}P_3 = \vec{N}_2 \tag{5.30}$$

has a solution P_3. The next order yields the equation

$$: P_4 : \vec{z} = \vec{N}_3 - \frac{1}{2}(: P_3 :)^2 \vec{z} \ . \tag{5.31}$$

If this potential problem for P_4 has a solution the next step to obtain an equation for P_5 is obvious. To show that all the appearing potential problems have a solution, we start with the assumption that P_k was previously found as a solution of the potential problem

$$: P_k : \vec{z} =_{k-1} \vec{z} + \vec{N} - e^{:P^{(k-1)}:}\vec{z} \ . \tag{5.32}$$

The potential problem for P_{k+1} is

$$: P_{k+1} : \vec{z} =_k \vec{z} + \vec{N} - e^{:P^{(k)}:}\vec{z} \ . \tag{5.33}$$

We call the right hand side $\vec{F}_k$ and note that it has no orders lower than k. This problem has a solution P_{k+1} if $J_{2d}F_k$ is symmetric to order $k-1$.

Let the symplectic matrix $I + E^{(k)}$ be the Jacobian of $e^{:P^{(k)}:}\vec{z}$, then the symplectic condition requires similar to equation (5.29) that

$$J_{2d}E^{(k)} + E^{(k)T}J_{2d} + E^{(k)T}J_{2d}E^{(k)} = 0 \ . \tag{5.34}$$

To ensure the symmetry of $J_{2d}F_k$, one needs to show that

$$J_{2d}(N - E^{(k)}) + (N^T - E^{(k)T})J_{2d} =_{k-1} 0 \ . \tag{5.35}$$

The equations (5.29) and (5.34) show that this condition is equivalent to

$$N^T J_{2d} N =_{k-1} E^{(k)T} J_{2d} E^{(k)} \ . \tag{5.36}$$

Since we have kept in mind that $\vec{N}$ is nonlinear and therefore the Jacobian N has no constant part and furthermore that $N =_{k-2} E^{(k)}$, we realize that the right and left side of equation (5.36) agree up to order $k-1$.

5.7 The Generating Function for the Linear Map

For the task of representing fringe-field maps which are to be stored as Taylor expansions of the magnetic field, it is important that all the manipulations can be done with parameter dependent maps and parameter dependent Lie exponents. The linear map $\vec{L}$ then corresponds to a matrix whose elements are Taylor expansions with respect of the parameters. In the specific case of SYSCA, the parameter is δ_B, the relative deviation of the pole-tip field from a reference value. The corresponding matrix L is symplectic to the expansion order of δ_B. However, if a specific value for δ_B is inserted the resulting matrix is in general not symplectic. Therefore a symplectic representation has to be found that agrees with $\vec{L}$ to the expansion order of the parameter

δ_B. The generating functions are a suitable approach. We are concerned with the six dimensional space of transverse momentum, energy, and the corresponding canonical variables. We will keep the arguments general, however, because the procedure is the same for any symplectic $2d$ dimensional space. The following matrices will all be either d or $2d$ dimensional. The symplectic matrix L will be written in terms of d dimensional submatrices:

$$L = \begin{pmatrix} A & B \\ C & D \end{pmatrix} . \tag{5.37}$$

The first d dimensions describe coordinates $\vec{q}$ and the second d dimensions describe the corresponding momenta $\vec{p}$. J_{2d} therefore has the structure

$$J_{2d} = \begin{pmatrix} 0 & I \\ -I & 0 \end{pmatrix} . \tag{5.38}$$

Because of symplecticity

$$L^{-1} = -J_{2d} L^T J_{2d} = \begin{pmatrix} D^T & -B^T \\ -C^T & A^T \end{pmatrix} \tag{5.39}$$

and therefore

$$LL^{-1} = \begin{pmatrix} AD^T - BC^T & BA^T - AB^T \\ CD^T - DC^T & DA^T - CB^T \end{pmatrix} = I . \tag{5.40}$$

The four commonly used generating functions depend on the initial and final positions $\vec{q}_{i/f}$ and momenta $\vec{p}_{i/f}$. The relationship between final and initial coordinates is established by the equations

$$(\vec{q}_i, \vec{q}_f) = (\partial_{\vec{p}_i}, -\partial_{\vec{p}_f}) F_1(\vec{p}_i, \vec{p}_f) , \tag{5.41}$$

$$(\vec{q}_i, \vec{p}_f) = (\partial_{\vec{p}_i}, \partial_{\vec{q}_f}) F_2(\vec{p}_i, \vec{q}_f) . \tag{5.42}$$

$$(\vec{p}_i, \vec{q}_f) = (-\partial_{\vec{q}_i}, -\partial_{\vec{p}_f}) F_3(\vec{q}_i, \vec{p}_f) , \tag{5.43}$$

$$(\vec{p}_i, \vec{p}_f) = (-\partial_{\vec{q}_i}, \partial_{\vec{q}_f}) F_4(\vec{q}_i, \vec{q}_f) . \tag{5.44}$$

How those generating functions can be computed and when they exist will be shown for the case of F_2. The symplectic matrix L and its inverse establish relations between

initial and final coordinates:

$$\begin{pmatrix} \vec{q}_f \\ \vec{p}_f \end{pmatrix} = \begin{pmatrix} A & B \\ C & D \end{pmatrix} \begin{pmatrix} \vec{q}_i \\ \vec{p}_i \end{pmatrix} , \tag{5.45}$$

$$\begin{pmatrix} \vec{q}_i \\ \vec{p}_i \end{pmatrix} = \begin{pmatrix} D^T & -B^T \\ -C^T & A^T \end{pmatrix} \begin{pmatrix} \vec{q}_f \\ \vec{p}_f \end{pmatrix} \tag{5.46}$$

which yield equations for $\vec{q}_i$ and $\vec{p}_f$ as functions of $\vec{p}_i$ and $\vec{p}_f$:

$$A\ \vec{q}_f = -B\vec{p}_i + \vec{q}_f , \tag{5.47}$$

$$A^T \vec{p}_f = \vec{p}_i + C^T \vec{q}_f . \tag{5.48}$$

In case the determinant of A does not vanish we get the potential problem

$$\begin{pmatrix} \vec{q}_i \\ \vec{p}_f \end{pmatrix} = \begin{pmatrix} A^{-1} & 0 \\ 0 & A^{-T} \end{pmatrix} \begin{pmatrix} -B & I \\ I & C^T \end{pmatrix} \begin{pmatrix} \vec{p}_i \\ \vec{q}_f \end{pmatrix} , \tag{5.49}$$

$$\begin{pmatrix} \partial_{\vec{p}_i} \\ \partial_{\vec{q}_f} \end{pmatrix} F_2 = \begin{pmatrix} -A^{-1}B & A^{-1} \\ A^{-T} & A^{-T}C^T \end{pmatrix} \begin{pmatrix} \vec{p}_i \\ \vec{q}_f \end{pmatrix} \tag{5.50}$$

which has a solution if the involved matrix is symmetric. The symplectic condition in equation (5.40) implies that $A^{-1}B$ is symmetric. Since the transposed of L is also symplectic we can conclude that $A^{-T}C^T$ is symmetric, too. Therefore F_2 exists whenever $det|A| \neq 0$. Similar relations can be obtained for the other generating functions:

$$F_1 \iff det|C| , \tag{5.51}$$

$$F_2 \iff det|A| , \tag{5.52}$$

$$F_3 \iff det|D| , \tag{5.53}$$

$$F_4 \iff det|B| . \tag{5.54}$$

This implies that there are linear maps without corresponding generating functions of the discussed types. According to figure (5.3), the SCOFF approximation yields good

results in first order. Therefore the linear part of a fringe-field map is closed to the identity. The determinants of A and D will therefore not vanish. In SYSCA we chose the generating function according to the submatrix with the greatest determinant.

5.8 Transformation between Cartesian and Canonical Coordinates

The motion of ions is governed by a Hamiltonian E that describes the energy:

$$\begin{aligned} \dot{x} &= \partial_{p_x} E \ , \quad \dot{p}_x = -\partial_x E \ , \\ \dot{y} &= \partial_{p_y} E \ , \quad \dot{p}_y = -\partial_y E \ , \\ \dot{s} &= \partial_{p_s} E \ , \quad \dot{p}_s = -\partial_s E \ . \end{aligned} \tag{5.55}$$

With the new independent variable s, measured along the central trajectory, we get new equations of motion which include the time t and the energy as dependent variables:

$$x' = \frac{\dot{x}}{\dot{s}} = \frac{\partial_{p_x} E}{\partial_{p_s} E} = -(\frac{\partial p_s}{\partial p_x})_E \ . \tag{5.56}$$

Similar manipulations for the other coordinates yield a set of Hamiltonian equations with the new Hamiltonian $K = -p_s$:

$$\begin{aligned} x' &= \partial_{p_x} K \ , \quad p_x' = -\partial_x K \ , \\ y' &= \partial_{p_y} K \ , \quad p_y' = -\partial_y K \ , \\ -t' &= \partial_E K \ , \quad E' = -\partial_{-t} K \ . \end{aligned} \tag{5.57}$$

This canonical transformation has already been discussed in [CS58]. A scaling with the initial momentum p_0 of the reference particle yields the new Hamiltonian $-p_s/p_0$ with the set of canonical variables

$$\vec{z}_{E_0} = (x, a = \frac{p_x}{p_0}, y, b = \frac{p_y}{p_0}, \tau = \frac{E_0}{p_0}(t_0 - t), \delta_{E_0} = \frac{E - E_0}{E_0}) \tag{5.58}$$

which can easily be verified by performing the scaling in the equations (5.57). This set is used in COSY INFINITY. In TRANSPORT the inclination x' and y' are used instead of the transverse momenta. Instead of the difference in time of flight τ and energy deviation δ_{E_0}, the difference in path length l and the momentum deviation δ_{p_0} are used. The TRANSPORT notation is more transparent and can be used for the presented scaling purpose. The canonical COSY INFINITY notation has to be used for the symplectic representations. The two notations are related by the following equalities:

$$x' = \frac{a}{\sqrt{(\frac{p}{p_0})^2 - a^2 - b^2}} \ , \quad y' = \frac{b}{\sqrt{(\frac{p}{p_0})^2 - a^2 - b^2}} \ , \tag{5.59}$$

$$l = l_i - \frac{v}{v_0}\frac{2+\eta_0}{1+\eta_0}(\tau - \tau_i) + (\frac{v}{v_0} - 1)s \ , \tag{5.60}$$

$$\delta_{p_0} = \frac{\sqrt{(E_0(1+\delta_{E_0}))^2 + 2E_0 mc^2(1+\delta_{E_0})}}{p_0 c} - 1 \tag{5.61}$$

where the subscript "i" indicates quantities corresponding to the initial plane and subscripts "0" denote values for the reference particle, v is the velocity and η is the ratio of energy to rest energy $\frac{E}{mc^2}$. The inverse transformation is

$$a = (\frac{p}{p_0})\frac{x'}{\sqrt{(1+x'^2+y'^2}} \ , \quad b = (\frac{p}{p_0})\frac{y'}{\sqrt{1+x'^2+y'^2}} \ , \tag{5.62}$$

$$\tau = \tau_i - \frac{v_0}{v}\frac{1+\eta_0}{2+\eta_0}(l - l_i - (\frac{v}{v_0} - 1)s) \ , \tag{5.63}$$

$$\delta_{E_0} = \frac{\sqrt{(p_0 c(1+\delta_{p_0}))^2 + (mc^2)^2} - mc^2}{E_0} - 1 \ . \tag{5.64}$$

The length of the reference trajectory s is usually the length of the element for which the maps are transformed. For fringe-field maps this length is zero.

It is important to realize that the transformation depends on the properties of the reference particle and on the length of the element. This information is not contained

in the map and have to be specified additionally.

Bibliography

[AH83] G. Alefeld and J. Herzberger. *Introduction to Interval Computations*. Academic Press, New York, 1983.

[Arn63] V. I. Arnol'd. Proof of a theorem of A. N. Kolmogorov on the invariance of conditionally periodic motions under small perturbations of the Hamiltonian. *Uspekhi Mat. Nauk*, 18:5:91–192, 1963. and translation in Russian Mathematical Surveys 18:6, 85–191 (1963).

[BBB64] K. L. Brown, R. Belbeoch, and P. Bounin. First- and second-order magnetic optics matrix equations for the midplane of uniform-field wedge magnets. *Review of Scientific Instruments*, 177:481, 1964.

[Ber87] M. Berz. The method of power series tracking for the mathematical description of beam dynamics. *Nuclear Instruments and Methods*, A528:431, 1987.

[Ber88a] M. Berz. Differential Algebraic treatment of beam dynamics to very high orders including applications to spacecharge. *AIP Conference Proceedings*, 177:275, 1988.

[Ber88b] M. Berz. High-order description of accelerators using differential algebra and first applications to the SSC. In *Snowmass Summer Meeting*. Snowmass, CO, 1988.

[Ber89] M. Berz. Differential algebraic description of beam dynamics to very high orders. *Particle Accelerators*, 24:109–124, 1989.

[Ber90a] M. Berz. Arbitrary order description of arbitrary particle optical systems. *Nuclear Instruments and Methods*, A298:426–440, 1990.

[Ber90b] M. Berz. Computer aspects of optics design and simulation: COSY INFINITY. *Nuclear Instruments and Methods*, A298:473–479, 1990.

[Ber91a] M. Berz. Forward algorithms for high orders and many variables. In *Automatic Differentiation of Algorithms*, Philadelphia, Pennsylvania, 1991. SIAM.

[Ber91b] M. Berz. Symplectic tracking through circular accelerators with high order maps. In *Nonlinear Problems in Future Accelerators*, pages 288–296, New York, 1991. World Scientific.

[Ber92a] M. Berz. Automatic differentiation as nonarchimedean analysis. In *Computer Arithmetic and Enclosure Methods*, pages 439–450. Elsevier Science Publishers B.V., 1992.

[Ber92b] M. Berz. COSY INFINITY version 6 reference manual. Technical Report MSUCL-869, National Superconducting Cyclotron Laboratory, MSU, East Lansing, MI, 1992.

[Ber93a] M. Berz. COSY INFINITY version 6. In *Nonlinear problems in accelerator physics*, Conf. Ser. No. 131, pages 125–133, London, 1993. Institute of Physics.

[Ber93b] M. Berz. Differential Algebraic formulation of normal form theory. In *Nonlinear problems in accelerator physics*, Conf. Ser. No. 131, pages 77–86, London, 1993. Institute of Physics.

[Ber94] M. Berz. *New features in COSY INFINITY*, volume 297 of *AIP Conference Proceedings*, pages 267–278. AIP Press, 1994.

[BH94a] M. Berz and G. H. Hoffstätter. Computation and application of Taylor polynomials with remainder bounds. *Submitted to Interval Computations*, 1994.

[BH94b] M. Berz and G. H. Hoffstätter. Exact bounds on the long term stability of weakly nonlinear systems applied to the design of large storage rings. *Interval Computations, to appear*, 1994.

[BHW87] M. Berz, H. C. Hofmann, and H. Wollnik. *COSY 5.0, the fifth order code for corpuscular optical systems*. *Nuclear Instruments and Methods*, A258:402, 1987.

[Bir27] G. D. Birkhoff. Dynamical systems. *American Mathematical Society Publications*, 9, 1927.

[BRCI77] K. L. Brown, F. Rothacker, D. C. Carey, and Ch. Iselin. TRANSPORT user's manual. Technical Report SLAC–91, Stanford Linear Accelerator Center, 1977.

[BS34] E. Brüche and O. Scherzer. *Geometrische Elektronenoptik*. Springer, Berlin, 1934.

[BS81] K. L. Brown and J. E. Spencer. Non-linear optics for the final focus of the single-pass-collider. *IEEE Transactions on Nuclear Science*, NS-28, 3:2568, 1981.

[BWRF93] J. S. Berg, R. L. Warnock, R. D. Ruth, and E. Forest. Construction of symplectic maps for nonlinear motion of particles in accelerators. Technical Report SLAC–PUB–6037, Stanford Linear Accelerator Center, 1993.

[BZWH91] M. Berz, M. Zhao, W. Wan, and G. H. Hoffstätter. New features in COSY INFINITY. Technical Report NSCL Annual Report, National Superconducting Cyclotron Laboratory, MSU, 1991.

[CS58] E. D. Courant and H. S. Snyder. Theory of the alternating-gradient synchrotron. *Annals of physics*, 3:1–48, 1958.

[Cse91] T. Csenes. Test results of interval methods for global optimization. *Computer Arithmetic, Scientific Computation and Mathematical Modelling*, 12, 1991.

[DF76] A. D. Dragt and J. M. Finn. Lie series and invariant functions for analytic symplectic maps. *Journal of Mathematical Physics*, 17:2215–2227, 1976.

[Eri91] J. Eriksson. *Parallel Global Optimization Using Interval Analysis, Licentiate Thesis*. PhD thesis, University of Umeå, Sweden, 1991.

[ES93] D. A. Edwards and M. J. Syphers. *An introduction to the physics of high energy accelerators*. Wiley series in beam physics and accelerator technology, M. Month (Editor). John Wiley& Sons, Inc., New York, 1993.

[FBI89] E. Forest, M. Berz, and J. Irwin. Normal form methods for complicated periodic systems: A complete solution using Differential Algebra and Lie operators. *Particle Accelerators*, 24:91–107, 1989.

[Gja93] I. M. Gjaja. A comparison of methods for long-term tracking using symplectic maps. In *Nonlinear problems in accelerator physics*, Conf. Ser. No. 131, pages 185–192, London, 1993. Institute of Physics.

[Han79] E. R. Hansen. Global optimization using interval analysis – the one-dimensional case. *J. Optim. Theor. and Appl.*, 29:331–334, 1979.

[Han80] E. R. Hansen. Global optimization using interval analysis -- the multidimensional case. *Numerische Mathematik*, 34:247–270, 1980.

[Han88] E. Hansen. *An Overview of Global Optimization Using Interval Analysis*, pages 289–307. Academic Press, New York, 1988.

[HB91] G. H. Hoffstätter and M. Berz. Fringe-field approximations. *NSCL Annual Report*, pages 236–241, 1991.

[HB92a] G. H. Hoffstätter and M. Berz. Applications of symplectic scaling. *NSCL Annual Report*, pages 206–209, 1992.

[HB92b] G. H. Hoffstätter and M. Berz. Survival times of particles in storage rings. Technical Report NSCL Annual Report, National Superconducting Cyclotron Laboratory, MSU, 1992.

[HB93a] G. H. Hoffstätter and M. Berz. Refinement of the normal form method for long term stability estimates. *NSCL Annual Report*, pages 182–185, 1993.

[HB93b] G. H. Hoffstätter and M. Berz. Rigorous stability estimates. *NSCL Annual Report, pages 186–189*, 1993.

[HB93c] G. H. Hoffstätter and M. Berz. Symplectic scaling, a DA based tool. In *Proceedings of PAC 93, Washington D.C.*, 1993.

[HB94] G. H. Hoffstätter and M. Berz. An efficient symplectic approximation for fringe-field maps. In *Computational Accelerator Physics*, volume AIP Conference Proceedings 297, pages 467–476, 1994.

[HBW90] B. Hartmann, M. Berz, and H. Wollnik. The computation of fringing fields using Differential Algebra. *Nuclear Instruments and Methods*, A297:343, 1990.

[Hel63] R. H. Helm. First and second order beam optics of a curved inclined magnetic field boundary in the impulse approximation. Technical Report 24, SLAC, 1963.

[HIW93] B. Hartmann, H. Irnich, and H. Wollnik. Analytical determination of 5th-order transfer matrices of magnetic quadrupole fringing fields. In *Nonlinear problems in accelerator physics*, Conf. Ser. No. 131, pages 87–96, London, 1993. Institute of Physics.

[Hof91] G. Hoffstätter. Geometrische Elektronenoptik angewandt auf ein durch Hexapole korrigiertes Mikroskop mit sub Ångström Auflösung. Master's thesis, Technische Hochschule Darmstadt, 1991.

[IF79] K. Ichida and Y. Fujii. An interval arithmetic method for global optimization. *Computing*, 23:85–97, 1979.

[Jan91] C. Jansson. A global minimization method: The one-dimensional case, Berichte des Forschungsschwerpunktes Informations- und Kommunikationstechnik. Technical Report Bericht 91.2, Technische Universität Hamburg–Harburg, 1991.

[Jan92a] C. Jansson. A global optimization method using interval arithmetic. *IMACS Annals of Computing and Applied Mathematics*, 1992.

[Jan92b] C. Jansson. A global optimization method using interval arithmetic. In *Computer Arithmetic and Scientific Computation, Proceedings of the SCAN 91*, Amsterdam, 1992. North–Holland, Elsevier.

[JK92] C. Jansson and O. Knüppel. A global minimization method: The multi-dimensional case, Berichte des Forschungsschwerpunktes Informations- und Kommunikationstechnik. Technical Report Bericht 92.1, Technische Universität Hamburg–Harburg, 1992.

[KE87] S. Kowalski and H. A. Enge. RAYTRACE user's manual. Technical report, Department of Physics MIT, 1987.

[Kol54] A. N. Kolmogorov. On the conservation of conditionally periodic motions for a small change in the Hamiltonian. *Dokl. Akad. Nauk SSST*, 98:527-530, 1954.

[KSYZ91] R. Kleiss, F. Schmidt, Y. Yan, and F. Zimmermann. On the feasibility of tracking with differential-algebra maps in long term stability studies for large hadron colliders. Technical Report CERN SL/92/02, DESY HERA 92-01, and SSCL-564, Superconducting Super Collider Laboratory, 1991.

[KSZ92] R. Kleiss, F. Schmidt, and F. Zimmermann. Experience with a simple method to "symplectify" differential algebra maps. Technical Report CERN SL/92-31 (AP) and DESY HERA 92-16, Superconducting Super Collider Laboratory, 1992.

[Kul89] U. Kulisch, editor. *Wissenschaftliches Rechnen mit Ergebnisverifikation – Eine Einführung.* Akademie Verlag, Ost–Berlin, Vieweg, Wiesbaden, 1989.

[LL83] A. J. Lichtenberg and M. A. Liebermann. *Regular and Stochastic Motion.* Springer, New York, 1983.

[Lya92] A. M. Lyapunov. *The General Problem of the Stability of Motion.* Taylor& Francis, London, Washington, DC, 1992. (Translated an edited by A. T. Fuller).

[May89] G. Mayer. *Grundbegriffe der Intervallrechnung*, pages 101–118. Akademie Verlag, Ost–Berlin, Vieweg, Wiesbaden, 1989.

[MH91] K. R. Meyer and G. R. Hall. *Introduction to Hamiltonian Dynamical Systems and the N-Body Problem.* Applied Mathematical Sciences 90. Springer Verlag, New York, 1991.

[Mic94] L. Michelotti. *Towards C++ object libraries for accelerator physics*, volume 297 of *AIP Conference Proceedings*, pages 264–266. AIP Press, 1994.

[Moh90] I. B. Mohd. An interval global optimization algorithm for a class of functions with several variables. *Journal of Computational and Applied Mathematics*, 31:373–382, 1990.

[Moo66] R. E. Moore. *Interval Analysis.* Prentice Hall, Engelwood Cliffs, New Jersey, 1966.

[Moo79] R. E. Moore. *Methods and Applications of Interval Analysis.* SIAM, Philadelphia, Pennsylvania, 1979.

[Moo88] R. E. Moore, editor. *Reliability in Computing: The Role of Interval Methods in Scientific Computations.* Academic Press, New York, 1988.

[Mos62] J. K. Moser. On invariant curves of area preserving mappings of an annulus. *Nachr. Akad. Wiss. Göttingen. Math. Phys. Kl. II*, pages 1–20, 1962.

[MR88] R. E. Moore and H. Ratschek. Inclusion functions and global optimization II. *Mathematical Programming*, 41:341–356, 1988.

[MW92] S. B. Mane and W. T. Weng. Minimal normal-form method for discrete maps. Technical Report AGS/AD/Tech Note No. 368, Brookhaven National Laboratory, 1992.

[MW93] S. B. Mane and W. T. Weng. Minimal normal-form method for discrete maps. *Physical Review E*, 48(1):523–542, 1993.

[Nay93] A. H. Nayfeh. *Method of normal forms.* Wiley series in nonlinear science. John Wiley & Sons, Inc., New York, 1993.

[Nek77] N. N. Nekhoroshev. An exponential estimate of the time of stability of nearly–integrable Hamiltonian systems. *Uspekhi Mat. Nauk*, 32:6:5–66, 1977. and translation in Russian Math. Surveys 32:6, 1–65 (1977).

[Poi99] H. Poincaré. *Les méthodes nouvelles de la méchanique céleste.* Gauthier–Villars, Paris, 1892, 1893, 1899. three volumes.

[PR71] E. Plies and H. Rose. Über die axialen Bildfehler magnetischer Ablenksysteme mit krummer Achse. *Optik*, 34, 1971.

[Pra33] Georg Prange. *Abhandlungen zur Strahlenoptik, W. R. Hamilton.* Akademische Verlagsgesellschaft, Leipzig, 1933.

[Pre92] D. Preikzas. MOPS reference manual. Technical report, Technische Hochschule Darmstadt, Darmstadt, Germany, 1992.

[Ral81] L. B. Rall. *Automatic Differentiation: Techniques and Applications. Computer Science No. 120.* Springer, 1981.

[Rat92] D. Ratz. *Automatische Ergebnisverifikation bei globalen Optimierungsproblemen.* PhD thesis, Universität Karlsruhe, Institut für Angewandte Mathematik, 1992.

[Ros87] H. Rose. Hamiltonian magnetic optics. *Nuclear Instruments and Methods in Physics Research*, A258:374–401, 1987.

[Ros90] H. Rose. Outline of a spherically corrected semiaplanatic medium-voltage transmission electron microskope. *Optic*, 85:19, 1990.

[RR88] H. Ratschek and J. Rokne. *New Computer Methods for Global Optimization.* Ellis Horwood Limited, Chichester, England, 1988.

[Sch91] F. Schmidt. SIXTRACK – A single particle tracking code. In *Nonlinear Problems in Future Accelerators*, pages 270–281, New York, 1991. World Scientific.

[Shc92] B. M. Sherrill. Initial operating experience with the a1200 fragment separator. *Nuclear Instruments and Methods*, B70:298–303, 1992.

[Sie52] C. L. Siegel. Über die Existenz einer Normalform analytischer Hamiltonscher Differentialgleichungen in der Nähe einer Gleichgewichtslösung. *Math. Ann.*, 128:144–170, 1952.

[Sie56] C. L. Siegel. *Vorlesungen über Himmelsmechanik.* Springer–Verlag, Berlin–Göttingen–Heidelberg, 1956.

[SSC94] J. M. Sanz-Serna and M. P. Calvo. *Numerical Hamiltonian Problems.* Applied Mathematics and Mathematical Computation 7. Chapman & Hall, London, 1994.

[Tal91] R. Talman. Long term prediction and the SSC. In *Nonlinear Problems in Future Accelerators*, pages 215–231, New York, 1991. World Scientific.

[Tur90] G. Turchetti. Nekhoroshev stability estimates for symplectic maps and physical applications. In *Number Theory and Physics, Springer Proceedings in Physics 47*, Berlin, Heidelberg, 1990. Springer–Verlag.

[Tur91] G. Turchetti. Beam stability analysis via normal forms and non perturbative methods. In *Nonlinear Problems in Future Accelerators*, pages 16–45, New York, 1991. World Scientific.

[vZ94] J. van Zeijts. *New features in the design code TLIE*, volume 297 of *AIP Conference Proceedings*, pages 285–290. AIP Press, 1994.

[War91] R. L. Warnock. Close approximation to invariant tori in nonlinear mechanics. *Physical Review Letters*, 66(14):1803–1806, 1991.

[WGB93] W. Wan, E. Goldmann, and M. Berz. Third-order achromats based on mirror symmetries. In *Nonlinear problems in accelerator physics*, Conf. Ser. No. 131, pages 201–207, London, 1993. Institute of Physics.

[WGB94] W. Wan, E. Goldmann, and M. Berz. *The design of a four cell third order achromat*, volume 297 of *AIP Conference Proceedings*, pages 143–149. AIP Press, 1994.

[WHB88] H. Wollnik, B. Hartmann, and M. Berz. Principles behind GIOS and COSY. *AIP Conference Proceedings*, 177:74, 1988.

[WHS85] G. Walster, E. Hansen, and S. Sengupta. *Test results for a global optimization algorithm*, pages 272–287. SIAM, Philadelphia, 1985.

[Wol65] H. Wollnik. Image aberrations of second order for magnetic and electrostatic sector fields including all fringing field effects. *Nuclear Instruments and Methods*, 38:56, 1965.

[Wol92] H. Wollnik. GIOS user's manual. Technical report, JLU Gießen, Germany, 1992.

[WR89] R. L. Warnock and R. D. Ruth. Bounds on nonlinear motion for a finite time. Technical Report SLAC–PUB–5020, Stanford Linear Accelerator Center, 1989.

[WR91] R. L. Warnock and R. D. Ruth. Stability of orbits in nonlinear mechanics for finite but very long times. In *Nonlinear Problems in Future Accelerators*, pages 67–76, New York, 1991. World Scientific. also SLAC–PUB–5304.

[WR92] R. L. Warnock and R. D. Ruth. Long-term bounds on nonlinear Hamiltonian motion. *Physica D*, 56(14):188–215, 1992. also SLAC–PUB–5267.

[WRGE89] R. L. Warnock, R. D. Ruth, W. Gabella, and K. Ecklund. Methods of stability analysis in nonlinear mechanics. Technical Report SLAC–PUB–4846, Stanford Linear Accelerator Center, 1989.

[Yan91] Y. Yan. Applications of differential algebra to single-particle dynamics in storage rings. Technical Report SSCL-500, Superconducting Super Collider Laboratory, 1991.

[Yan93] Y. Yan. Performance of an implicit algorithm for symplecitic one-turn-map tracking. Technical Report SSCL-Preprint-157, Superconducting Super Collider Laboratory, 1993.

[Yan94a] Y. Yan. Success in one-turn maps for dynamic apperture studies - a brief review. In *Stability of Particle Motion in Storage Rings*, volume 292 of *AIP Conference Proceedings*, pages 177-181. AIP Press, 1994.

[Yan94b] Y. T. Yan. *Zlib and related programs for beam dynamics studies*, volume 297 of *AIP Conference Proceedings*, pages 279-284. AIP Press, 1994.